NASA
SPACE VEHICLE
DESIGN CRITERIA
(CHEMICAL PROPULSION)

NASA SP-8110

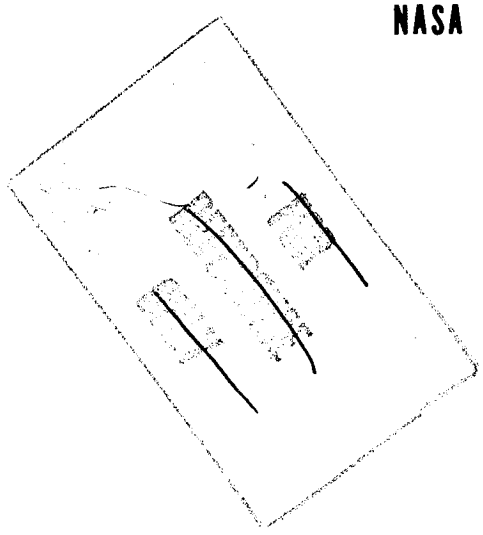

LIQUID ROCKET ENGINE TURBINES

JANUARY 1974

NATIONAL AERONAUTICS AND SPACE ADMINISTRATION

FOREWORD

NASA experience has indicated a need for uniform criteria for the design of space vehicles. Accordingly, criteria are being developed in the following areas of technology:

Environment
Structures
Guidance and Control
Chemical Propulsion

Individual components of this work will be issued as separate monographs as soon as they are completed. This document, part of the series on Chemical Propulsion, is one such monograph. A list of all monographs issued prior to this one can be found on the final pages of this document.

These monographs are to be regarded as guides to design and not as NASA requirements, except as may be specified in formal project specifications. It is expected, however, that these documents, revised as experience may indicate to be desirable, eventually will provide uniform design practices for NASA space vehicles.

This monograph, "Liquid Rocket Engine Turbines," was prepared under the direction of Howard W. Douglass, Chief, Design Criteria Office, Lewis Research Center; project management was by Harold Schmidt assisted by Lionel Levinson. The monograph was written by S. B. Macaluso, Rocketdyne Division, Rockwell International Corporation, and was edited by Russell B. Keller, Jr. of Lewis. To assure technical accuracy of this document, scientists and engineers throughout the technical community participated in interviews, consultations, and critical reviews of the text. In particular, B. R. Branstrom of Pratt & Whitney Aircraft Division of United Aircraft Corporation; R. R. Duane of Bell Aerospace Company, Division of Textron; T. T. Thomas of General Electric Company (Evendale); and R. G. Stabe of the Lewis Research Center individually and collectively reviewed the monograph in detail.

Comments concerning the technical content of this monograph will be welcomed by the National Aeronautics and Space Administration, Lewis Research Center (Design Criteria Office), Cleveland, Ohio 44135.

January 1974

For sale by the National Technical Information Service
Springfield, Virginia 22151
Price – $5.00

GUIDE TO THE USE OF THIS MONOGRAPH

The purpose of this monograph is to organize and present, for effective use in design, the significant experience and knowledge accumulated in development and operational programs to date. It reviews and assesses current design practices, and from them establishes firm guidance for achieving greater consistency in design, increased reliability in the end product, and greater efficiency in the design effort. The monograph is organized into two major sections that are preceded by a brief introduction and complemented by a set of references.

The State of the Art, section 2, reviews and discusses the total design problem, and identifies which design elements are involved in successful design. It describes succinctly the current technology pertaining to these elements. When detailed information is required, the best available references are cited. This section serves as a survey of the subject that provides background material and prepares a proper technological base for the *Design Criteria* and Recommended Practices.

The *Design Criteria*, shown in italics in section 3, state clearly and briefly what rule, guide, limitation, or standard must be imposed on each essential design element to assure successful design. The *Design Criteria* can serve effectively as a checklist of rules for the project manager to use in guiding a design or in assessing its adequacy.

The Recommended Practices, also in section 3, state how to satisfy each of the criteria. Whenever possible, the best procedure is described; when this cannot be done concisely, appropriate references are provided. The Recommended Practices, in conjunction with the *Design Criteria,* provide positive guidance to the practicing designer on how to achieve successful design.

Both sections have been organized into decimally numbered subsections so that the subjects within similarly numbered subsections correspond from section to section. The format for the Contents displays this continuity of subject in such a way that a particular aspect of design can be followed through both sections as a discrete subject.

The design criteria monograph is not intended to be a design handbook, a set of specifications, or a design manual. It is a summary and a systematic ordering of the large and loosely organized body of existing successful design techniques and practices. Its value and its merit should be judged on how effectively it makes that material available to and useful to the designer.

CONTENTS

LIST OF FIGURES

LIST OF TABLES

LIQUID ROCKET ENGINE TURBINES

1. INTRODUCTION

This monograph deals with the specialized requirements and techniques used for designing axial-flow turbines for rocket engine turbomachinery. The design factors that distinguish rocket engine turbines from those developed for other turbodrive applications are associated with

- Comparatively short but severe service life
- Strict limitations on size and weight
- High energy content of working fluids (propellants)
- High specific work output
- Requirements for rapid start and short run duration
- Severe thermal shock conditions
- High stage loadings and stresses.

Noteworthy advancements in rocket turbine design have been made since the early developments in the Redstone[1] rocket engine program. This engine contained a comparatively-low-speed turbine of conservative design driven by decomposed hydrogen peroxide. The pressure-compounded turbines for the Atlas vehicle and H-1 engines, which use LO_2/RP-1 working fluids, were typical of the next generation turbine designs. In the dual-shaft, series-installed turbines developed for the J-2 engines for the Saturn V S-II stage, liquid hydrogen (LH_2) and liquid oxygen (LO_2) were used as working fluid. Concurrent with these developments, five- and six-stage nuclear rocket turbines also were designed and developed, together with the LO_2/RP-1 turbine for the 1 500 000-lbf[2]-thrust F-1 engine for the Apollo booster. The 30-in.-pitch-diameter F-1 turbine was evolved from accumulated missile and space vehicle turbomachinery experience, and exemplifies current state-of-the-art turbine design; it is a two-row velocity-compounded configuration and develops 60 000 horsepower at a design speed of 5600 rpm. The current technology now serves as a base for developing turbines for the Space Shuttle engines and for continuing advances in rocket turbine technology. Developed rocket turbines have reliably

[1]Symbols, materials, and engines and vehicles are defined or identified in Appendix A.
[2]Factors for converting U.S. customary units to the International System of Units (SI units) are given in Appendix B.

demonstrated service lives of 6000 seconds; however, new requirements call for operational capabilities of up to 10 hours.

The attainment of turbine predicted performance will be more critical in the next generation rocket engines than in the past engines because more horsepower will be developed per unit turbine size and because a closer interdependence will exist among turbine efficiency, engine specific impulse, and chamber pressure. This monograph provides guidelines for predicting turbine performance, sizing gas-path elements, and avoiding problems associated with mechanical design and development. Typical problems and solutions in past rocket engine programs include the following:

- Changes to the turbine design pressure ratio affected gas-path energy distribution, and the turbine nozzles and blading had to be modified or redesigned.
- Differential expansion and component cracking at weld joints during operation required modification of turbine casing and manifold design.
- Blading failed during turbine operation, and changes were made to blade/disk attachments and to blade/shroud configurations in order to reduce stress levels and stress concentrations.
- Forged rotor disks failed because of poor material ductility; this condition was corrected by increasing the solution-heat-treat temperature specified for the disk forgings.

The material in the monograph is organized along the lines of the design and development effort necessary to produce a turbine that satisfies the requirements imposed on it. A new turbine design is initiated with preliminary studies that establish design state conditions, turbine size, and performance estimates. Operational requirements of the oxidizer and fuel pumps and of the propellant feed system are used to establish turbine design horsepower, speed, pressure ratios, working-fluid properties, and operational characteristics. This preliminary turbine analysis is supplemented with layout studies of gas-path elements and candidate turbine configurations. The in-depth aerodynamic and detailed mechanical design of turbine hardware is subsequently accomplished during the turbomachinery development program. Final design drawings are evolved with the coordinated efforts of stress analysts, materials specialists, and machine-design personnel. This process requires close direction by the responsible turbine engineer to ensure that all design details related to turbine geometry, gas-path configuration, performance, and turbine mechanical integrity are maintained.

Equally important to the development of a good turbine design are the tasks associated with fabrication, prototype assembly, and development testing. The degree of success attained during the development program ultimately rests with the ability to transform into operational hardware what has been evolved during the preceding analytical and design phases. Thus, the successful development of a flight-ready turbine depends on the skill and experience of all the aforementioned kinds of personnel; their influence on the final design will vary in accordance with the specific requirements of the application and the utilization of good engineering judgment.

2. STATE OF THE ART

Turbines for rocket engines are developed to meet specific performance and turbomachinery-installation requirements. Representative designs for turbines used to drive production and experimental rocket engine turbomachinery are illustrated in figures 1 through 10. These configurations depict various approaches used in the mechanical design and arrangement of turbine manifolding, casing, shafting, rotor assembly, gas-path detail, and component retention.

Figure 1 illustrates the turbine design used in the XLR-99 rocket engine that powered the experimental X-15 aircraft. Distinguishing features are the design of the single rotor, which carries two rows of blades, and the cone-type disk retainer and support. The split turbine shroud retains the turbine stator. The change in manifold cross-sectional area depicts the constant-velocity manifold design used in this assembly.

The Mark 3 turbine in figure 2 is a two-stage design used in the turbomachinery for the Thor, Jupiter, and Atlas booster engines and in the Saturn H-1 engine. This turbine has an interstage seal package located at the base of the rotors, and drive pins locate the rotors and transmit power to the shaft. Turbine casing loads are transmitted to the turbopump through the torus and short-coupled retaining diaphragm. The turbine rotor blades are welded to the first- and second- stage disks. Speed reduction between the turbine and the two propellant pumps is obtained by a 4.83-to-1 gearbox.

The Mark 5 turbine shown in figure 3 is a single-row, 7.64-in. pitch-diameter design that employs an extended dual diaphragm as the main structural member of the casing; the torus is supported at the nozzle. This type of torus/diaphragm configuration is most suitable in low-horsepower applications.

The mechanical-design details of the Mark 10 LO_2/RP-1 turbine are illustrated in figure 4. This unit provided power for the turbopumps for the F-1 engines used in the Apollo Saturn V booster. The shroud, manifold, and diaphragm in this design comprise a single subassembly; shroud and manifold are attached to the pump at the torus outer diameter with radial pin retainers. The production nozzle was fabricated from Rene 41 by machining the vanes and inner shroud and welding an outer shroud to the vanes. An improved development version of this nozzle design is currently being fabricated by electrical-discharge machining of Rene 41 forgings. The turbine rotors are designed with conventionally shrouded impulse-type blades and fir-tree attachments; curvic couplings and bolts retain the turbine rotors to the turbopump shaft.

The Mark 15-fuel (LH_2) turbine design appears in figure 5. This is the high-pressure turbine in the series-installed turbines for the J-2 engines used in the Saturn S-II and S-IVB stages (turbine exhaust from this unit is used subsequently as working fluid in the low-pressure

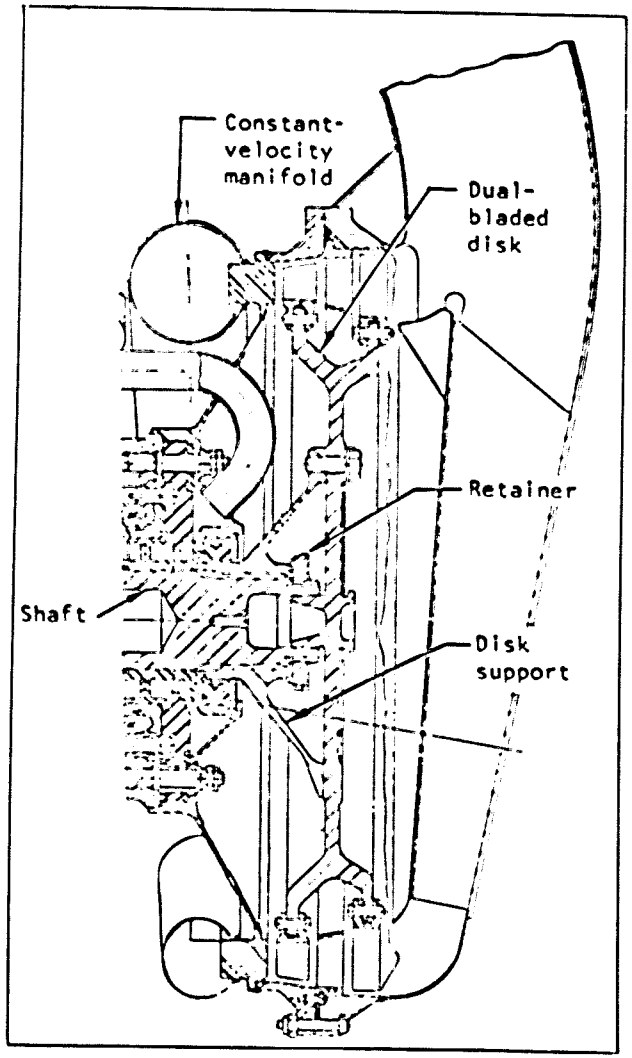

Figure 1. – X-15 turbine assembly.

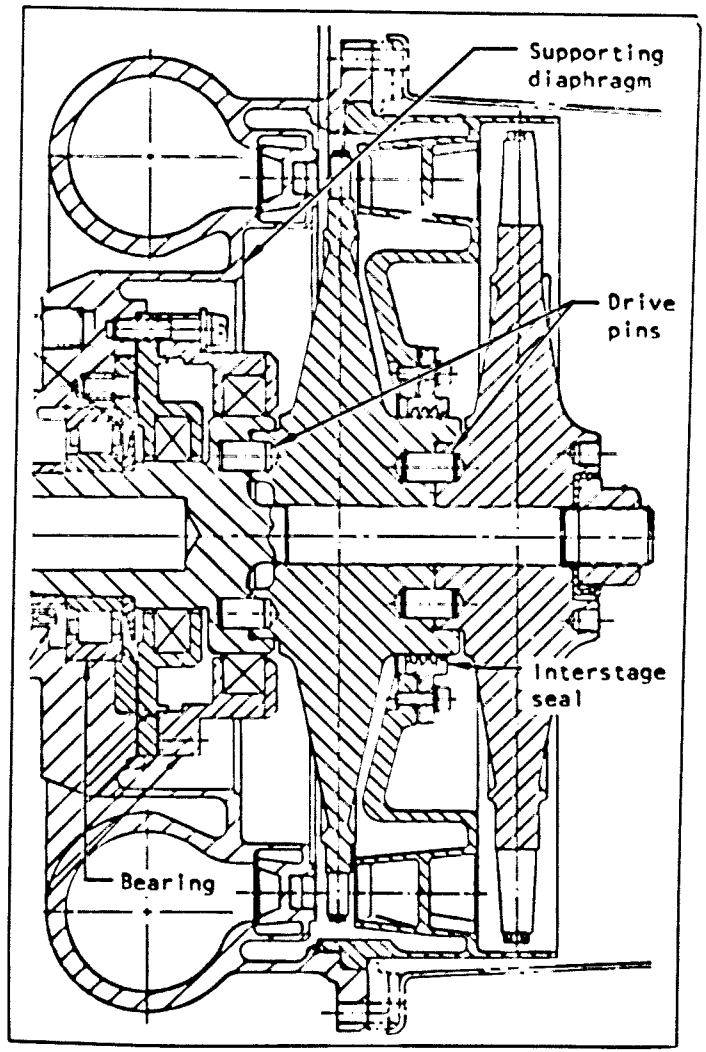

Figure 2. – Mark 3 turbine assembly (H-1 engine).

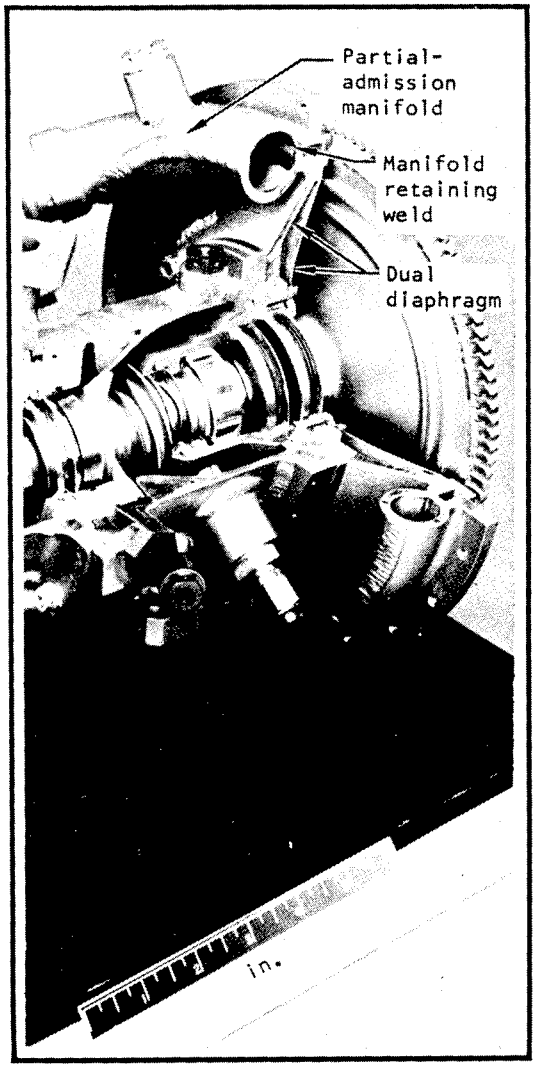

Figure 3. – Mark 5 turbine assembly (aircraft rocket).

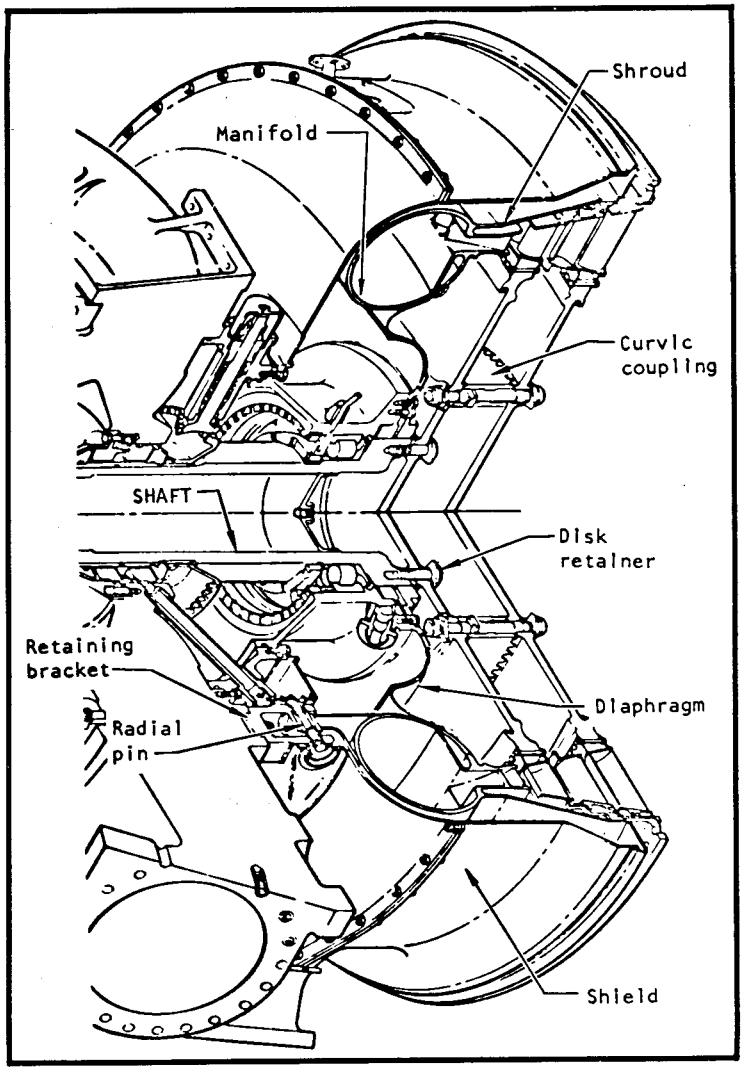

Figure 4. – Mark 10 turbine assembly (F-1 engine).

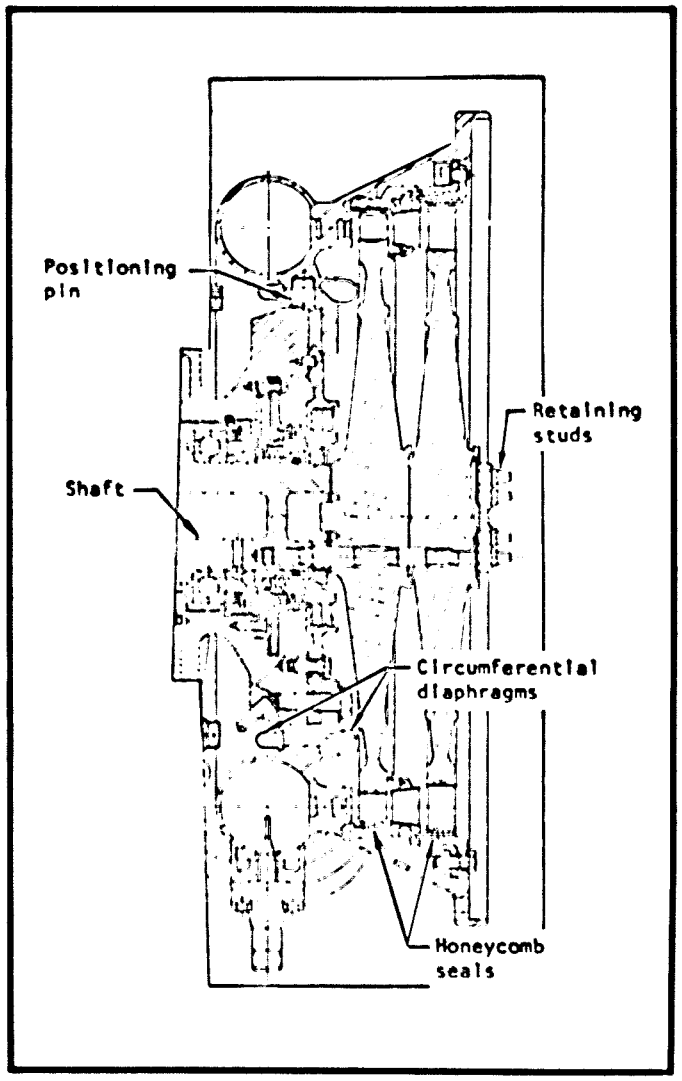

Figure 5. – Mark 15-F turbine assembly (J-2 fuel).

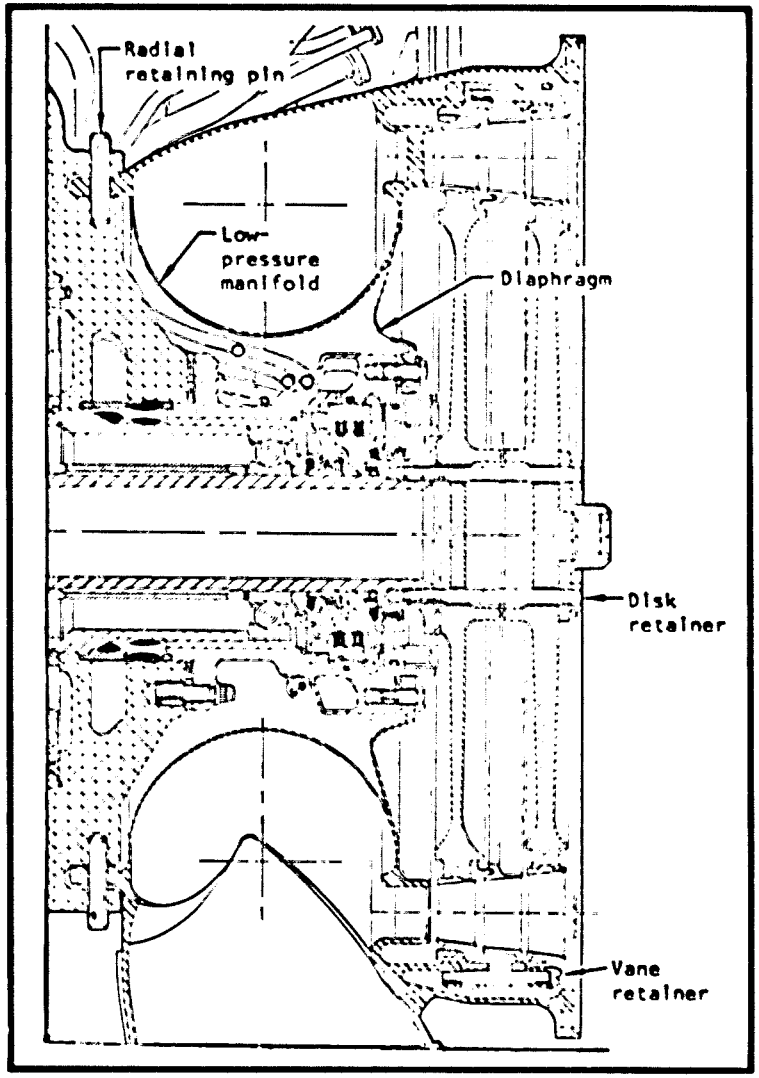

Figure 6. – Mark 15-O turbine assembly (J-2 oxidizer).

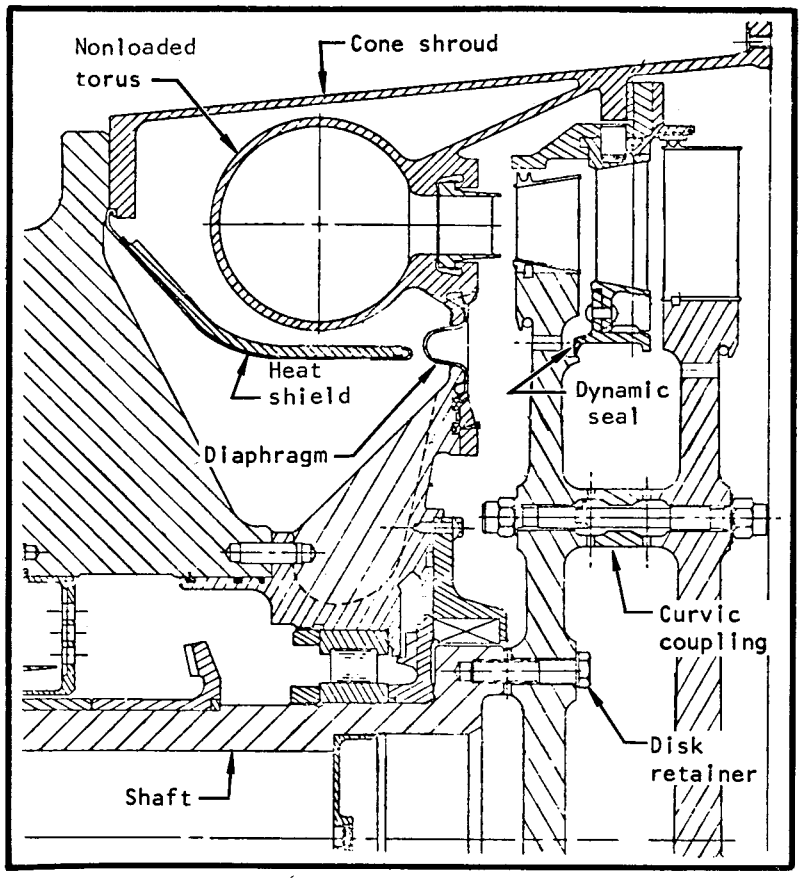

Figure 7. — Alternate design, Mark 10 turbine assembly (F-1 engine).

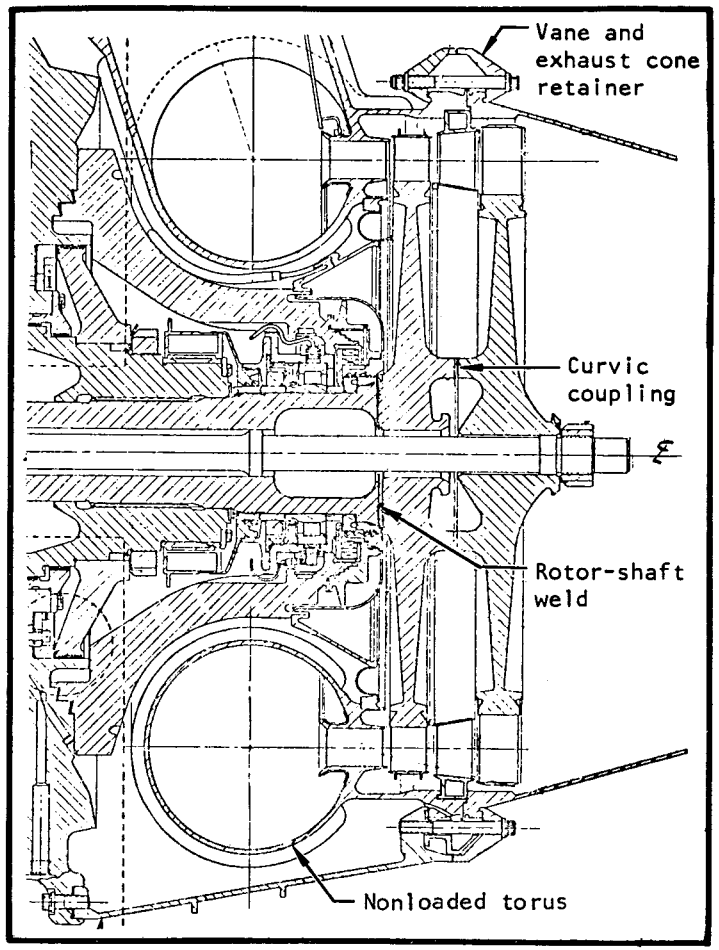

Figure 8. — M-1 fuel turbine assembly.

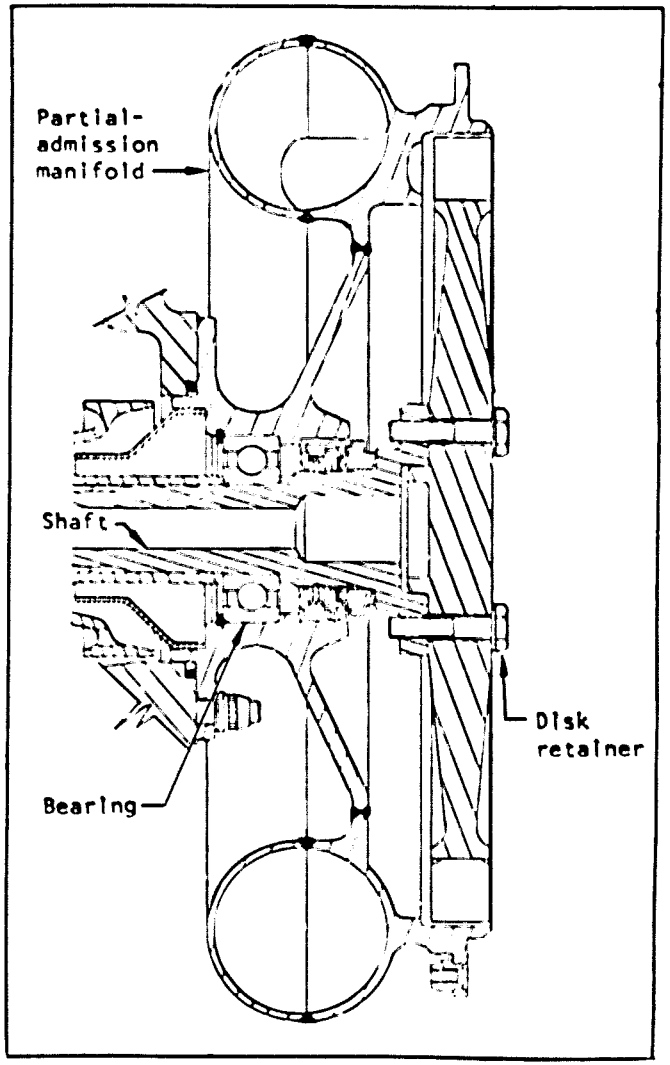

Figure 9. – Agena LR81-RA-11 turbine assembly.

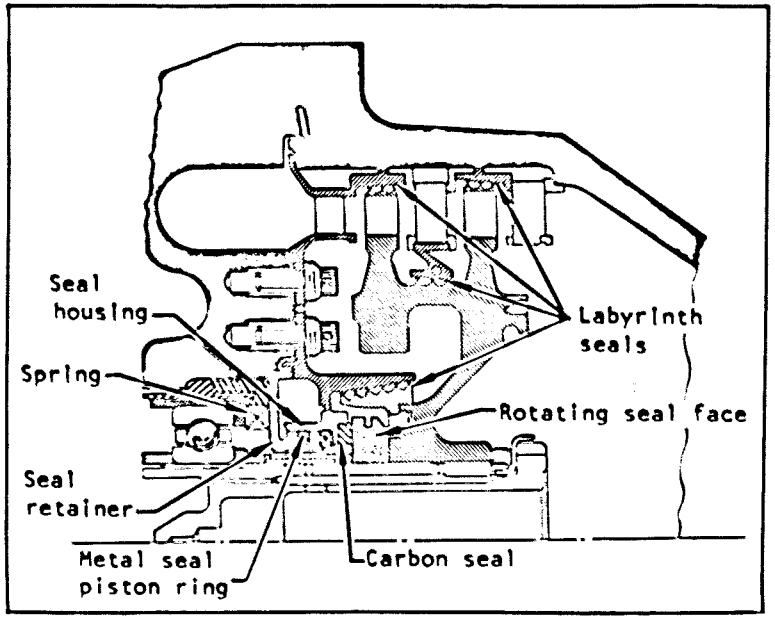

Figure 10. – RL10 A3-3 turbine assembly.

Mark 15-oxidizer (LO_2) turbine. The turbine is mounted to the turbopump with a short-coupled diaphragm containing radial pins for axial positioning. A circumferential "hat" section and U-diaphragm perform the sealing function at the radial joint. Honeycomb rotor tip seals are carried by the stator ring and retainer. Turbine torque transmission and disk retention are accomplished with a stud drive.

The J-2 engine series-installed oxidizer turbine (Mark 15-0), which utilizes exhaust gas from the Mark 15-F turbine as working fluid, is illustrated in figure 6. It incorporates a unitized low-pressure torus-and-shroud configuration that does not require the numerous welds of a separate torus and nozzle. Radially installed roll pins retain the manifold at the outer diameter, and a conventional diaphragm at the inner diameter provides a seal at that juncture.

The alternate Mark 10 turbine, which is designed with a nonloaded torus, is illustrated in figure 7. Higher turbine inlet temperatures and pressures can be accommodated in this type of torus/shroud configuration than in a turbine that does not incorporate a separate torus design. This 30-in.-pitch-diameter turbine has developed 60 000 horsepower during development tests.

The turbine illustrated in figure 8 was designed to provide power for the liquid-hydrogen turbopump used in the M-1 engine. The turbine shroud and exhaust cone join to form a clamp configuration for retaining the stator and torus outer support. The first-row rotor is electron-beam welded to the turbine shaft, and the second row is retained with a tie-bolt-and-lock configuration. The interface of the first and second rotors incorporates a curvic coupling. Turbine blades are attached to the rotors by electron-beam welding.

The single-row turbine assembly illustrated in figure 9 is used in the LR81-BA-11 Agena engine. This is a 7.89-in.-pitch-diameter, partial-admission design that uses IRFNA/UDMH at 1400° F as working fluid. At the design speed of 24 800 rpm, the turbine develops 365 horsepower.

The model A3-3 two-stage turbine shown in figure 10 is used in the RL 10 engine. This is a 5.9-in.-pitch-diameter design that uses heated hydrogen as working fluid; it develops 660 horsepower at a design speed of 28 670 rpm. Blading is fully shrouded, and labyrinth seals are incorporated to minimize blade and interstage leakage. The conical web between the disk and the bore is designed to reduce the effects of disk thermal growth, minimize hub distortion, and aid in preventing imbalance. The turbine case and integral disk and blades are fabricated of aluminum alloy. The shrouds are brazed to the blade tips and vane roots. Turbine exit guide vanes are utilized to minimize discharge whirl losses.

Design data representative of these and other turbine configurations developed for space vehicles are listed in table I, and a tabulation of typical materials used in the fabrication of these turbines appears in table II. Turbine designs that appear in figures 1 through 10 are cross referenced in tables I and II.

Table 1 — Design Data for Representative Operational and Advanced Development Turbines

Rocket engine	Turbine designation	Turbine status	Type	No. of stages	Power MJ/s	Speed rpm	Pitch diameter m	Working fluid	Propellant enthalpy kJ/kg	Inlet total temperature °K	Inlet total pressure psia	Pressure ratio	Velocity ratio U/C_i	Efficiency $\eta_s/T.S$ %	Assembly
RL10	Mark 2	Former production	Zero NC	1	295	48 667	20.00	H_2O_2	423	680	890	22	–	89.0	–
H-1	Mark 3	Production	PC	2	4 000	31 600	9.00	LO_2/RP-1	1290	1200	600	17.7	0.47	62.5	Fig. 2
Atlas Sustainer	Mark 4	Production	PC	2	1 660	38 000	6.00	LO_2/RP-1	995	1075	760	23	0.39	64.3	–
AR	Mark 5	Former production	Impulse	1	300	27 000	2.64	H_2O_2	876	1364	680	22	–	–	Fig. 3
E-1	Mark 6	Former development	Zero NC	1	14 860	8 900	22.00	LO_2/RP-1	617	1400	650	25	0.20	62.5	–
Nuclear	Mark 9	Former production	PC	6	13 500	32 800	3.90	GH_2	1132	60	800	15.2	–	–	–
F-1	Mark 10	Production	Zero NC	1	56 356	5 890	34.90	LO_2/RP-1	847	1550	920	16.3	0.20	60.4	Fig. 4
H-2	Mark 14	Former development	Zero NC	1	7 650	34 300	16.07	LO_2/RP-1	1000	1700	525	13.9	0.21	58.9	–
J-2	Mark 15 oxidizer	Production	Zero NC	1	2 604	16 650	15.50	LO_2/LH_2	587	260	82	3.16	0.11	68.4	Fig. 4
J-2	Mark 15 fuel	Production	Zero NC	1	6 745	26 000	12.50	LO_2/LH_2	1464	1200	620	6.35	0.18	60.1	Fig. 5
XLR	Mark 15 oxidizer	Former development	Impulse	1	250	32 800	6.00	LO_2/LH_2	860	1200	450	9.0	–	–	–
XLR	Mark 15 fuel	Former development	PC	2	4 000	27 000	9.00	LO_2/LH_2	1160	1200	450	16.4	–	–	–
NERVA	Mark 25	Former production	PC	5	20 000	34 000	7.97	GH_2	1162	60	1000	10	–	29.5	–
J-2X	Mark 26 fuel	Former development	Zero NC	1	12 700	28 000	12.50	LO_2/LH_2	1535	1050	920	2	–	–	–
J-2S	Mark 26 fuel	Former development	Zero NC	1	10 800	28 000	10.5	LO_2/LH_2	1283	1200	889	3.30	–	66.0	–
J-2S	Mark 26 oxidizer	Former development	Zero NC	1	3 260	16 000	13.5	LO_2/LH_2	613	260	100	2.68	–	54.2	–
M-1	M-1 oxidizer	Former development	Zero NC	1	24 600	5 550	33.0	LO_2/LH_2	508	260	194	1.82	0.13	54.0	–
M-1	M-1 fuel	Former development	Zero NC	1	54 138	12 900	25.58	LO_2/LH_2	1355	1000	904	5.8	0.19	65.0	Fig. 9
RL-10	A-3-3	Production	PC	2	660	24 670	5.90	GH_2	338	60	700	1.82	0.35	24.7	Fig. 10
Agena	LR-79-9-11	Production	Impulse pump admission	1	367	24 800	3.89	IRFNA/UDMH	611	1400	475	37.7	0.14	41.0	Fig. 9

NOTE AC = axial-flow compressor
PC = pressure compressor
AR = [illegible]

Table II. – Materials Successfully Used for Turbine Components

Turbine designation	Manifold and nozzle*	Rotor blades**	Rotor disks	Stator vanes**
Mark 3	Hastelloy B, cast	Stellite 21	16-25-6	Hastelloy B, cast
Mark 4	M: 19-9DL N: Hastelloy B, cast	Stellite 21	16-25-6	Hastelloy B, cast
Mark 9	Inconel X-750	Inconel X-750	Inconel X-750	Inconel X-750
Mark 10 (D_m = 35 in.)	Rene 41	Alloy 713C	Rene 41	Stellite 21
Mark 10 (D_m = 30 in.)	M: Hastelloy C N: Stellite 21	Alloy 713C	Inconel 718	Stellite 21
Mark 15-O	310	Stellite 21	16-25-6	Stellite 21
Mark 15-F	Hastelloy C	Alloy 713C	Inconel 718	Stellite 21
Mark 25	Inconel X-750	Inconel 718	Inconel 718	Inconel X-750
Mark 29-O	321	Stellite 21	16-25-6	Stellite 21
Mark 29-F	Hastelloy C	Alloy 713C	Inconel 718	Hastelloy C
Summary (10 turbines)	Hastelloy B, cast 19-9DL Inconel X-750 Rene 41 Hastelloy C Stellite 21 310 321	Stellite 21 Inconel X-750 Alloy 713C Inconel 718	16-25-6 Inconel X-750 Rene 41 Inconel 718	Hastelloy B, cast Inconel X-750 Stellite 21 Hastelloy C

*The manifolds in most designs are welded from more than one alloy; the principal alloy used for the manifold is listed above. The nozzle is part of the welded manifold assembly for all the listed turbines. M designates manifold material; N, nozzle material.

**For rotor blades and stator vanes:

- Stellite 21 and alloy 713C are available only in the cast form (casting alloys).
- In the Mark 3 and 4 turbines, the blades were attached to the disk by welding; in the Mark 9 and 25, integrally machined with the disk. In the other listed turbines, fir-tree blade attachments were used.

Representative engine cycles and installations for which rocket turbines are developed appear in figure 11. In-depth discussions of the design of engine cycles and propellant feed systems are presented in reference 1; basic concepts involved in turbine design and application are treated in reference 2.

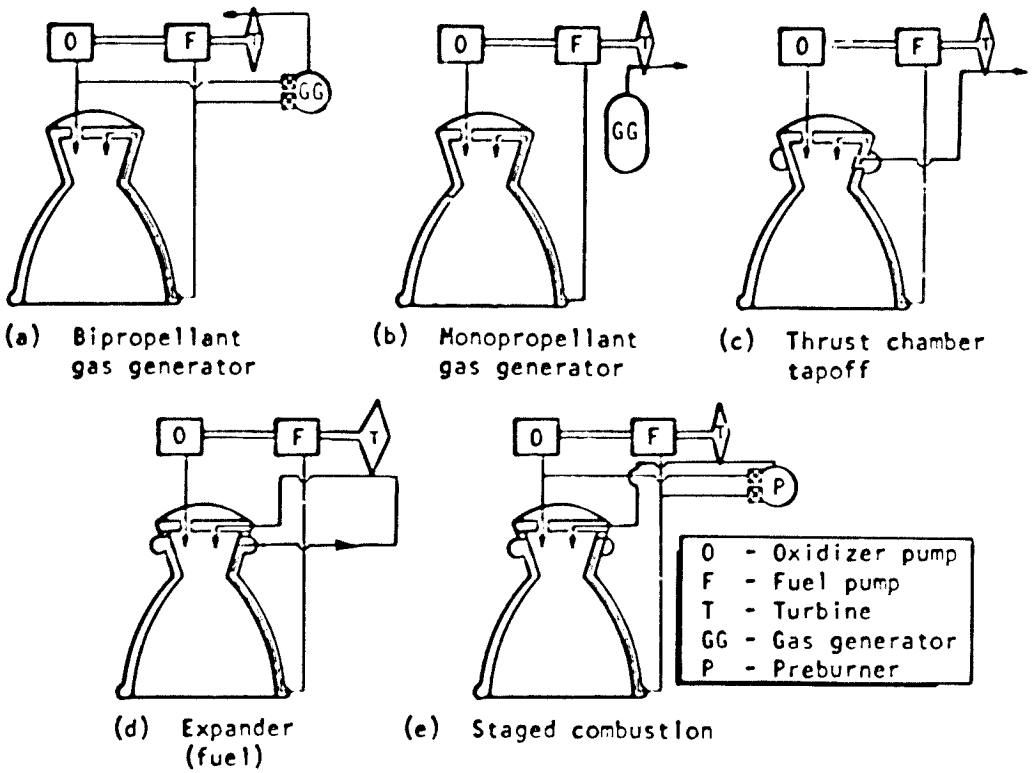

Figure 11. - Typical rocket engine cycles and turbine installations.

A new turbine design is evolved, as part of the overall turbopump design, from studies of candidate configurations and component schemes that best satisfy the requirements of the turbine gas path, the turbomachinery, and the rocket engine propellant-feed system. Development of a turbine design includes the following major phases:

(1) Preliminary design analysis
(2) Aerothermodynamic design of the turbine gas path

(3) Design of nozzle, stator, and blade profiles
(4) Mechanical design of the turbine assembly and selection of materials.

The design process always requires iterative aerothermodynamic, stress, and mechanical-design adjustments before the turbine design is completed and considered ready for fabrication and performance evaluation.

Final design drawings for turbine subassembly and assembly include, in addition to detail dimensions for fabrication, the functional design dimensions that define blading profiles, gas-path flow angles, critical flow areas, and diameters required after components are machined, heat treated, welded, and assembled.

In successful turbine development programs, rigid engineering control of all design, processing, and fabrication changes is established at one change-control point within the engineering program or development staff. Engineering, manufacturing supplier, and vendor changes made to turbine hardware can be initiated only by using change-control procedures. Equally important, close adherence to the dimensions and specifications set forth on the final design drawings must be required from all suppliers. Only in this manner can the objectives of the design, analysis, and development phases be achieved in the working hardware.

2.1 PRELIMINARY DESIGN ANALYSIS

A principal requirement in the design of a turbine for a rocket engine system is the efficient utilization of high-energy working fluid in the smallest obtainable flightweight configuration. Past designs for rocket engine turbines have been developed for comparatively short service lives when compared with other turbine applications. To date, total operational times of up to 6000 seconds have been reliably demonstrated by turbine assemblies; current design specifications, however, require 10-hour service lives. Rocket engine turbines normally undergo rapid starts, which impose severe thermal shock conditions on turbine components. Additionally, these turbines operate with extremely high stage loadings and stresses during their comparatively short run durations.

The preliminary design analysis investigates performance tradeoffs among candidate turbine designs required for an engine application. Turbine inlet temperature and pressure, inlet-to-exhaust pressure ratio, mass flowrate, shaft speed, staging needs, and any pertinent parameters affecting turbine performance and size are investigated with parametric analyses (ref. 3). Estimates of component and blading stresses are also established from preliminary layouts to ensure that the aerothermodynamic design can be developed into a workable mechanical configuration. The final design selection is influenced by tradeoff factors of turbine life, weight, complexity, and cost established by the type of service or mission for

which the rocket engine is being designed. Normally, these factors are evaluated in conjunction with the overall engine design. Computers have proven to be valuable analytical tools for this type of study. Automatic plotting equipment, which develops design curves from computer program output data, has been used effectively.

2.1.1 Pressure Ratio, Mass Flowrate, and Engine Performance

Rocket turbine performance is linked directly to the design values of turbine pressure ratio and mass flowrate. A gas-generator-cycle turbine (fig. 11(a)) attains the best turbine performance with a minimum design mass flowrate; this condition results in the best possible engine performance in terms of specific impulse. Figure 12 presents a typical plot of tau factor τ (the ratio of mass flowrate of turbine working fluid [$\dot{w}_t$, lbm/sec] to primary

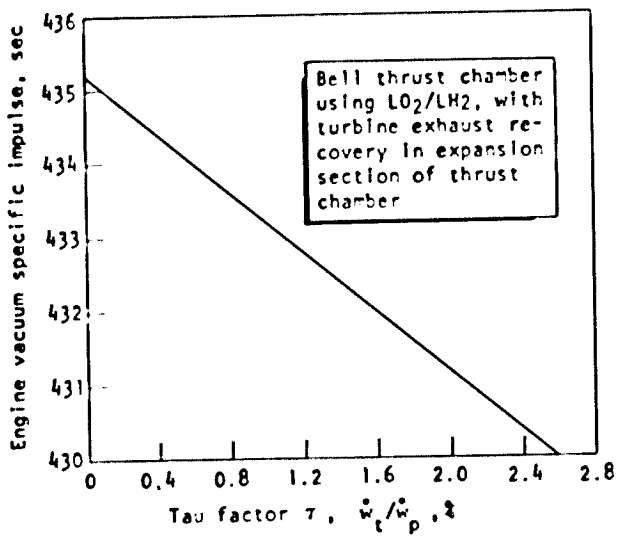

Figure 12. – Typical effect of tau factor on engine specific impulse.

mass flowrate of thrust chamber propellant [$\dot{w}_p$, lbm/sec]) versus engine specific impulse. Note that as tau factor decreases, a corresponding gain in engine specific impulse is realized. A topping-cycle (staged-combustion) turbine design (fig. 11 (e)), however, is more concerned with minimizing turbine pressure ratio in order to obtain the highest turbine efficiency. In this cycle, turbine exhaust is subsequently injected into the thrust chamber at

a fixed design chamber pressure; therefore, a reduction in turbine pressure ratio translates into lower required turbine inlet pressure, reduced propellant pump discharge pressure, and lower turbine horsepower required to drive the turbopump.

2.1.2 Working-Fluid Properties

To develop the gas-path energy and velocity distribution, flow area, and turbine power relationships required for a good design, the turbine designer depends on the use of accurate data on working-fluid gas properties. Working-fluid data for frozen-equilibrium state conditions are used for turbine design analyses because these data best represent the gas properties delivered by the gas generator (or other working-fluid source) to the turbine inlet. A tabulation of turbine working-fluid properties for propellant combinations used in operational and development engines appears in table III (these gas properties are included as reference data only and are not intended for use in a formal turbine design). Analyses performed with inaccurate values for specific heat C_p, ratio of specific heats γ, and specific gas constant R will contain errors in turbine energy distribution and efficiency and in gas-path area relationships. Therefore, the responsibility for establishing turbine working-fluid gas properties and for seeing that these data agree with properties used in the engine-system analysis is established before a new design is initiated.

2.1.3 Isentropic Velocity Ratio

The design isentropic velocity ratio determines the range of efficiency in which a proposed new turbine design operates. The velocity ratio for a single stage configuration is $\frac{U}{C_o}\left(\frac{\text{pitchline velocity}}{\text{theoretical spouting velocity}}\right)$; however, for a multistage turbine design, the numerator of the velocity-ratio term represents the square root of the sum of the squares of the pitchline velocities of each stage. Therefore, the precise expression for velocity ratio for either a single stage or multistage turbine is $\sqrt{\Sigma U^2}/C_o$. However, in this monograph, the velocity ratio will be consistently expressed as U/C_o, it being understood that for a multistage turbine $U = \sqrt{\Sigma U^2}$.

The plot of velocity ratio versus turbine efficiency presented in figure 13 illustrates the variation in peak efficiency for 1-, 2-, and 3-row impulse staging and for reaction staging. This general type of curve serves to establish and compare initial estimates of efficiency for new designs.

A plot of efficiency versus isentropic velocity ratio for experimental, development, and in-service rocket turbines appears in figure 14. Design velocity ratios for two-row configurations used in gas-generator and tapoff engine cycles range from 0.10 to 0.40, and

Table III. – Turbine Working-Fluid Gas Properties

Working fluid*	Chamber pressure of working-fluid source, psi	Turbine inlet temperature (T_{oi}), $^{\circ}R$	Ratio of specific heats (γ)	Specific heat at constant pressure (C_p)	Specific gas constant (R), (ft-lbf)/(lbm-$^{\circ}R$)
LOX/RP-1	1000	1100	1.097	0.635	44
		1300	1.115	0.648	52
		1500	1.132	0.656	59
		1600	1.140	0.660	63
		1700	1.148	0.662	67
LOX/LH_2	1500	1000	1.374	1.998	423
		1200	1.364	1.910	396
		1500	1.348	1.802	362
		1700	1.337	1.738	341
		1900	1.326	1.687	323
LF_2/LH_2	750	900	1.395	2.765	626
		1100	1.388	2.608	574
		1300	1.380	2.509	529
		1500	1.373	2.318	491
		1700	1.366	2.192	457
$FLOX/CH_4$	750	1300	1.176	0.857	100
		1500	1.189	0.855	106
		1700	1.215	0.834	113
		1900	1.233	0.810	116
		2100	1.242	0.791	117
Hydrogen	–	700	1.396	3.481	766
		800	1.394	3.490	766
		900	1.392	3.501	766
		1000	1.390	3.516	766
		1100	1.388	3.531	766
$\frac{N_2O_4}{50\text{-}50}$**	1500	1700	1.248	0.726	112
		1750	1.249	0.719	111
		1800	1.254	0.708	111
		1850	1.260	0.694	111

*Products of combustion of propellant combinations listed
**Hydrazine/UDMH

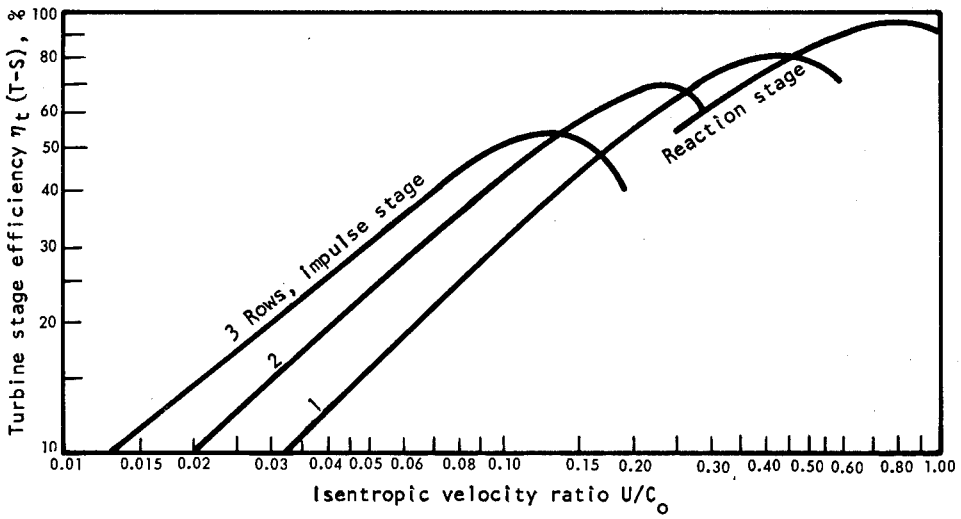

Figure 13. — Typical curves for velocity ratio vs efficiency for impulse and reaction staging.

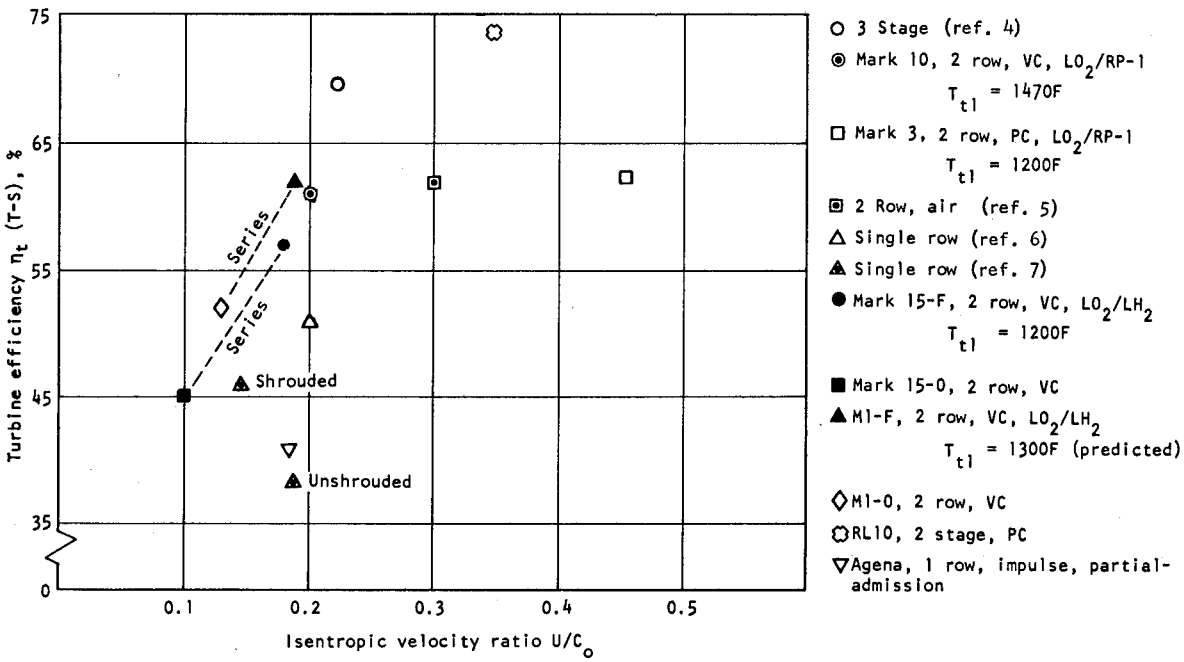

Figure 14. — Efficiency data from operations and test for some representative turbine designs.

corresponding efficiencies vary from 35 to 65 percent. Staged-combustion and expander-cycle turbines are capable of attaining efficiencies above 80 percent because the lower turbine system pressure ratios generally permit operation in a more efficient range of velocity ratio. Pitchline velocities of current turbine designs vary from 1000 to 1500 ft/sec; associated inlet temperatures for LO_2/RP-1 and for LO_2/LH_2 turbines range from 1000° to 1500° F. Rocket engine turbines have been operated successfully without cooling at inlet temperatures of 1700° F.

2.1.4 Staging

The number of stages designated in a new turbine design depends on (1) the quantity of working-fluid energy available to the turbine and (2) the tradeoff between gain in turbine efficiency and the extra turbine stages and added weight required for the performance increase. During staging studies, pressure ratio(s) and available energy allocation are varied in candidate configurations to determine which design develops the highest efficiency with the smallest pitch diameter and least number of stages.

Production turbine designs have been limited to single- and two-row axial-flow configurations principally because of size and weight restrictions on flight-type turbomachinery. A third rotor has been utilized in some proposed turbine designs that employ high-energy working fluids (e.g., LF_2/LH_2); this practice ensures that the energy available to the turbine is used more efficiently. Designs with three or more rotors have the disadvantage of requiring either an outboard-bearing installation or an independently supported turbine shaft. Five- and six-stage designs have been successfully developed and have demonstrated predicted performance in experimental nuclear-rocket turbine configurations (Mark 25, table I).

Impulse-type staging usually is specified in new designs with velocity ratios below 0.35. These designs normally operate with high-energy working fluids and at pressure ratios that raise the theoretical stage spouting velocities into the supersonic region.

Reaction staging normally is utilized in low-pressure-ratio (<2) turbines that operate with isentropic velocity ratios above 0.45.

2.2 TURBINE AEROTHERMODYNAMIC POINT DESIGN

2.2.1 Gas-Path Energy Balance, Velocity and Pressure Distribution, and Power

The results of preliminary design studies are used in the aerothermodynamic analysis to establish the final turbine design. Station-to-station state conditions and performance data are calculated together with required flow areas for all points in the gas path. Practices used throughout industry for the aerothermodynamic-analysis phase of turbine design deal with energy distribution, staging, gas-path geometry, and performance. Current practices are exemplified by Stewart's design approach (ref. 8), which is in terms of work and speed requirements, and by the method of Ainley and Mathieson (refs. 9 and 10), which uses blade flow and pressure loss to generate the design. A widely used design procedure that develops equivalent results was evolved by H. D. Emmert (ref. 11). The turbines for the J-2 and F-1 engines used in the Saturn vehicles as well as numerous successful research and development configurations were designed with the Emmert procedure. This procedure is presented in this monograph.

The relationships among temperature, pressure, and energy conventionally used to develop a turbine gas-path energy are shown in the entropy-enthalpy diagram in figure 15. To facilitate accounting for energy relationships in a nozzle (or stator) and rotor, subscripts 1 and 2 are assigned to the first two gas-path elements. A three-rotor assembly would therefore have energy quantities accounted for in six successive elements.

The total effective energy Δh_e available for developing turbine stage work is comprised of the effective gas-expansion and kinetic energies available in the stator and blade gas paths. These energies are established initially with the use of two-dimensional friction and loss coefficients developed from turbine design experience and experimental data and substantiated in rocket turbine development programs.

The effective expansion energy available in a nozzle or blade is equal to the working-fluid isentropic enthalpy drop Δh_s minus turbulence and wall-friction losses within the blade passage. The expression for isentropic enthalpy drop is

$$\Delta h_s = \frac{RT}{J}\left[\frac{\gamma}{\gamma-1}\right]\left[\frac{\left(\frac{p_{t1}}{p_{s2}}\right)^{\frac{\gamma-1}{\gamma}}-1}{\left(\frac{p_{t1}}{p_{s2}}\right)^{\frac{\gamma-1}{\gamma}}}\right] \tag{1a}$$

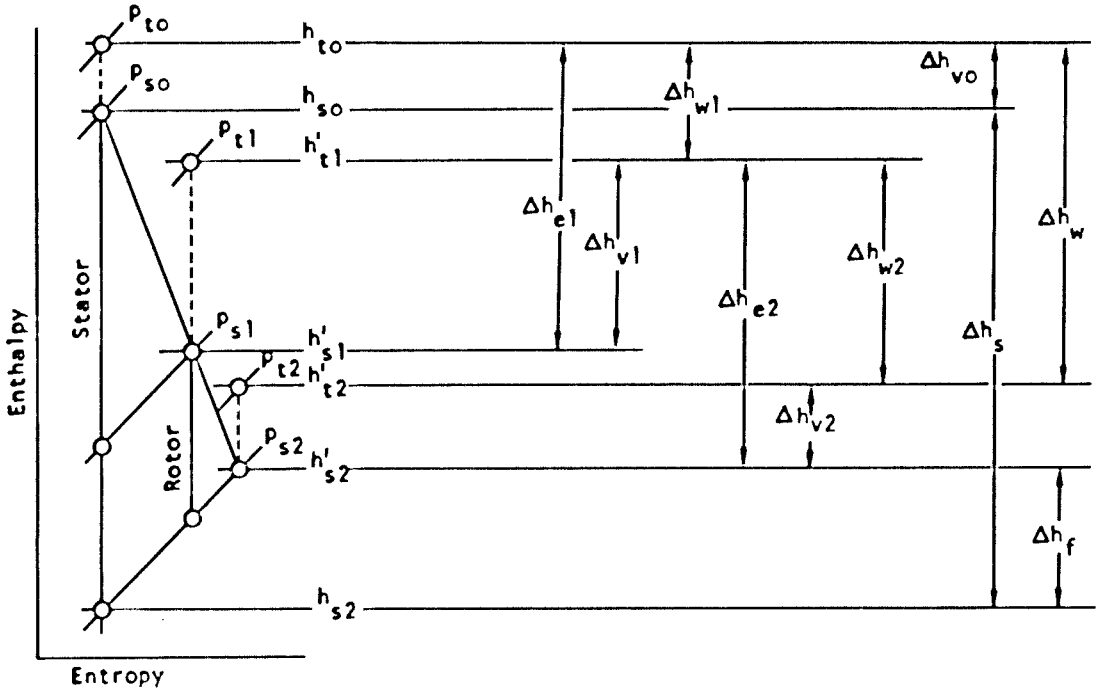

Δh_{vo}	=	Kinetic energy	Stator inlet
p_{to}	=	Total pressure	Stator inlet
h_{to}	=	Total enthalpy	Stator inlet
p_{so}	=	Static pressure	Stator inlet
h_{so}	=	Static enthalpy	Stator inlet
Δh_{e1}	=	Kinetic energy	Stator outlet
p_{t1}	=	Total pressure	Rotor inlet
h'_{t1}	=	Total enthalpy	Rotor inlet
p_{s1}	=	Static pressure	Rotor inlet (+stator outlet)
h'_{s1}	=	Static enthalpy	Rotor inlet (+stator outlet)
$\Delta h'_{v1}$	=	Kinetic energy	Rotor inlet
Δh_{e2}	=	Kinetic energy	Rotor outlet
p_{t2}	=	Total pressure	Exhaust
h'_{t2}	=	Total enthalpy	Exhaust
p_{s2}	=	Static pressure	Rotor outlet (+exhaust)
h_{s2}	=	Static enthalpy	Rotor outlet (+exhaust)
Δh_{v2}	=	Kinetic energy	Exhaust
h'_{s2}	=	Isentropic static enthalpy	Exhaust
Δh_{s}	=	Stage isentropic enthalpy drop	
Δh_{w}	=	Stage actual enthalpy drop (blading work)	
Δh_{f}	=	Stator and rotor blade losses	

Figure 15. – Entropy/enthalpy diagram relating gas-path energy, temperature, and pressure.

or

$$\Delta h_s = \frac{RT}{J}\left[\frac{\gamma}{\gamma - 1}\right]\left[1 - \left(\frac{p_{s2}}{p_{t1}}\right)^{\frac{\gamma - 1}{\gamma}}\right] \tag{1b}$$

where

Δh_s = isentropic enthalpy drop

R = specific gas constant

T = working-fluid temperature

J = energy conversion factor

γ = ratio of specific heats

p_{t1} = turbine total inlet pressure

p_{s2} = turbine exhaust static pressure

Expansion-energy loss coefficient φ^2, which corrects for expansion-energy losses, is obtained as a function of blade deflection angle φ and blade width b from a plot like that in figure 16; the data in figure 16 has been used in a number of successful turbine designs. The effective expansion energy Δh_{es} is therefore

$$\Delta h_{es} = (\Delta h_s)(\varphi^2) \tag{2}$$

where φ^2 is the expansion-energy loss coefficient empirically determined as $f(\theta, b)$.

The kinetic energy to a gas-path element is equivalent to the working-fluid inlet velocity. The kinetic energy of a velocity vector representing the working fluid entering a stator or rotor must be corrected for friction and incidence losses and for energy losses induced by the magnitude of the inlet relative Mach number. The kinetic-energy loss coefficient ψ^2, which corrects for friction losses, is evolved as a function of the expansion-energy loss coefficient:

$$\psi^2 = 2\varphi^2 - 1 \tag{3}$$

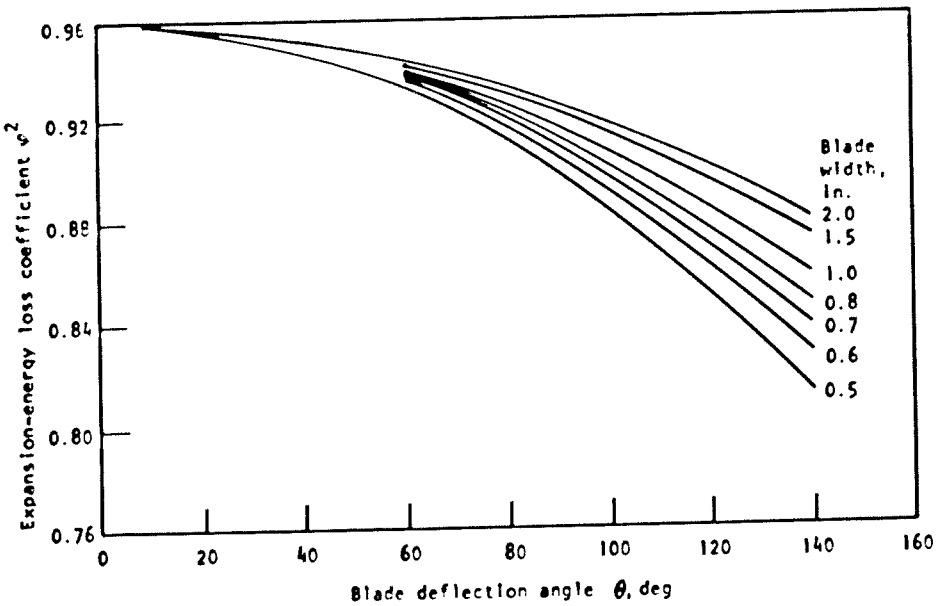

Figure 16. – Expansion-energy loss coefficient as a function of blade deflection angle and blade width.

Figure 17 shows blade incidence-angle coefficient C_i plotted as a function of incidence

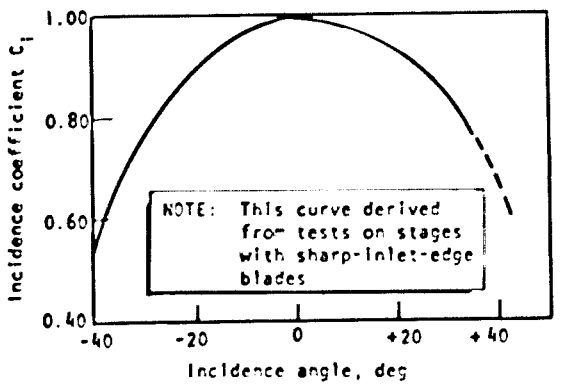

Figure 17. – Incidence angle vs incidence coefficient.

angle; figure 18 shows Mach number coefficient C_m plotted as a function of inlet relative Mach number. The effective (or corrected) kinetic energy Δh_{cv} at a stator or rotor inlet therefore is

$$\Delta h_{cv} = (\Delta h_v)(\psi^2)(C_i)(C_m) \tag{4}$$

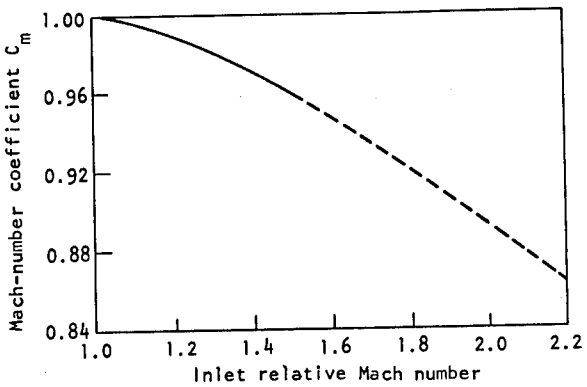

Figure 18. – Mach-number coefficient vs inlet relative Mach number.

where Δh_v is the kinetic-energy equivalent entering a stator or rotor.

The total effective energy Δh_e available to each stator and rotor as the flow progresses through the gas path is the sum of the effective expansion and kinetic energies:

$$\Delta h_e = \Delta h_{es} + \Delta h_{ev} \tag{5a}$$

$$= (\Delta h_s)(\varphi^2) + (\Delta h_v)(\psi^2)(C_i)(C_m) \tag{5b}$$

Note that the expansion-energy quantity varies with the stator or rotor pressure ratio [eq. (1)], whereas the kinetic-energy quantity is a function of fluid velocity entering the element from the upstream stator or blade [eq. (4)].

Expansion and kinetic energy considerations have been developed separately in the above discussion; however, during the actual fluid flow in the turbine, the mix of expansion energy and kinetic energy occurs simultaneously. The energy loss coefficients φ^2 and ψ^2 account for wall-friction, turbulence, and circulatory-flow losses; in addition, effects of reheat are experienced by the working fluid during the flow process.

The parameter that links fluid flow and energy transfer with changes in momentum and work quantities is fluid velocity. Pertinent absolute and relative velocity notations are illustrated in the turbine velocity diagram in figure 19.

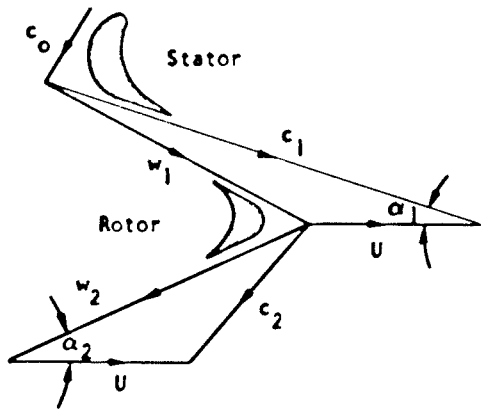

c_o = absolute fluid velocity, stator inlet

c_1 = absolute fluid velocity, stator outlet

U = blade velocity (= pitchline velocity)

w_1 = relative fluid velocity, rotor inlet

w_2 = relative fluid velocity, rotor outlet

c_2 = absolute fluid velocity, rotor outlet

α_1 = exit vector angle, vane

α_2 = exit vector angle, blade

Figure 19. – Turbine velocity diagram.

Respective effective energies leaving the stator and rotor are Δh_{c1} and Δh_{c2}:

$$\Delta h_{c1} = \frac{c_1^2}{2gJ} \tag{6}$$

$$\Delta h_{c2} = \frac{w_2^2}{2gJ} \tag{7}$$

where g is the acceleration due to gravity.

Diagram factors for calculating energy equivalents of blading work in the gas-path elements are developed from stator and rotor velocity-triangle outlet velocities and vector relationships. To calculate the overall blading work, the total change in tangential velocity is separated into two parts and referenced at the nozzle (or stator) and blade exits:

$$\text{Diagram factor (stator) } E_{d1} = \frac{U}{c_1}\left(2\cos\alpha_1 - \frac{U}{c_1}\right) \tag{8}$$

$$\text{Diagram factor (rotor) } E_{d2} = \frac{U}{w_2}\left(2\cos\alpha_2 - \frac{U}{w_2}\right) \tag{9}$$

Diagram work $\Delta h_{w\,d}$ for a single-row stage therefore is

$$\Delta h_{w\,d} = (\Delta h_{e\,1} \cdot E_{d\,1}) + (\Delta h_{e\,2} \cdot E_{d\,2}) \tag{10a}$$

$$= \left(\frac{c_1^{\,2}}{2gJ}\right)\left[\frac{U}{c_1}\left(2\cos\alpha_1 - \frac{U}{c_1}\right)\right] + \left(\frac{w_2^{\,2}}{2gJ}\right)\left[\frac{U}{w_2}\left(2\cos\alpha_2 - \frac{U}{w_2}\right)\right] \tag{10b}$$

Turbine diagram efficiency $\eta_{t\,d}$ is established as the ratio of turbine diagram work to isentropic available energy:

$$\eta_{t\,d} = \frac{\Delta h_{w\,d}}{\Delta h_s} \tag{11}$$

Turbine efficiencies generally are quoted on a total-to-static (T-S) basis, where available energy for calculating turbine efficiency is established from the relationship of total inlet pressure to static exit pressure; the energy equivalent of turbine exit velocity therefore is charged to the turbine. In an expander-type cycle, where turbine exhaust is subsequently utilized in the thrust chamber, efficiency is quoted on a total-to-total (T-T) pressure basis; the turbine is not charged with the kinetic energy of turbine exit velocity. The overall engine-system pressure schedule accounts for both turbine static and dynamic pressures and defines the station location in the turbine assembly at which inlet and exit pressures are taken.

Detailed treatments of the analysis of turbine geometry and design performance are presented in references 12 through 15.

2.2.2 Partial-Admission Turbine

The partial-admission turbine is used in applications that, because of limitations imposed by design horsepower, mass flowrate, and required flow area, would require excessively small blade heights for full-admission (360°) nozzle configurations. Pitch diameters cannot be reduced to accommodate larger blading in these designs because of velocity-ratio considerations. Blading heights, however, can be increased to practical design limits under the circumstances by adjusting the nozzle arc of admission. To accomplish this, performance tradeoffs between full-admission small-blade and partial-admission blade designs are conducted before the nozzle arc of admission is selected.

The following kinds of losses are accounted for in the analysis of a partial-admission gas path:

(1) Windage loss when the blading passes through the inactive portion of the nozzle arc
(2) Expansion loss contributed by loss of working-fluid momentum at the boundary between the active and inactive portions of the nozzle arc
(3) Loss due to working fluid that enters the rotor blades and mixes with inactive gases in blade paths
(4) Losses attributed to blading clearances (sec. 2.3.8). In reentry configurations, axial clearance between nozzle exit and rotor entry and the effect of disk deflection on this clearance are of extreme importance to the maintenance of pressure distribution and control of leakage losses between stages.

Loss analyses that accurately separate and predict partial-admission losses have not been developed. However, loss relationships that have been evolved empirically and substantiated by experimental tests enable designers to predict performance of a partial-admission turbine. For example, a partial-admission loss analysis developed in reference 16 has been verified by other investigators as noted in reference 17.

Figure 20 presents typical efficiency data for a partial-admission turbine (3.75-in. pitch diam.) plotted against velocity ratio for various arcs of admission. These data were developed experimentally at the NASA-Lewis Research Center and are reviewed in reference 18. The curves in figure 20 clearly indicate that the turbine efficiency falls off if the velocity ratio is reduced or if the turbine arc of admission is reduced.

In a partial-admission turbine the efficiency reduction $\eta_{l\,W}$ due to rotor pumping and windage is given by the expression

$$\eta_{l\,W} = 5.6\times10^{-5}\left(\frac{U}{C_o}\right)^2 \rho N\left(\frac{1-F}{F}\right) \qquad (12)$$

where

ρ = density of working fluid

F = active fraction of nozzle admission

Stenning (ref. 10) developed an efficiency correction $\eta_{l\,SM}$ that combined scavenging and momentum-loss factors:

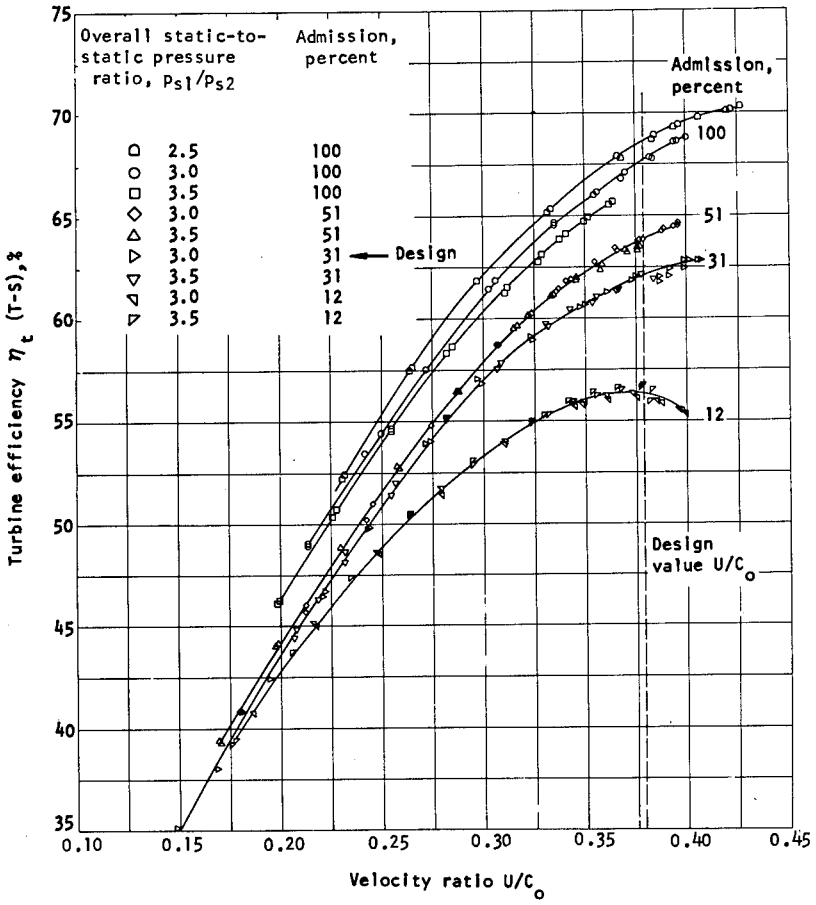

Figure 20. — Efficiency vs velocity ratio for a partial-admission turbine with various arcs of admission (adapted from ref. 18).

$$\eta_{TSM} = \left[\frac{1 + K\left(1 - \frac{p}{3f}\right)}{1 + K}\right] \eta_{FA} \tag{13}$$

where

K = $\dfrac{\text{velocity leaving the wheel}}{\text{velocity entering wheel}}$

p = blade pitch

f = nozzle arc length

η_{FA} = turbine efficiency with full admission

The expression that establishes performance $\eta_{P\,A}$ for a partial-admission turbine includes the combined windage, scavenging, and momentum-loss corrections to full-admission efficiency:

$$\eta_{P\,A} = \left[\frac{1 + K\left(1 - \frac{p}{3f}\right)}{1 + K}\right]\eta_{I\,A} - 5.6\times10^{-5}\left(\frac{U}{C_o}\right)^2 \rho N\left(\frac{1 - F}{F}\right) \qquad (14)$$

Losses in high-energy-propellant, high-pressure-ratio partial-admission designs are not as critical as those that occur in low-pressure-ratio subsonic turbines. High-energy and high-momentum working fluids can cope with windage, expansion, and mixing losses and sustain a smaller percentage loss of overall available energy in overcoming these partial-admission gas-path conditions.

2.2.3 Stage Reaction

A reaction-stage design differs from an impulse-stage design in that a portion of the reaction-blade motive force is developed from kinetic energy contributed by the pressure drop sustained across the rotor. The total available kinetic energy results from the combined pressure drops in the nozzle and the rotor. The percentage of stage reaction R_s therefore can be expressed as

$$R_s = \frac{\Delta h_r}{\Delta h_s} \times 100 \qquad (15)$$

where

Δh_r = enthalpy drop in the rotor

Δh_s = enthalpy drop across the stage

Reaction blading normally is designed with the amount of reaction varying from 25 to 50 percent. The percent reaction that is required varies with working-fluid energy and its influence upon blading entrance and exit vectors. Reaction-type blades are used in staging that operates in the velocity-ratio range above 0.40 and in the subsonic pressure-ratio regime. The maintenance of gas-path pressure gradients is more critical in reaction staging than in impulse staging because of the close dependence of gas-path state conditions on pressure distribution.

Impulse blading for two-row, velocity-compounded turbines is not designed as pure impulse configuration; in practice, a total of 10-percent stage reaction is provided across the second stator and rotor to prevent adverse pressure gradients and negative reaction at the blade roots.

2.2.4 Intake Manifold Sizing

When turbine pressure distribution is analyzed, the flow through the inlet manifold is treated as a throttling process, the working fluid undergoing no enthalpy loss; however, a pressure loss is sustained. Manifold configurations containing a single radial inlet have been successfully designed with a 2- to 5-percent drop in the overall pressure available to the turbine; in current gas-generator-cycle designs, a maximum pressure loss of 2 percent is sustained. Full (360°) axial-entry manifold designs containing centerbodies extending from the shaft centerline to the nozzle inner diameter normally have inlet pressures specified at the nozzle inlet plane, with the turbine sustaining no manifold loss; in this case, the engine pressure schedule accounts for pressure differentials between the gas generator (or preburner) and turbine nozzle inlet. Staged-combustion-cycle designs normally incorporate this kind of no-loss, axial-entry configuration.

Manifold areas are increased from 10 to 25 percent over those required to pass design mass flows as a precaution against excess manifold pressure drop whenever manifold flow areas are sized for entrance velocities between Mach 0.25 and Mach 0.30. Constant-diameter rather than constant-velocity manifold designs normally are designated in new designs because of ease of fabrication and lower cost. Manifolds designed with noncircular cross sections for the purpose of accommodating turbomachinery mechanical-design and installation requirements have not exhibited any fluid-flow disadvantages; this type of noncircular configuration is exemplified by the manifold configuration for the J-2 oxidizer turbine appearing in figure 6.

2.3 NOZZLE, VANE, AND BLADE GEOMETRY

Turbine blading design deals with the development of nozzle, vane, and blade profiles that will develop the required gas-path vector-diagram relationships and pass the working-fluid mass flow at design operating conditions. Blading inlet and exit angles, turning angles, fluid velocities, flow areas, chord and blade width data, pitch diameters and blade heights, and trailing-edge data are used to evolve design blade profiles.

Representative configurations of state-of-the-art stator vanes and rotor blades used in production rocket engine turbines appear in figure 21. Note the various blade shapes, sealing

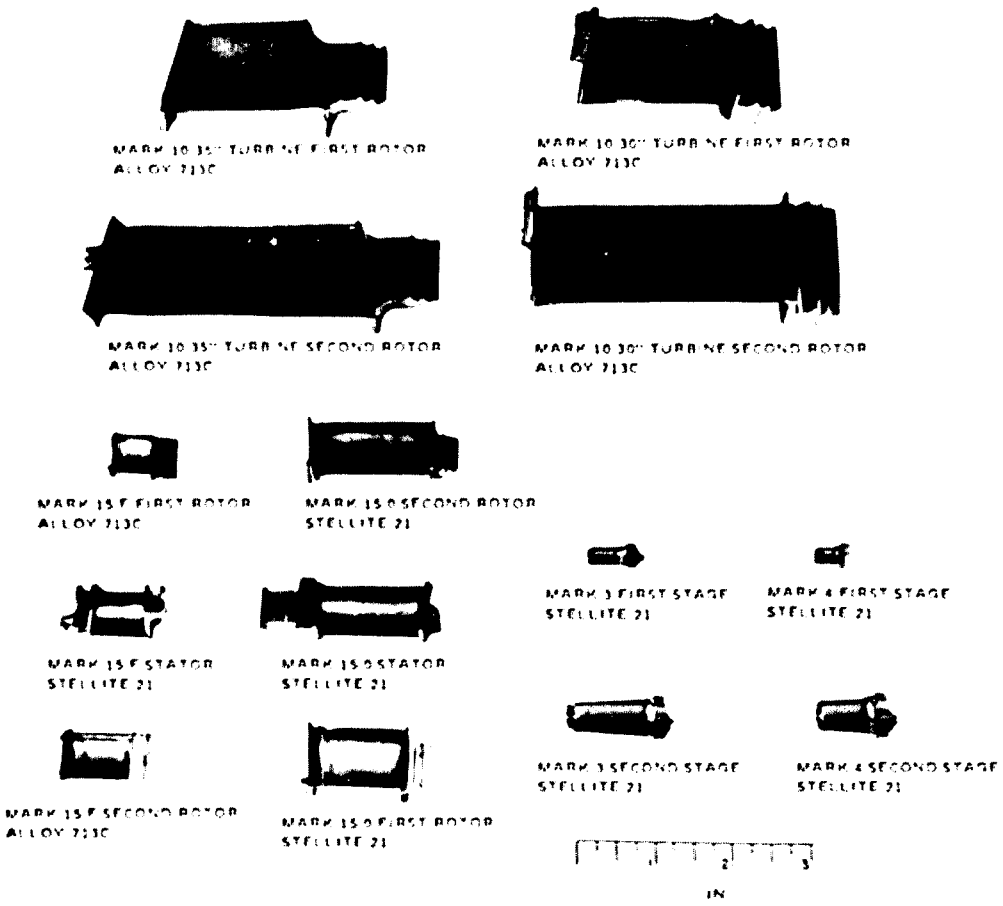

Figure 21. – Vane and blade designs for representative production turbines.

provisions, blade attachment methods, and shrouding. Each blade was designed to meet a specific set of operating requirements in its respective turbine gas path. The pictured blading profiles were developed with straight-line sections combined with circular arcs or parabolic arcs or both to form the flow-path suction and pressure surfaces and the leading and trailing edges. Blading sizing data for three representative production and development rocket turbines appear in table IV.

During the profile design phase, blades are drawn approximately 10 times actual size or on any other convenient scale that provides an accurate definition of profile and gas-path relationships. The geometric relationships among principal blading design parameters are illustrated in figure 22.

Table IV. – Nozzle, Stator-Vane, and Rotor-Blade Data for Representative Turbines

Turbine	Type	D_m	Nozzle N			1st Rotor 1-R			Stator S			2nd Rotor 2-R		
			Z	H	b	Z	H entrance/exit	b	Z	H entrance/exit	b	Z	H entrance/exit	b
Mark 10	2R-VC	34.90	61	1.55	3.00	119	1.862/2.484	1.50	130	2.604/3.372	1.50	109	3.683/4.223	1.50
Mark 15-F	2R-VC	12.50	43	0.42	0.700	97	0.53	0.596	115	0.640/0.770	0.596	93	0.88	0.585
M-1-F	2R-VC	23.00	37	1.492	2.175	80	1.741	1.350	67	1.931/2.309	1.360	78	2.683	1.500

Notes: D_m = pitch diameter, in.
Z = number of blades or vanes
H = height, in.
b = axial width, in.

2.3.1 Leading and Trailing Edges

Leading-edge design is more critical in blading with supersonic inlet velocity than in blading with subsonic entrance conditions, because of the danger of shocks developing from convergence of compression waves at the blade entrance. Supersonic blades are designed with thin leading edges to avoid the development of entrance shocks, whereas subsonic designs can incorporate larger leading-edge radii because these blades are less sensitive to the effect of small variations in the angle between the inlet vector and blade leading edge. Elliptical leading edges are preferred to circular configurations whenever the geometry of blading pressure and suction surfaces permits their use.

The trailing-edge geometry helps form the flow-controlling throat section and is prone to develop excessive exit losses if improperly sized. Minimum exit losses are sustained in trailing edges designed with the smallest radii allowed by stress limitations. The trailing-edge coefficient C_e for vanes and blades is defined as

$$C_e = \frac{\text{throat opening}}{\text{throat opening} + 2\,(\text{trailing-edge radius})} \tag{16}$$

Values for C_e less than 0.90 are avoided in new blading because of the excessive wake losses that can otherwise develop. Details of trailing-edge design and its influence on stage performance are presented in reference 19.

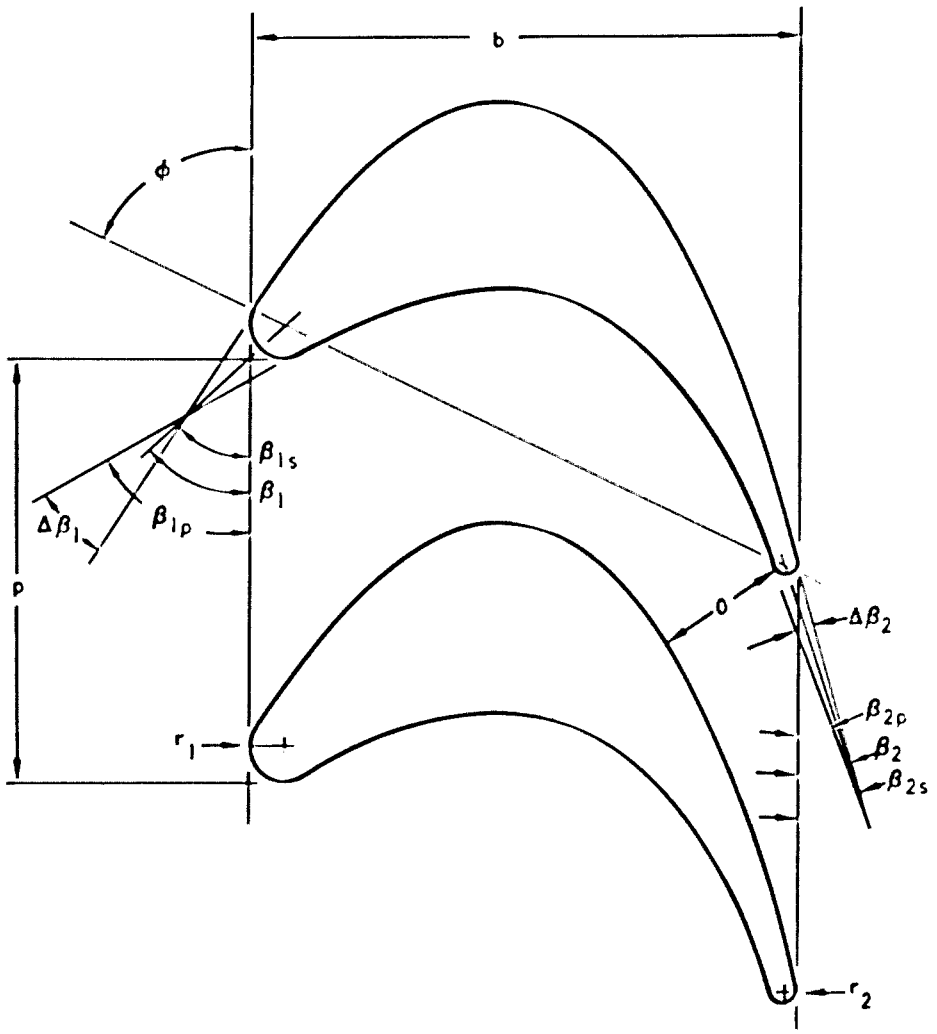

p	Pitch	β_2	Blade discharge angle
b	Axial width	$\Delta\beta_2$	Trailing-edge divergence
o	Throat opening	p/b	Pitch-width ratio
r_1	Leading-edge radius	o/p	Opening coefficient
r_2	Trailing-edge radius	α_2	Exit vector angle = arcsin (o/p)
ϕ	Chord angle	Θ	Blade deflection angle = $180° - (\beta_1 + \alpha_2)$
β_{1p}	Inlet angle (pressure surface)	t_1	Leading-edge thickness = $2r_1$
β_{1s}	Inlet angle (suction surface)	t_2	Trailing-edge thickness = $2r_2$
β_1	Blade inlet angle	C_e	Edge coefficient = $o/(o + t_2)$
$\Delta\beta_1$	Leading-edge divergence		
β_{2p}	Discharge angle (pressure surface)		
β_{2s}	Discharge angle (suction surface)		

Figure 22. – Nozzle, vane, and blade design parameters.

2.3.2 Pressure and Suction Surfaces

The designs for blading pressure and suction surfaces are evolved with practices that were originally developed for steam and air-breathing turbines and subsequently adapted for rocket engine turbines. Initially, the flow channel is developed as the pressure and suction surfaces are defined as described below. These new blade profiles are analyzed with methods for predicting and checking the velocity of the fluid on the blade pressure and suction surfaces. The primary objective is to avoid excessive local accelerations, which normally result from high rates of turning in the blade path. Unnecessary local acceleration of the working fluid is avoided because of the diffusion losses that occur when the fluid subsequently decelerates. If the analysis of blade-path velocity distribution (sec. 2.3.7) shows any overspeed condition, corrective adjustments to the blade profile are made.

Circular arc blading is used principally in parallel-sided impulse blade designs containing no provisions for radial equilibrium. The construction details of the pressure and suction surfaces in this type of blade are illustrated in figure 23. The required gas-path exit vector angle α_2 (noted as 21° in the illustration) fixes the blade trailing-edge geometric angle (β_2, fig. 22) and is formed by the straight-backed exit plane of the suction surface. The straight-back, impulse-type blade normally is designed for supersonic applications, and no correction is applied for efflux-angle deviation (sec. 2.3.3). The gas-path inlet vector angle is used to define the blade inlet angle β_1 (fig. 22). For symmetrical blades, the chord angle is set at 90°; for nonsymmetrical blading, the chord angle initially is fixed between 30° and 70° and subsequently is adjusted, together with pitch and throat opening, to obtain the required total flow area and height relationships as the blade or nozzle design is developed during successive blade layouts. The pressure and suction surfaces are constructed with circular arcs of appropriate radii. These arcs are drawn, as illustrated, tangent to the blade trailing and leading edges. The resultant blade path is developed by drawing the adjacent blade suction surface at a distance equivalent to blade pitch p from the initially evolved blade design. The flow path formed by these suction and pressure profiles should contain no discontinuities or abrupt curve sections that can develop loss-producing local accelerations. The resultant gas path should converge at a constant rate as flow progresses from the blade entrance to exit plane.

A parabolic blade design layout, normally used for subsonic applications, is initiated with the same approach used for the circular-arc configuration. Construction details of a parabolic (pressure) profile are illustrated in figure 24; parameters involved in the development of this profile are those identified in figure 22. The gas-path inlet vector angle is used as the blade inlet angle β_1. The blade exit angle β_2 is established by applying adjustments for exit-vector angle deviation (sec. 2.3.3) and unguided turning (sec. 2.3.4) to the gas-path exit vector angle α_2. These exit-angle adjustments normally are applied at the suction surface between the exit plane and blade throat opening.

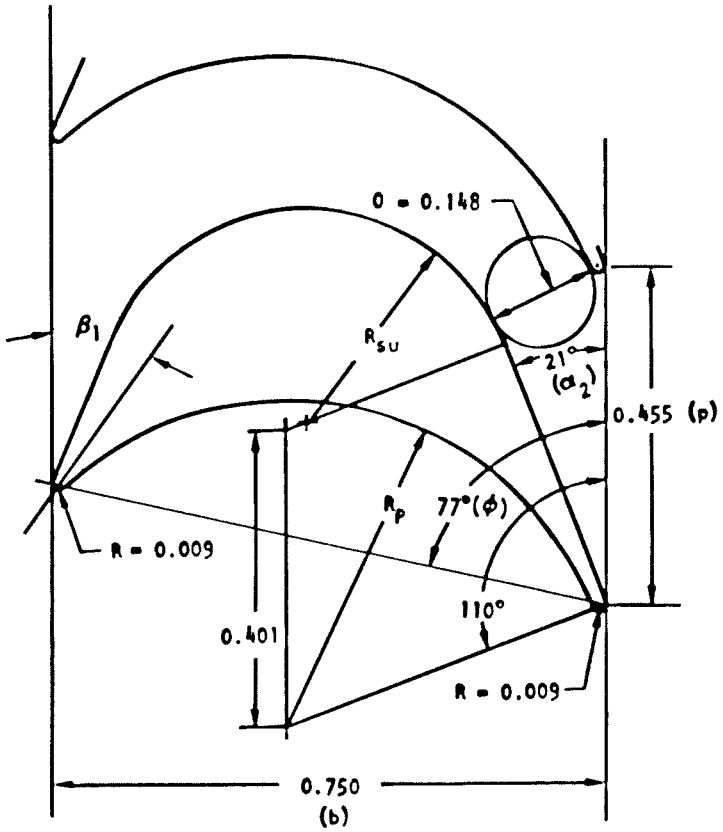

Figure 23. – Details of a circular-arc blade design.

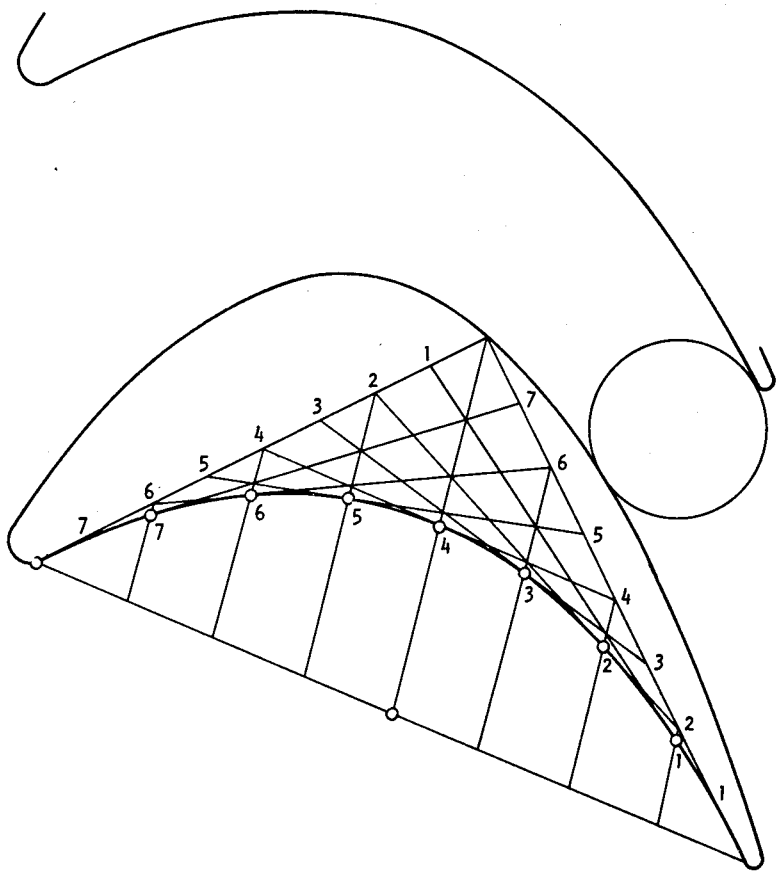

Figure 24. — Development of a parabolic suction-surface profile.

Blades have also been designed with combinations of circular and parabolic arcs. These blades are developed with parabolic arcs adjacent to the entrance and exit sections of the suction profile. The profile center section is constructed with a circular arc that blends with the parabolic sections at the entrance and exit portions of the design. The pressure surface in this combination-type profile normally is established with a circular arc.

If changes are necessary after a blade profile is established, the designer may, instead of redrawing the basic layout, modify it by use of plastic curves that simulate either parabolic or circular arc sections.

Background information on techniques for blade design is presented in references 20 and 21, and data on designing supersonic blading for turbomachinery appear in references 22, 23, and 24.

2.3.3 Deviation of Exit Vector Angle

Working fluid leaving a nozzle or blade, at exit Mach numbers less than one, experiences a flow deviation that in effect reduces turning in the exit vector. Therefore, additional turning is designed into the vane or blade design to correct for the turning loss caused by the flow deviation. This flow deviation (exit-vector-angle deviation) is equal to the difference between the gas-flow exit angle α_2 and the blade exit angle β_2. A plot illustrating deviation of the exit vector angle as a function of exit Mach number and exit vector angle appears in figure 25. These data are used to correct for exit-vector-angle deviation.

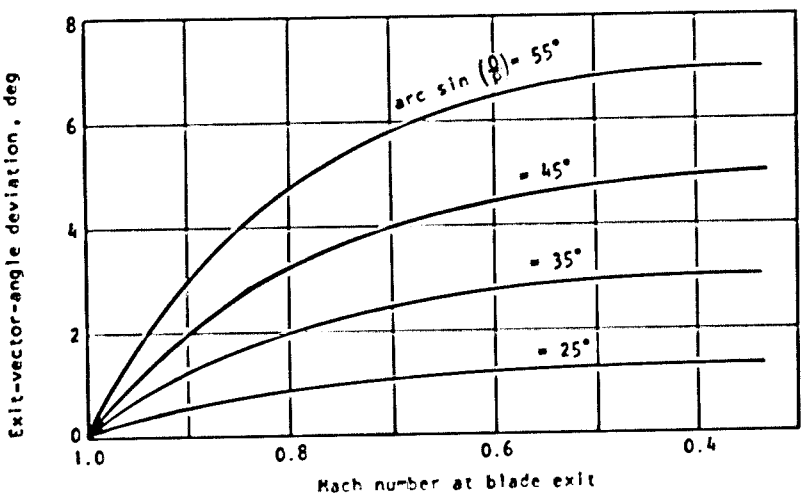

Figure 25. – Exit-vector-angle deviation as a function of Mach number and exit vector angle.

2.3.4 Unguided Turning

Unguided turning refers to the continuation of working-fluid turning that is provided along the blade suction surface after the fluid passes the throat section. In effect, the turning

continues in the absence of an adjacent pressure surface in this portion of the blade path. Unguided turning is incorporated in blade designs to distribute the total turning over a longer path to help avoid local accelerations along the profile surfaces. From 8° to 12° of unguided turning normally is provided at the blade root, and up to 15° at the tip.

Unguided turning normally is provided in subsonic, reaction-type blading. Supersonic blades, however, are designed with straight-backed suction surfaces that contain no unguided turning downstream of the throat. The use of unguided turning in blade profile design and development is discussed in reference 9.

2.3.5 Pitch

The pitch parameter p defines the circumferential spacing between adjacent gas-path elements and helps establish the number of vanes and blades contained in a nozzle or rotor assembly. A rotor with too many blades incurs excessive losses from friction, whereas with too few blades the required total turning in the blade path is reduced because effective flow control is lost in the excessively wide channels between blades. Prominent among the various established design practices used to evolve pitch/chord design relationships for reaction-type blading are (1) the procedure that utilizes profile drag and blading exit-angle relationships described in references 9 and 25 and (2) the technique dealing with blade lift and Zweifel loading coefficients as reported in reference 26.

The design practice described herein deals with blade lift and Zweifel loading coefficients. The results obtained with this design procedure have been found to be in good agreement with pitch and blade solidities established by other investigators and used for various turbine applications. Reference pitch/chord design relationships as a function of exit flow angles are presented in figure 26 (adapted from ref. 27). The Zweifel loading coefficient ψ is used principally to establish pitch/chord parameters as a function of inlet and exit vector angles for gas-path elements in subsonic, reaction-type blading. These blades can be designed with unguided turning downstream of the throat. The loading coefficient is established by the following relationship:

$$\psi = \frac{p}{b} \sin(2\alpha_2) \left[\frac{\tan \alpha_2}{\tan \alpha_1} + 1 \right] \tag{17}$$

The loading coefficient (Zweifel number) values used for reaction-blade designs range from 0.70 to 1.15. The resultant pitch and chord parameters are used to develop blade-profile geometric relationships discussed previously.

Opening coefficient. – The ratio of throat (minimum blade passage) opening to blade pitch for straight-back, impulse-blade designs is established with opening coefficient O/p data

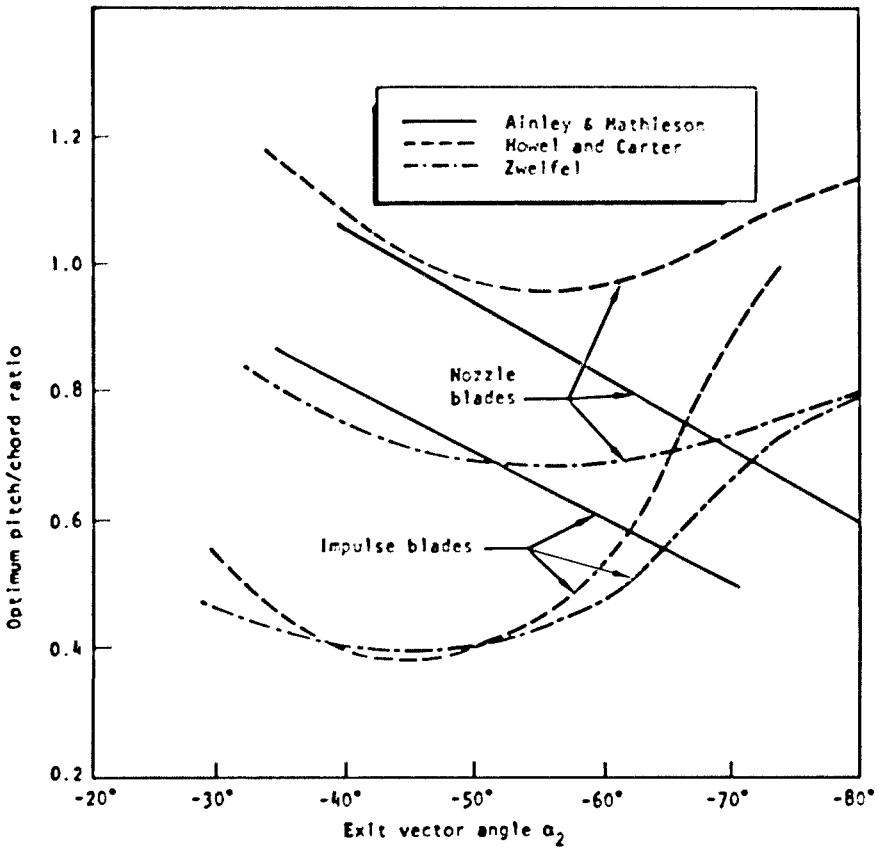

Figure 26. – Pitch/chord ratio data as a function of exit vector angle (adapted from ref. 27).

presented in figure 27. The blade opening coefficient is initially selected from this plot as a function of the sine of the exit vector angle α_2 :

$$\sin \alpha_2 = \frac{O}{p} \tag{18}$$

During the design process, the O/p value may be adjusted slightly, as the blade profiles are developed, to satisfy stress and flow-continuity requirements. Appropriate adjustments are always made to the gas-path design analysis if any nozzle or blade exit angles are changed during the blade layout process.

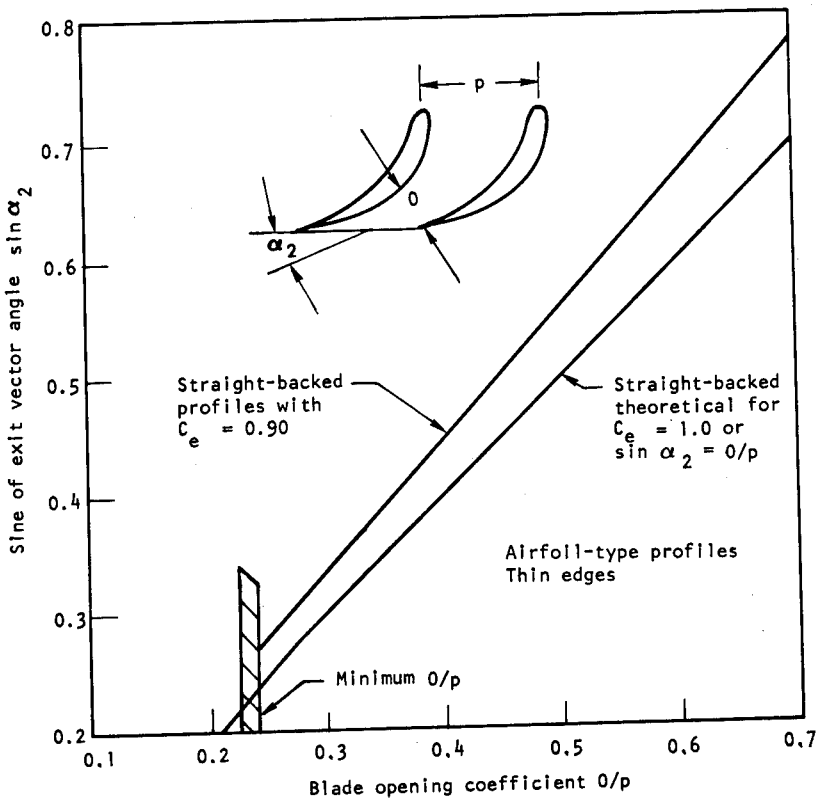

Figure 27. — Exit vector angle vs blade opening coefficient.

2.3.6 Radial-Equilibrium (Free-Vortex) Blading

Blading losses resulting from root-to-tip velocity (and flow) variations in parallel-sided blades with constant entrance and exit angles are minimized when the blading is designed for radial-equilibrium conditions. Parallel-sided blades normally are developed with state conditions and vector quantities that exist at the pitch line. In reality the blading experiences velocity changes that affect the vector diagram at all radii away from the pitch diameter. Past experience with both supersonic and subsonic turbines indicates that this variation is not significant in typically short, untwisted blading; no blading redesigns have been required to correct for effects of blade radial velocities and static-pressure gradients.

However, all state-of-the-art high-performance blades that are longer than one inch in height are designed to comply with requirements for radial equilibrium, viz., the product of blade radius R and the respective tangential velocity c_{u1} is constant at all radii along the blade length:

$$Rc_{u1} = \text{constant} \tag{19}$$

This condition is based on the assumption that stagnation temperature and pressure are constant at all radii and that equal quantities of working-fluid energy are available along the length of the blade to develop a uniform work output. Flow conditions are in radial equilibrium along the entrance and discharge of each blade. The free-vortex blade profile that results is twisted from root to tip and provides for more turning at the blade root than at the tip, as illustrated in figure 28. Note that the pictured blade design is tapered; radial equilibrium can be applied to either tapered or straight blading.

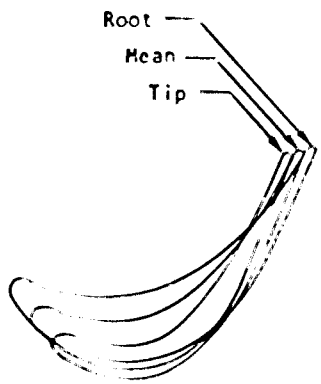

Figure 28. – Blade designed for radial equilibrium.

2.3.7 Blade-Path Velocity Distribution

After the blade designs are completed, the velocity distributions along the pressure and suction surfaces are predicted analytically, and adjustments are made to any blading profile that exhibits excessive velocity and pressure gradients. Techniques for predicting the blade-to-blade and blade root-to-tip fluid velocity distribution are reported in references 28 and 25, respectively. The combination of these two analyses provides the capability of developing a quasi-three-dimensional-flow prediction of blading velocity characteristics. A

single computer program for predicting these blade-path velocities by use of a finite-difference stream function is given in reference 29; supporting information appears in reference 30.

An alternate method, which has been used to predict blade-path flow conditions, deals with ideal velocity and pressure distributions. In this approach, profile-boundary-layer corrections are made with the assumption that turbulent-boundary-layer conditions exist on all blade pressure and suction surfaces. Applicable blade-path flow analyses for compressible laminar and turbulent boundary layers are reviewed in references 31 and 32. Corrections are made for effects of vane and blade trailing-edge thicknesses, which create blockage and flow discontinuities downstream of the trailing edges and ultimately contribute to blading pressure losses. Additional information on compressible flow losses downstream of blade rows, in terms of boundary-layer characteristics, is reported in reference 33.

The mathematical solutions for these velocity-prediction analyses are complex and time consuming if established by hand calculations. Solutions are most efficiently accomplished with computer programming.

Blade-path velocity and pressure distributions are established with the analytical prediction techniques described above. The evaluation of new design nozzle and rotor configurations with cascade tests, however, has not been a common practice in rocket turbine programs, primarily because of short development schedules. The initial substantiation of effective flow areas and of predicted performance has been accomplished successfully by nozzle blowdown and model turbine tests with cold working fluids (air and GN_2). There have been no reported incidents of turbines designed with the procedures described herein that failed to start during development test programs.

2.3.8 Blade Shrouding and Clearance

Experimental test data indicate that turbine rotors with shrouded blades, when compared with unshrouded blade designs, are capable of providing a 2- to 6-point efficiency advantage in impulse-type staging. The performance advantage is attributed to the reduced amount of blade-tip unloading and leakage of the shrouded configuration. An increase in blade-tip clearance in effect permits a greater percentage of leakage flow and thereby produces an accompanying loss in stage performance. Current production turbines developing 500 horsepower or more, including the turbines for the J-2, F-1, and M-1 engines, normally have shrouded blades. The unshrouded blade configurations have been used more extensively in designs having blades less than 1/2 in. in height and developing 400 horsepower or less. In some turbine designs, shrouds are used for structural purposes to minimize the effects of mechanical vibrations. Highly loaded stages sometimes cannot utilize blade shrouding because the shrouding contributes to excessively high blading stresses. In these instances,

Table V. – Representative Blade Axial and Tip Clearances

Turbine		Axial clearance		Tip clearance	
		in.	% Chord	in.	% Blade height
Mark 10	1st rotor	0.476	32	0.030	0.7
	2nd rotor	0.342	23	–	–
Mark 15-O	1st rotor	0.150	20	0.010	0.8
	2nd rotor	0.150	20	0.012	0.7
Mark 15-F	1st rotor	0.100	17	0.0075	1.4
	2nd rotor	0.090	15	0.008	0.9

minimum leakage losses are achieved with shroudless blading designed with the tip-clearance volume recessed into the turbine casing; the blade tip extends into the tip-clearance volume a minimum of 0.005 in. Blade axial and radial clearances for three representative production turbines appear in table V.

Test experience indicates that the influence of blade radial clearance on turbine efficiency varies with turbine pitch diameter. The clearance loss effects are more pronounced in a small-turbine configuration because the leakage flow area generally represents a greater percentage of the main-flow annulus area. These losses are affected principally by the blade-tip sealing provisions, clearance, and pressure differentials. Tip seal requirements vary with the design and with turbine gas-path state conditions. When mechanically possible, for best performance the blade tip clearance is designated as one percent of the blade height; if design constraints prevent this, the clearance is maintained as small as possible. A plot that illustrates the manner in which tip clearance affects turbine performance appears in figure 29. Details of seal clearance losses are reviewed in reference 34; typical seal test data are presented in references 35 and 36.

The axial clearance between stators and rotors varies between 15 percent and 35 percent of vane chord in production turbine designs. Results of tests that have evaluated the influence of axial clearance on turbine performance indicate that minimum blade-path losses result when the ratio of axial clearance to upstream vane chord ratio is 0.25. In one reaction-turbine design, an axial clearance 0.25 times vane chord width was unobtainable because of mechanical constraints associated with sealing geometry and blade cooling; the axial clearance between the nozzle discharge and the blade inlet plane was fixed at a value 0.35 times the nozzle vane chord. Test results with this axial clearance indicate that no appreciable performance loss was incurred.

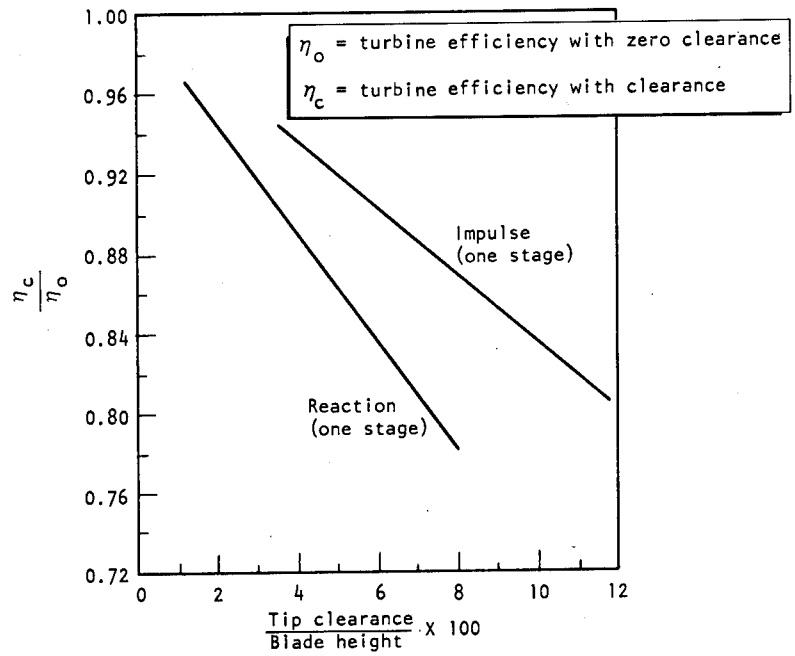

Figure 29. – Effect of blade tip clearance on turbine efficiency.

2.4 MECHANICAL DESIGN AND STRUCTURAL ANALYSIS

Loads and stresses at maximum power conditions are of principal importance in turbine structural design. Experience with turbines for the F-1, J-2, and other production engines indicates that selection of a mechanical-design speed in excess of the predicted maximum is required to compensate for any uncertainties in the speed prediction; a mechanical-design speed 10 percent greater than the predicted maximum speed has proved adequate. The resultant centrifugal loads are 20 percent higher than the predicted maximum loads. Correspondingly, the mechanical-design loads (pressures, torques, etc.), with the exception of the thermal loads, have been established 20 percent in excess of the predicted maximums. Mechanical-design thermal loads are assumed to be equal to the predicted maximums. This procedure of working with the mechanical-design speed and loading and the resultant mechanical-design stresses has provided a means of establishing the maximum allowable operating conditions with some flexibility so that they can be adjusted as experience is gained with the hardware and as the limits of speed, load, and stresses are more firmly established.

The designation of operational stresses in the design of turbine components is divided into two basic categories:

(1) Primary stresses. — These stresses result from centrifugal loads, internal pressures, external loads, etc.; they must be sustained by the component without failure.

(2) Secondary stresses. — These stresses result from component deflections induced by internal or external restraints. Secondary stresses are generally considered less critical than primary stresses because they can be relieved by yielding. Thermal stresses, discontinuity stresses, and certain types of bending or deflection-limited stresses also are considered to be secondary stresses.

The structural integrity of a component customarily is ensured by establishment of a value greater than unity for the ratio of the stress capability of the component (material and configuration) to the calculated stress on the component. In specifying this ratio, the design safety factor, it is the practice to consider only the minimum guaranteed material properties, i.e., the strength that is expected to be met by 99 percent of the material samples with 95 percent confidence (ref. 37).

Stress rupture has not been a major consideration in state-of-the-art rocket turbines designed for approximately 1/2-hour life. New design objectives, however, require 10-hour service lives. Therefore, in the future, turbine designs will deal with stress-rupture-strength considerations.

2.4.1 Blading

2.4.1.1 MECHANICAL DESIGN

The kinds of curves illustrated in figure 30 are used to establish preliminary estimates of acceptable centrifugal stresses in blading designs. These curves provide allowable design values of the $A_a N^2$ (annulus area times nominal speed squared) parameter as a function of blade temperature. The plotted data contain allowances for the variation between nominal and maximum turbine speed, for the gas bending stress in the blade, and for the effect of stress concentration(s). The blade weight used in these calculations generally is reduced from that of a solid untapered blade by assuming that the blade is tapered or hollowed or both. By carrying this weight reduction to practical limits, the centrifugal stress is minimized. The general form of the equation for the allowable $A_a N^2$ is

$$(A_a N^2)_{allow} = \left(\frac{F_{tu}}{FS}\right) K_t - R_2 \sigma_F \left(\frac{1800g}{\pi \rho R_o R_1^2}\right) \qquad (20)$$

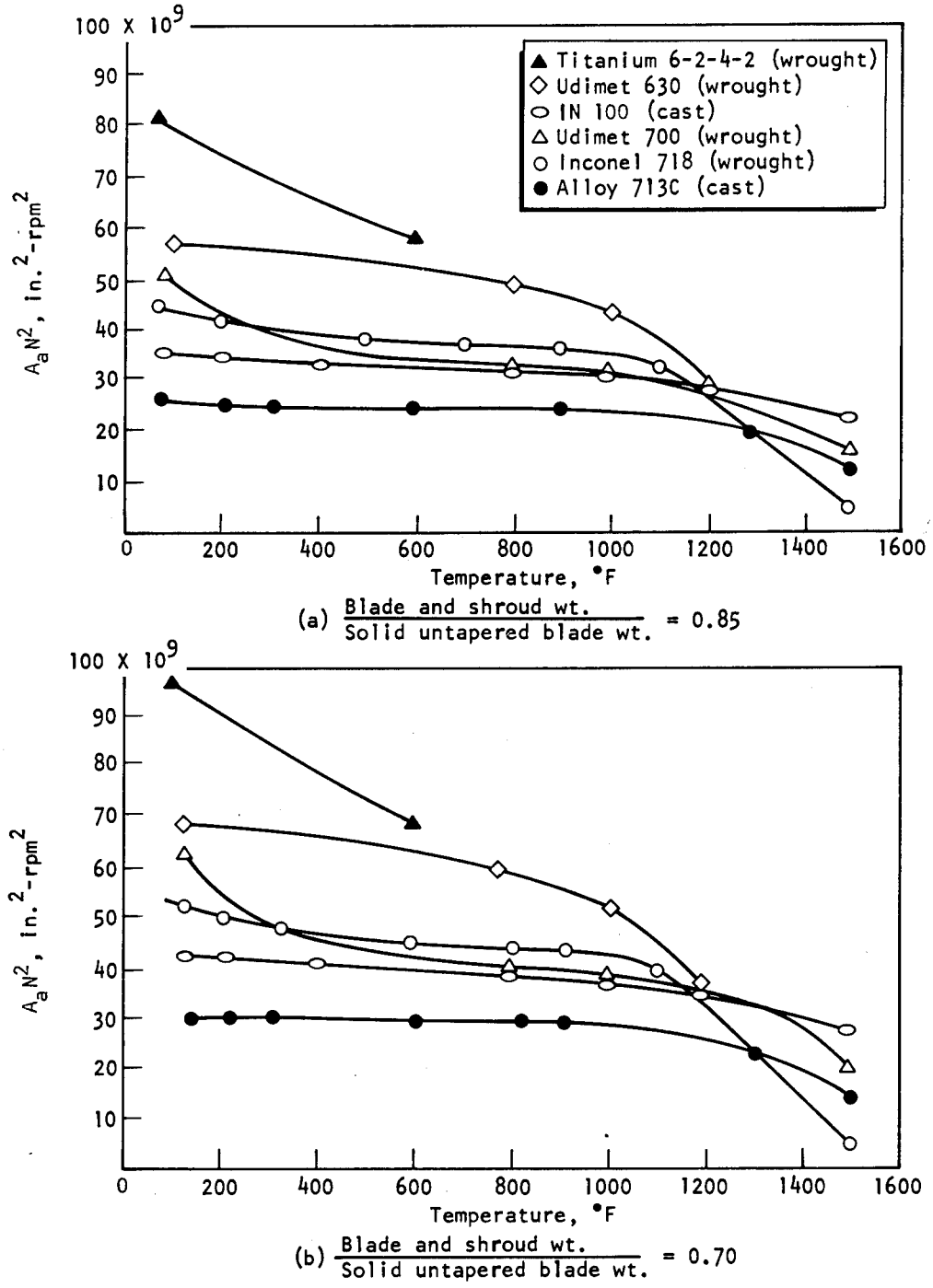

Figure 30. – Allowable A_aN^2 vs blade temperature for various metals and blade weights.

where

$$A_a N^2 = \pi D_m H N^2 \quad (21)$$

F_{tu} = ultimate tensile strength

FS = factor of safety

K_t = stress concentration factor

R_2 = fraction of gas bending force that is alternating weight of a solid

σ_g = gas bending stress

g = acceleration due to gravity

ρ = density of blade material

R_w = ratio of actual blade weight to weight of a solid untapered blade

R_1 = ratio of maximum to nominal turbine speed

D_m = pitch diameter

H = blade height

N = nominal turbine speed

Blade dimensions established during the preliminary design generally are adjusted during subsequent analysis phases. The geometry, solidity, speed, and gas loading are determined from aerothermodynamic analysis. The gas-bending-stress requirements are satisfied by scaling the blade shape and by adjusting the number of blades to maintain constant solidity. Resonant frequencies of the blade must be avoided; in some instances, blade profile designs have had to be modified to alter natural frequencies.

Rocket engine turbines have been designed successfully with blades that are mechanically retained, integrally machined with the disk, or welded to the disk. The mechanically attached blades can be replaced individually; their attachment interfaces often provide some friction damping of vibratory motion. Integrally machined blades result in lighter weight disks and have higher natural blade frequencies. Welded blades normally have small slots between blades that are potential origins for thermal fatigue cracking.

The fir-tree mechanical blade attachment has been used for most of the production turbines for high-thrust engines. The fir-tree geometry varies from configurations with two or three

relatively large lobes to configurations containing a larger number of small lobes. The geometry and tolerances of the fir tree are adjusted to distribute the load between the lobes. The blade above the attachment often is hollow and contains a full radius at the bottom of the central hole, as shown in figure 31, to provide a more uniform transition for load distribution. Interaction between stress concentrations normally is eliminated by positioning

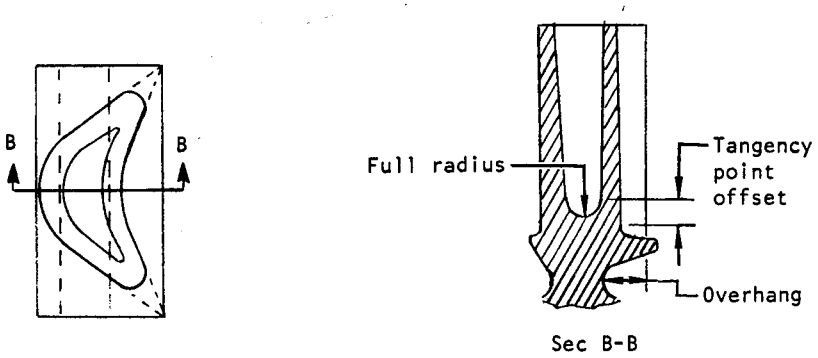

Figure 31. – Blade construction details.

the hole/radius tangency point outboard of the blade/platform fillet tangency point. The blade-to-platform fillet is designed to minimize the stress-concentration factor. Section 2.4.1.2 discusses the variation of stress-concentration factor for a circular blade-root fillet radius as a function of the local blade thickness. A minimum stress-concentration factor of 1.25 is achieved when the blade-root fillet radius equals the local profile thickness.

The blade normally is stacked to induce a centrifugal bending moment that will offset the power bending moment and to minimize the extraneous centrifugal bending stresses. The shroud and blade are positioned (by shifting and tilting) to optimize the bending stress in both the blade and blade attachment. The blade is toleranced to realize the full advantage of this stacking; tolerances that are too large will overshadow the gain. Thickness variations within ±0.003 in. have been utilized successfully.

Large variations in blade thickness induce excessive thermal stresses during thermal transient conditions. Therefore, long, thin leading and trailing edges, as shown in phantom in figure 31, and thick sections without internal holes are avoided whenever possible. Additionally, blades designed with the leading and trailing edges extending a small distance beyond the fir-tree neck, as illustrated in figure 31, have more flexibility at the blade-root cross section. This characteristic tends to reduce thermal stresses. Too great an overhang is avoided because it results in an uneven stress distribution in the fir-tree neck. To provide for a uniform load transmission from the blade to the fir-tree neck, a smooth transition must be incorporated in the design.

The axial spacing between adjacent blade rows is checked to ensure that it does not contribute significantly to the intensity of the vibratory disturbance on the downstream blade. Blade excitation is reduced as axial spacing is increased.

Provisions that maintain blade radial clearances help prevent blade tip rubbing. Tip contact may induce large vibratory stresses that can result in premature fatigue failure. Designs with honeycomb seals are an exception; some rubbing is permitted with this type of seal configuration.

2.4.1.2 STRUCTURAL ANALYSIS

In the structural analysis of the blade, all critical stress locations are analyzed; stresses are computed, and the effects on stress of variations in dimensional tolerances are determined. Thus the structural adequacy of the design is analytically substantiated.

Centrifugal stress. — The centrifugal load for rotor blades consists of a direct component and a bending component. The direct centrifugal stress σ_c is

$$\sigma_c = K_t' (F_c/A) \tag{22}$$

where

K_t' = stress-concentration factor

F_c = centrifugal "weight" of blade ($MR\omega^2$)

A = cross-sectional area of blade

M = mass of blade (W/g)

R = radius of blade centroid

ω = rotational speed in rad/sec

The stress-concentration factor K_t' is a function of the fillet radius and blade thickness, as indicated in figure 32. The centrifugal bending stress σ_{cb} is a result of the bending about both the minimum and maximum principal axes:

$$\sigma_{cb} = \pm K_t' \left(\frac{M_{cmin}}{Z_{min}} \pm \frac{M_{cmax}}{Z_{max}} \right) \tag{23}$$

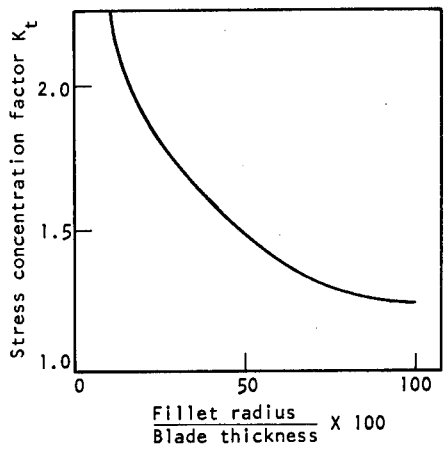

Figure 32. – Stress-concentration factor as a function of fillet radius and blade thickness.

where

$M_{c\,min}$ = bending moment about the minimum-moment-of-inertia axis

$M_{c\,max}$ = bending moment about the maximum-moment-of-inertia axis

Z_{min} = section modulus about minimum axis

Z_{max} = section modulus about maximum axis

The signs, section modulus, and stress-concentration factors are chosen so that they are consistent with the point(s) under consideration. These points usually include the leading edge, trailing edge, and midpoint. Stresses also vary along the blade height; the maximum stress locations normally are near the fillet tangency location on the blade and in the neck of the fir tree. If the blade is twisted, the twisting stress is included with the centrifugal bending.

Gas bending stress. – The force exerted on the blades and shrouds by the working fluid is referred to as the "gas bending force." The gas bending stress σ_p induced by this force also results in bending about both the minimum and maximum principal inertia axes:

$$\sigma_p = \pm K_t' \left(\frac{M_{p\,min}}{Z_{min}} \pm \frac{M_{p\,max}}{Z_{max}} \right) \tag{24}$$

where

$M_{p\,min}$ = gas bending moment about the minimum principal inertia axis

$M_{p\,max}$ = gas bending moment about the maximum principal inertia axis

Z_{min} = minimum section modulus compatible with the point

Z_{max} = maximum section modulus compatible with the point

Mean stress. - The mean stress at any point in the blade σ_m is obtained by adding the centrifugal (direct and bending) and gas bending stresses:

$$\sigma_m = \sigma_c \pm \sigma_{cb} \pm \sigma_p \tag{25}$$

Vibratory stress. - Vibratory loading is the major cause of rotor blade failures. For nonresonant conditions, the alternating stress σ_{alt} is assumed to be a fraction of the gas bending stress σ_p' induced by the gas force on the blade profile only (i.e., excluding the contribution of the gas forces on the shroud):

$$\sigma_{alt} = R\sigma_p' \tag{26}$$

where

R = ratio of alternating stress to gas bending stress

σ_p' = gas bending stress induced by the gas force on the profile only

In many designs, the fraction R is assumed to be equal to unity for nonresonant conditions, i.e., when a known safe margin is maintained between the operating speeds and resonant speeds. To predict the resonant speeds, the blade natural frequencies are calculated, generally by finite-element techniques that account for the increase in natural frequency due to centrifugal stiffening of rotor blades.

A typical graph of the stress limits for safe operation is shown in figure 33; a margin is maintained on resonant speeds to minimize blade vibratory stresses. The allowable ranges of operating speed for a typical case are illustrated by the interference diagram in figure 34.

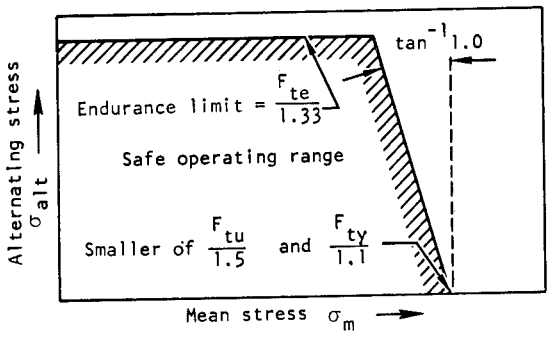

Figure 33. – Safe operating limits on blade mean stress and alternating stress.

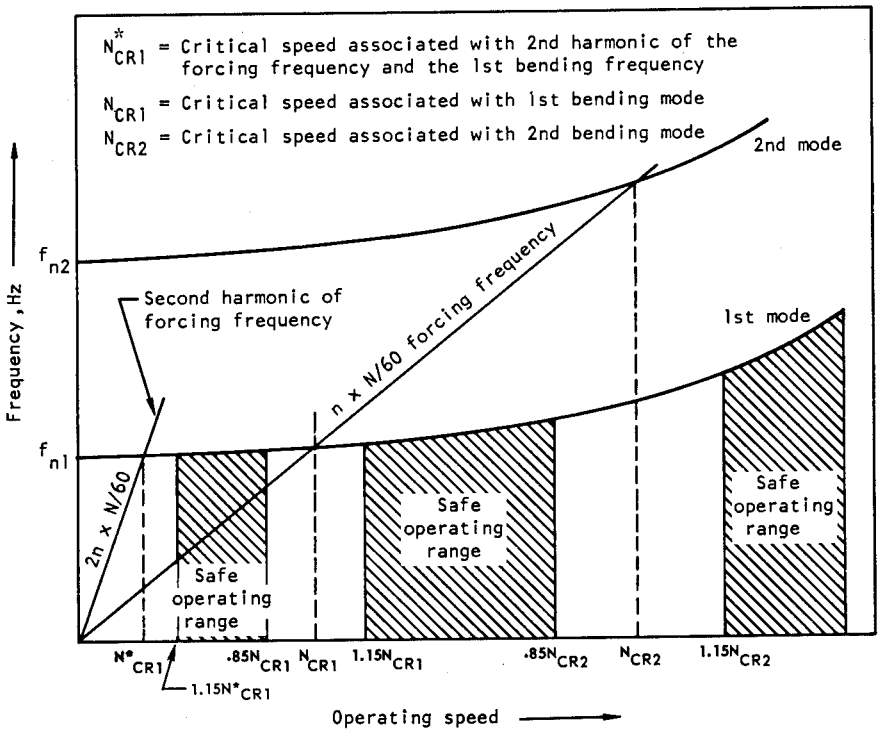

Figure 34. – Safe operating speed range for turbine blades related to critical speeds and forcing frequencies.

When a safe margin cannot be maintained (e.g., because of throttling requirements), a large resonance magnification may occur. In this case, the alternating stress can be calculated from the expression:

$$\sigma_{alt} = F_m R_2 \sigma_p' A_s \qquad (27)$$

where

F_m = mode receptiveness factor

R_2 = fraction of gas bending stress that is alternating

A_s = amplification factor in a damped system

The factor F_m, related to the energy required to excite a particular mode, has been approximated as 0.87, 0.066, and 0.041 for the first, second, and third cantilever bending modes, respectively (ref. 38). For this type of analysis, a modified R value (R_2 = 0.25 nominal) is more appropriate. The value of 1.0 for R mentioned previously has an allowance for a limited resonant magnification; the reduced value of R is a function of the stator-to-rotor spacing.

Component vibration testing normally is conducted for all blade designs to verify the natural frequency analysis. In cases where the turbine operates near resonance, the alternating stresses are measured during operation.

Thermal stress. – Rocket engines usually are started a limited number of times in service, and consequently low-cycle fatigue has not been a major design consideration. Therefore, the thermal stresses that result from gradients within the blade cross section generally have not been predicted analytically, but have been minimized by previously discussed design practices. However, low-cycle fatigue becomes a more important design consideration as turbine life requirements increase. The thermal stress in these long-life applications may be calculated by the analytical approach reviewed in reference 39.

Blade attachment stress. – The load distribution between the lobes of the attachment section is a function of the combined bending, bearing, and shear deformation spring rates, the relative thermal growths, and the tolerance conditions. The design is optimized to balance the stresses and additionally to effect a load distribution between the lobes by varying the lobe and neck geometries and by properly spacing the load flats on the blade relative to those of the disk.

2.4.2 Nozzle

The nozzle converts the potential energy of the working fluid into kinetic energy by reducing the temperature and pressure of the fluid as it passes through the vane channel(s). The kinetic energy subsequently is converted to work as the fluid passes through the rotor blading.

2.4.2.1 CONFIGURATION

A good nozzle design does not sustain any load that distorts the nozzle assembly and deflects the orientation of the nozzle exit gases during operation.

In torus designs that transmit the turbine casing load through the nozzle inner and outer shrouds, the loading is concentrated through the heavier leading-edge section of the nozzle vane. Loading of the distortion-prone trailing edge is then minimized.

In designs with pressures above 500 psi and temperatures above 1200° F, nozzle-to-turbine casing alignment, concentricity, and positioning are best maintained by separating the manifold/nozzle and turbine casing subassemblies. In this type of configuration, the casing loads are transmitted directly to component attachment points and completely bypass the nozzle.

2.4.2.2 PASSING FREQUENCY

High alternating stresses in rotor blades are introduced when nozzle passing frequencies coincide with rotor-blade natural frequencies. Passing frequencies can be altered by changing the number of nozzles and varying the range of operating speed. Rotor-blade natural frequencies may also be modified by adjusting blade shrouding design or modifying blade profiles.

2.4.2.3 FLOW-AREA CONSISTENCY

A design practice that helps control the dimensional accuracy of nozzles requires that the physical nozzle area be noted on nozzle design drawings as a functional dimension. This practice helps avoid excessive turbine-to-turbine nozzle area variations. In practice, nozzle flow areas are checked experimentally by conducting nozzle flow tests with air or GN_2. Figure 35 illustrates a typical nozzle flow test installation. In this type of test setup, to help establish the test component's flow characteristics, a calibrated orifice is installed in series upstream of the nozzle being flow checked.

Figure 35. – Manifold/nozzle assembly (J-2 oxidizer turbine) installed in nozzle flow test facility.

During any turbine development testing program, precautionary measures are taken to ensure that all combustion of propellants that forms the working fluid takes place in the gas generator (or at its origin) and is not allowed to continue in the manifold and nozzle.

Development and production experience with various nozzle designs indicates that a cast nozzle configuration is easier to fabricate and provides a better control of effective flow areas than either the machined or the welded vane-and-shroud designs. In one instance involving a 35-in.-pitch-diameter production configuration, the consistency with which physical nozzle area met flow specifications was improved significantly when a machined nozzle was modified so that it could be cast.

2.4.3 Stator

The stator is an assembly of a stationary row of vanes that redirect the working fluid between two rows of impulse blades. Ideally, no pressure drop is sustained in the stator; in practice, however, some design provisions are made to preclude adverse pressure gradients, as noted in section 2.3.2.

Stators for production turbines can be cast single-ring assemblies; assembled with cast stator segments normally containing 8 to 12 vanes per segment, as shown in figure 36; or assembled from individually cast or wrought vanes that are assembled with circumferential-type retaining devices, as depicted in figure 37. Stator retention is accomplished by clamping between turbine casing flanges, or by assembly-to-stator attachment rings. These components are always designed with antirotation devices and provisions for thermal expansion.

Stators usually have both inner and outer shrouds that can impart large thermal loads to the blades if not properly designed. This load is eliminated by designing the blades with radial freedom at the inner shroud or by segmenting the outer shroud when the design permits.

The selection of stator chord and number of stator vanes depends on solidity, frequency requirements of the turbine rotor blades, axial space limitations, and stator stress and natural frequency limits.

Selection of materials for stator vanes is based on the stator design. If the vanes are designed to have radial freedom to eliminate thermal stress, ultimate and fatigue strength are prime properties. However, if radial freedom is not permitted, material low-cycle fatigue properties become an additional design consideration.

Honeycomb seal strips used in conjunction with rotor-blade shroud labyrinths (fig. 5) have proven to be durable when welded or brazed to the stator seal platform. This installation method avoids the loosening or buckling that has occurred in some mechanically retained designs. The honeycomb seal strip installation normally is combined with the stator installation.

2.4.4 Rotor Assembly

Two basic types of rotor designs are used in production turbines:

(1) The configuration with a relatively small shaft and a simple one- or two-rotor installation. No extensive provisions are included for rigid disk support at any points other than at the shaft. This type of rotor is used in designs not limited by rotordynamic considerations.

(2) The design comprised of a number of disks retained at a large distance from the shaft center line. This type of rotor is generally employed when stiffness and precise balance are required. The assembly is designed to maintain positive piloting and normality of the disk to minimize component imbalance whenever possible.

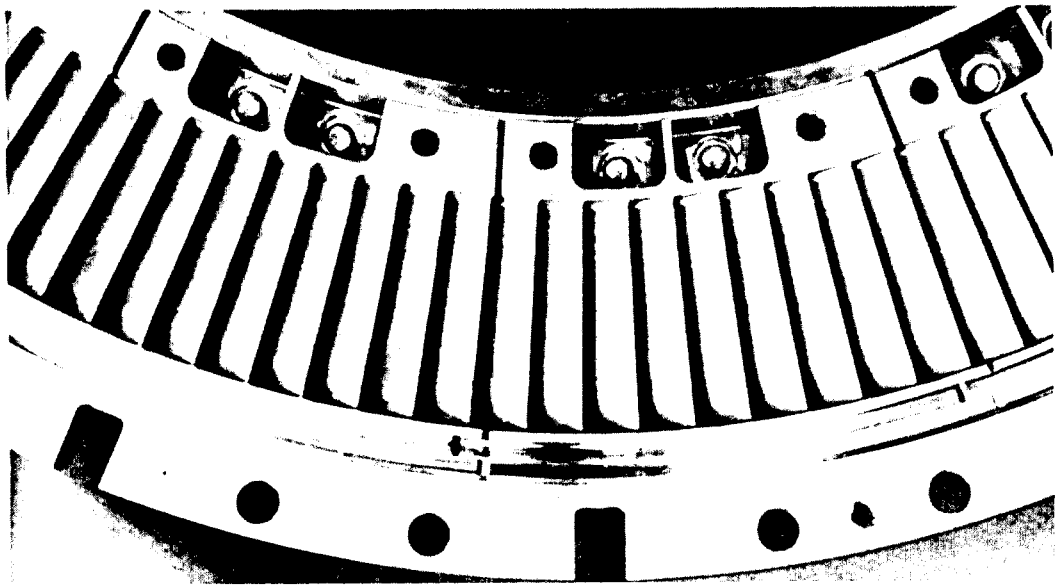

Figure 36. – Portion of a stator assembled from cast stator segments containing 9 stator vanes per subassembly.

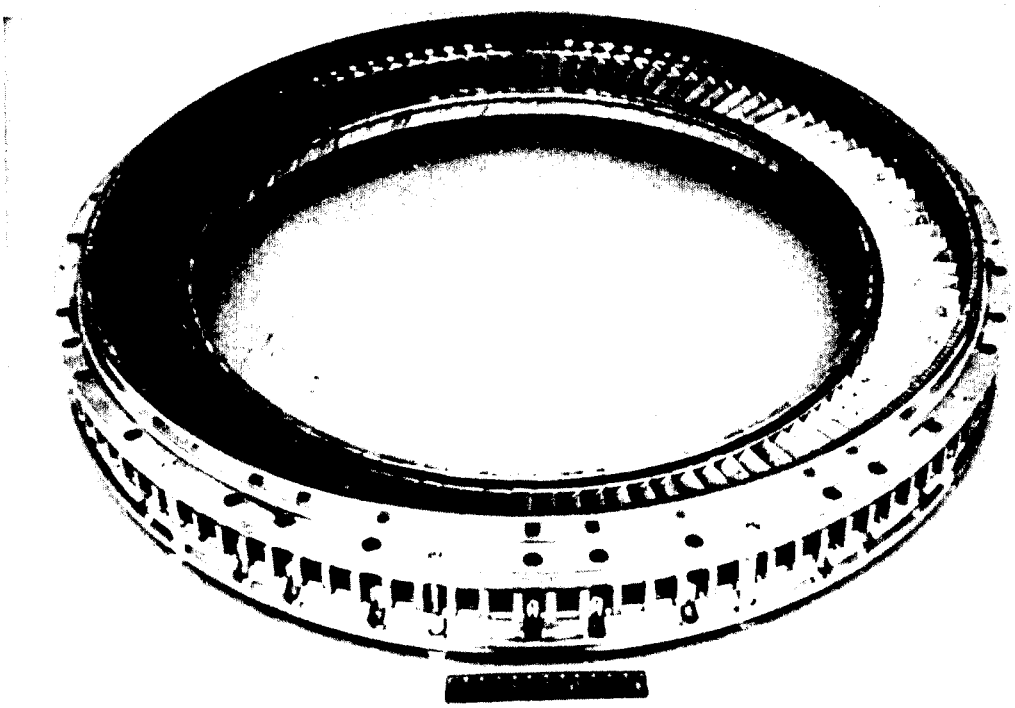

Figure 37. – Stator assembled from individually cast vanes.

For most one- and two-row turbine designs, a low-speed (1000 to 2000 rpm) multiplane balance has proven adequate. The basic rotor is initially balanced, and the assembly is rebalanced as each component is added; the needed corrections are made to the added component. A more precise balance can be obtained by balancing the assembly at the design speed; this normally is not required.

Fatigue resistance is also a consideration in rotor design. To optimize the fatigue strength, generous fillet radii are incorporated at all changes in cross sections.

2.4.4.1 DISK

2.4.4.1.1 Configuration

A turbine rotor disk is designed to support the rotor blades in addition to its own weight and to satisfy rotordynamic design considerations.

Assembly of the rotor is generally simplified if the disk has a central hole, because only a single disk retainer is then required. On the other hand, in highly loaded designs centrifugal or thermal growth of the disk at the inner diameter often makes it difficult to maintain a positive pilot. A lighter weight design can be obtained with a solid disk, the solid disk being thinner and lighter than a disk of equivalent strength having a central hole. The use of a solid disk is generally mandatory for high-tip-speed rotors.

A large transition radius normally is employed between the disk rim and neck to obtain uniform transition of rim loading into the neck of the disk. Since the rim and neck proportions directly influence the required thickness at the disk center, a lightweight disk design is obtained by minimizing these thicknesses. Attention must be given to the placement of holes, curvics, splines, or other stress raisers. Axial symmetry is maintained in the disk insofar as practical, so that the lateral bending stresses are minimized.

Turbine disk material selection is based on ductility and tensile strength, because these properties govern the burst speed. Yield strength is also important because it limits the allowable peak radial stress.

2.4.4.1.2 Structure

A preliminary disk profile normally is obtained by selecting the neck thickness such that the radial stress (assuming the weight outside the neck to be dead weight) is equal to approximately 90 percent of the material yield strength minus an allowance (10 000 to 20 000 psi) for thermal stress. Once the neck thickness and radius are established, the basic disk profile is determined from the constant-stress disk relation discussed in reference 40. The profile is modified as required to facilitate the inclusion of seal and balance-ring

attachments, curvic couplings, and assembly needs. The stresses and vibration natural frequencies normally are calculated with lumped-parameter techniques as described in references 41 through 44; electronic computer programs facilitate the use of these analytical methods.

Burst speed. – The disk burst speed is predicted by the procedure outlined below. All stresses are calculated for the mechanical design speed N_d and include thermal effects. The disk average tangential stress σ_{AT} is given by the expression

$$\sigma_{AT} = \frac{1}{A} \sum_{i} (\sigma_{ti} \Delta A_i) \tag{28}$$

where

A = disk gross cross-sectional area

σ_{ti} = local tangential stress

ΔA_i = area increment

The average tangential stress is corrected for area reductions due to any eccentric holes (e.g., holes of a concentric bolt circle). Therefore the corrected average tangential stress $\sigma_{AT\,corr}$ is

$$\sigma_{AT\,corr} = \left(\frac{A}{A'}\right) \sigma_{AT} \tag{29}$$

where

A' = net area = (gross area) – (bolt hole area)

The maximum tangential stress $\sigma_{t\,max}$ is determined from the stress distribution and stress-concentration effects. The stress-concentration factor K_t' for spline teeth in a central hole, or for eccentric holes, is determined from the equation

$$K_t' = 1.4 - 0.02\,e \tag{30}$$

where e is the elongation.

For an elongation larger than 20 percent and for a disk having a central hole with no splines and no eccentric holes, $K_t' = 1.0$. The maximum tangential stress $\sigma_{t\,max}$ is the greater of the two stresses

$$\sigma_{t1} = K_t' \sigma_{td} \tag{31}$$

or

$$\sigma_{t2} = \sigma'_{tmax} \tag{32}$$

where

σ_{td} = local tangential stress at discontinuity

σ'_{tmax} = peak tangential stress

The design factor F_d is a measure of how nearly the disk approaches the ideal (constant-stress) disk configuration:

$$F_d = \frac{\sigma_{ATcorr}}{\sigma_{tmax}} \tag{33}$$

This design factor and the material elongation are used in determining the fraction $F_b \left(= \frac{\sigma_{ATburst}}{F_{tu}} \right)$ of the material ultimate tensile strength that can be utilized (fig. 38).

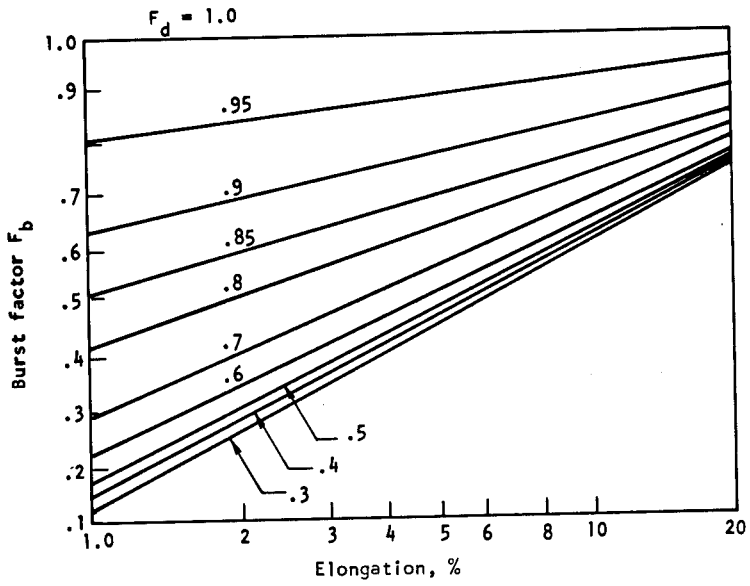

Figure 38. – Disk burst factor as a function of ductility and design factor F_d.

The elongation and material strength are based on an average temperature weighted on the basis of the area of the material at temperature. Design-factor data have been developed with experience gained during development of the engines for the Atlas and Thor vehicles and in the programs for the J-2 and F-1 rocket engines.

The burst speed N_b is given by

$$N_b = N_d \sqrt{\frac{F_b F_{tu}}{\sigma_{AT}}} \tag{34}$$

For alloys exhibiting low elongation (less than 2 or 3 percent), the burst speed is based on peak stress:

$$N_b = N_d \sqrt{\frac{F_{tu}}{\sigma'_{tmax}}} \tag{35}$$

Yield speed. – A disk made of a low-yield-strength material may undergo gross yielding of the cross section prior to burst. The speed at which yielding will occur, N_y, is given by

$$N_y = N_d \sqrt{\frac{F_{ty}}{\sigma_{AT}}} \tag{36}$$

where

F_{ty} = yield tensile strength

Disk vibration. – In general, disks are designed so that the modes of vibration having two or more nodal diameters are above the operating speed range. The critical speeds for the higher diametral modes are often lower than those for the second diametral mode. Therefore, a number of diametral modes must be considered in selecting the design. Critical speeds vary with run time because of changing thermal stress distribution and modulus of elasticity. Consequently, the critical speeds are calculated as a function of run time to ensure that the design is free of critical speeds in the operating range. The umbrella modes can be excited by pressure or shaft oscillations but normally are not an important consideration since the stimulus usually is not present.

A 15-percent margin on second- and higher-order diametral critical speeds, as noted in figure 39, has proved adequate.

Structural limitations. – Disks designed to have burst speeds equal to or greater than 120 percent of the mechanical-design speed have demonstrated structural adequacy. The disk is

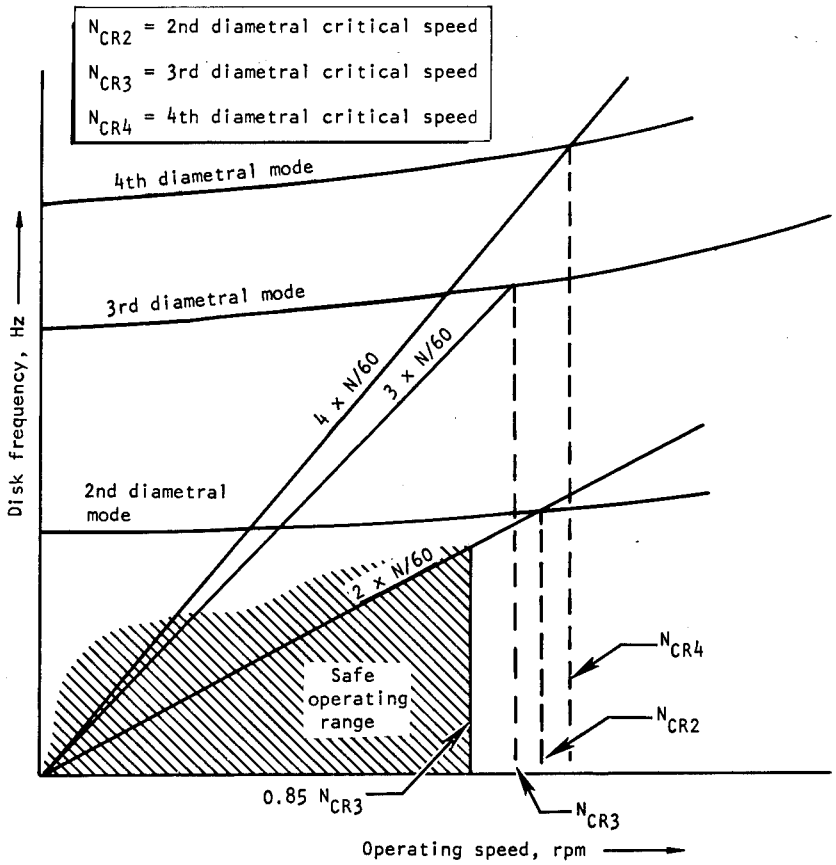

Figure 39. – Limits on disk operating speed related to disk frequency.

designed to prevent local yielding of the entire cross section and to maintain a 1.1 safety factor on yield strength for the maximum radial and compressive tangential rim stresses. To ensure this, the calculated yield speed is maintained equal to or greater than 105 percent of the mechanical-design speed.

2.4.4.1.3 Structural Testing

Normally each new turbine disk is spin tested if the mechanical-design speed is greater than 50 percent of the operational burst speed. The test is made to provide a partial measure of quality assurance and to preyield highly stressed areas. All areas of the disk normally are

subjected to strains in excess of the room-temperature equivalent mechanical-design strains. The spin speed is limited to 90 percent of the room-temperature burst speed. Due consideration is given to the safety of personnel during these spin tests.

For many turbines the margin on critical speed is near the recommended minimum. Designs that fall in this category normally are evaluated by vibration testing to verify the calculated natural frequencies.

2.4.4.2 SHAFT

Detailed information on the design of turbopump shafts and couplings is presented in reference 45. The turbine shaft is subjected typically to a combination of shear, bending, and tensile stresses. The combined stress state in the shaft is not calculated as such; instead, the ultimate safety factor FS_u is calculated directly. The calculation includes both alternating and steady stresses and considers the combined loading effects, as indicated in the following equation (ref. 46):

$$FS_u = \left[\left(\frac{\sigma_o}{L_b F_{ty}} + \frac{K_{tf}\sigma_{alt}}{F_{te}} \right)^2 + 3\left(\frac{\tau_o}{L_s F_{ty}} + \frac{K_{tsf}\tau_{alt}}{F_{te}} \right)^2 \right]^{-1/2} \tag{37}$$

where

L_b = limit design factor for bending

$$= \frac{16}{3\pi}\left(\frac{1 - (d_i/d_o)^3}{1 - (d_i/d_o)^4} \right)$$

L_s = limit design factor for shear, $L_s = \frac{\pi}{4} L_b$

σ_o = steady normal stress

τ_o = steady shear stress

τ_{alt} = alternating shear stress

F_{te} = endurance limit for the required number of cycles

K_{tf} = fatigue notch factor for tensile stress

K_{tsf} = fatigue notch factor for shear stress

d_i = inner diameter of hub shear section

d_o = outer diameter of hub shear section

The terms $L_b F_{ty}$ and $L_s F_{ty}$ in equation (37) have an upper limit of F_{tu}, the material ultimate strength. If either of these terms is equal to or larger than F_{tu}, it is replaced by F_{tu}.

Shafts designed to have a safety factor of 1.5 on failure, calculated from equation (37) on the basis of mechanical design loads, have proved to be structurally adequate. In the absence of calculated or test results, the alternating torsional load is assumed to be equal to 5 percent of the steady torsional load.

2.4.4.3 FASTENERS

Disks retained by either tie bolts or a shaft experience changes in loads during the transition from static to operating conditions. These loads can be divided into two classes: (1) those induced by differential growth, and (2) those contributed by applied loads. The contributors to differential growths include thermal effects and Poisson-type effects. Applied loads include those due to axial pressure differentials, separating action of curvic couplings, and bending moments and shear forces resulting from rotating imbalance forces and rotordynamic motion. The fastener load during operation is determined from the preload, the differential growth, the applied loads, and the spring rates of the individual components of the rotor assembly fastener. A typical bolt load diagram is illustrated in figure 40. The differential growth and applied load effects are treated separately for convenience. In this example, the remaining preload in the fastener is less than the initial preload by the amount of the loss due to differential growths. The operating load is a function of the remaining preload plus the gain due to applied loads. The safety factor on separation is taken normally as the ratio of applied load that will cause separation to the applied loads, equivalent to A/B. A 50-percent margin on fastener separation (i.e., A/B = 1.5) usually is adequate.

The direct tensile stress in the bolt thread is calculated from the minimum minor-diameter area of the fastener. The bending stress resulting from nut-and-bolt overhang is included for bolts arranged in conventional patterns.

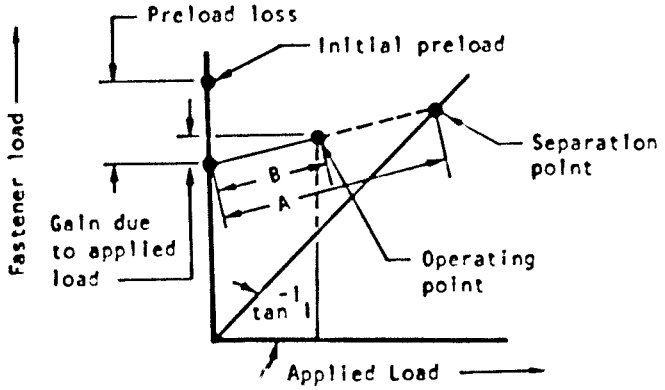

Figure 40. – Fastener load diagram.

2.4.4.3.1 Locking Devices

Locking devices for threaded retainers for rotating components are designed to withstand yielding and failure from high acceleration and deceleration loads experienced during turbine start and shutdown transient conditions.

2.4.4.4 TORQUE TRANSMISSION

Curvic couplings have been found to be most satisfactory for transmitting high torque between turbine rotors and the shaft. Experience with the F-1 Mark 10 turbine (table I) has proved that these couplings are effective in maintaining concentric and normal relationships among rotating components under all operating conditions. Figure 41 depicts the mechanical details of the curvic coupling used between the two rotors in the alternate design Mark 10 (F-1 engine) turbine assembly appearing in figure 7. In low-horsepower turbines, the torque transmission and retaining functions can be provided satisfactorily by drive pin(s) and shaft bolt arrangements as shown in the turbine design in figure 3.

Rotors have also been successfully coupled to the shaft by electron-beam welding as shown in the M-1 turbine design in figure 8. Other torque transmission techniques that have proven successful include

- Integrally machined rotor and shaft
- Involute splines
- Combination of a concentric pilot and retaining bolts

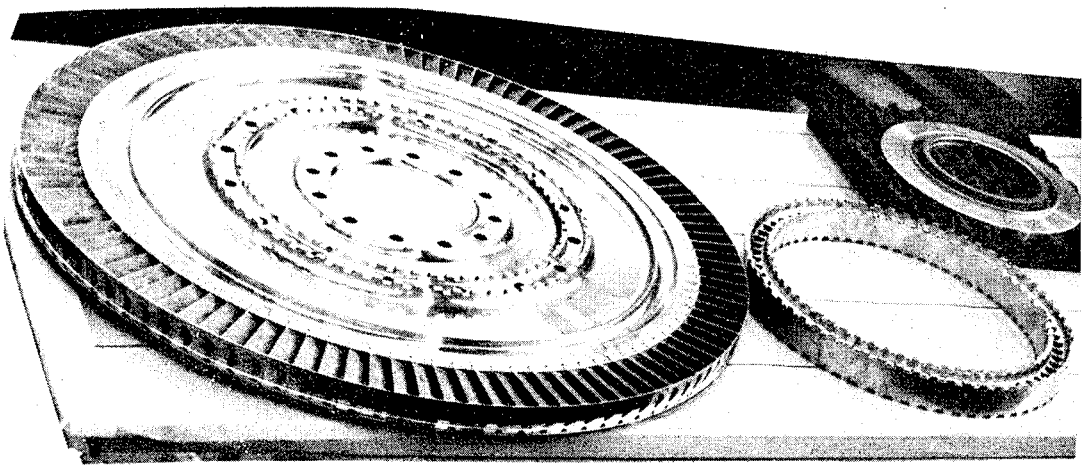

Figure 41. — Rotor and curvic coupling for alternate Mark 10 turbine.

Studs and bolts in curvic couplings and in shaft flanges have on occasion developed thread binding that made turbine rotor disassembly difficult. The binding was attributed to the accumulation of turbine exhaust products and foreign matter on exposed retaining threads. This condition has been averted in new designs by eliminating the exposure of threads to the turbine environment, thereby precluding accumulation of combustion products thereon.

Additional details on the design of coupling devices are presented in reference 45.

2.4.5 Casing, Manifold, and Diaphragm

2.4.5.1 CONFIGURATION

The turbine casing-and-manifold assembly is coupled to the propellant pump or to a pump gearbox to form the turbopump assembly. The design of the casing, manifold, and diaphragm deals principally with the technique of transmitting operational loads through flightweight structures without deforming the structure. The basic design problem is to evolve an acceptable interface of a high-temperature turbine with a propellant pump; this problem is particularly difficult when the propellant is cryogenic.

The design requirements range from those for low-power, relatively simple configurations to those for high-horsepower, high-temperature, highly loaded assemblies; the former often are cast, whereas the latter usually incorporate forged, machined, rolled, and cast components assembled by bolting and welding.

Tooling and fabrication costs for manifolds, casings, and diaphragms in past programs indicate that these components have been as expensive as any other components in the turbopump assembly. Relatively simple configurations have required significant development effort on problems associated with

- Geometry of weld joints
- Capability of the hardware for sustaining thermal growth
- Transmission of operating loads
- Capability of components to sustain high stresses without affecting adjacent turbine parts

The solution to these problems in general has consisted of tailoring the design and fabrication of casings and manifolds to the specific application, as outlined below and as illustrated in figures 42 through 45.

Low power, low temperature. – In small turbines for low-horsepower applications with inlet temperatures below 500° F, the torus preferably is retained at the nozzle interface as shown in figure 42. The principal structural support for the casing is provided by the diaphragm. As the design inlet pressure(s) increase, the torus construction method changes from the sheet-metal-type construction in figure 6 to the cast design discussed in section 2.4.5.2.

Low inlet pressure. – Unitized manifold and scroll casing designs fabricated of sheet metal are structurally suited for turbines with inlet pressures below 100 psi. This configuration is exemplified by the manifold for the series-installed J-2 oxidizer turbine shown in figures 6 and 43. A relatively large manifold area is required in this design because the source of working fluid is the low-pressure exhaust gas from the J-2 fuel turbine (fig. 5). This type of sheet-metal construction is not as complex as that required in a separate torus and shroud assembly, and it has good load-transmitting capability. Radially installed roll pins retain the manifold to the pump outer flange, and a conventional diaphragm is used at the inner attachment circle.

Moderate inlet pressure. – The welded torus and casing assembly in figure 44 has been used for turbine designs with inlet pressures up to approximately 1000 psi. The turbine is attached to the turbopump at the torus outer surface with radial pins passing through partial flanges on the torus; a conventional diaphragm with a retaining flange is used for the inner diameter. However, distortion and cracking of the welded assembly at pressures near 1000 psi limits the effective use to more moderate pressures such as 500 psi. The illustrated

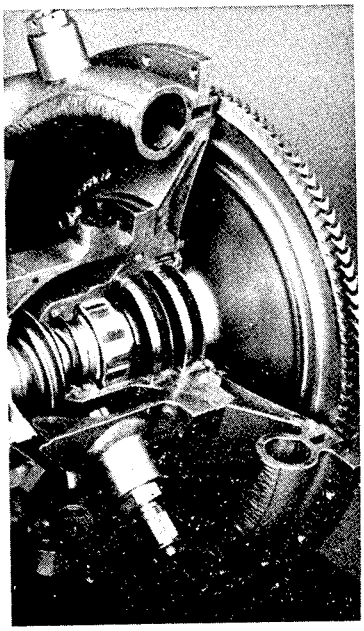

Figure 42. – Manifold-diaphragm design for low-power application

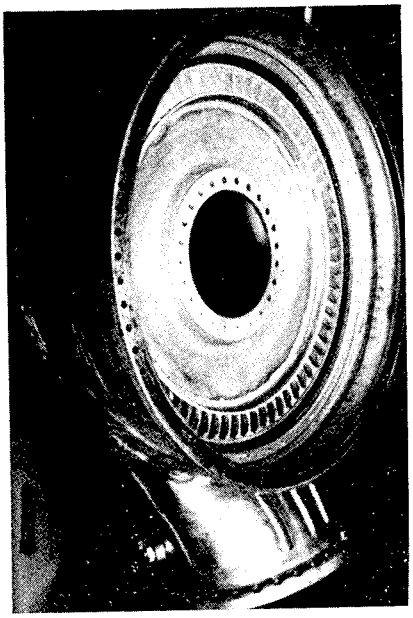

Figure 43. – Unitized shroud, casing, and manifold configuration for low inlet pressure.

Figure 44. – Welded manifold and casing assembly.

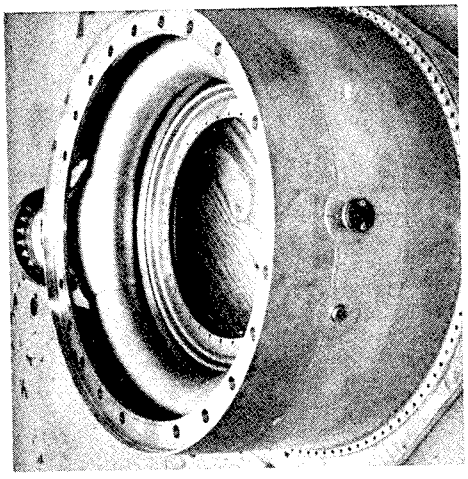

Figure 45. – Separated manifold and shroud design.

manifold design is used in the 56 000-horsepower F-1 production turbine. Note the inlet guide vanes located downstream of the manifold entrance flange.

High inlet pressure. – The manifold and turbine shroud assembly appearing in figure 45 was developed for high-temperature, high-thermal-stress designs that operate with turbine inlet pressures above 1000 psi. In this configuration the turbine casing loads are transmitted through the outer shroud without imposing any primary loads upon the torus.

Additional design details of the independently supported manifold appear in figures 7 and 8. This configuration currently is being utilized in turbines with manifold pressures of 500 psi and above, because this casing design helps avoid the distortion and cracking often experienced with the welded torus and casing assembly illustrated in figure 44.

Configuration for test. – The simplified nonflight manifold and casing configuration, shown in figure 46, is designed for use in model and full-scale turbine test programs with cold-gas

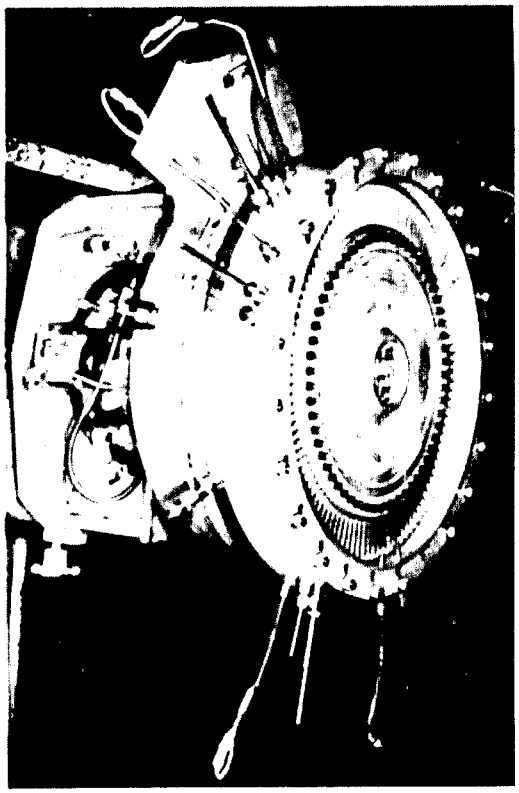

Figure 46. – Manifold and casing configuration for test.

working fluids. These nonflight manifold/casing assemblies are fabricated with a minimum of machining operations and cost. Nozzle assemblies are easily removable to permit performance evaluation of different nozzle designs in the model turbine. Note the gas-path instrumentation provisions in the turbine casing.

2.4.5.2 STRUCTURE

The manifold assembly is the primary turbine casing structure in many turbine designs. The inlet manifold and casing are designed with sufficient strength to withstand component thermal gradients, applied external loads, and gas-flow pressure loads. In general, the thermal stresses are minimized by utilizing thin, uniform-thickness sections.

When practical, the manifold is designed so that the structural loads imposed by ducts, mounts, external pressures, etc., are not carried through the torus assembly to the support structure. Manifolds with integral nozzle vanes occasionally have exhibited thermal fatigue cracking in the vane area. When space and aerothermodynamic considerations allow, this fatigue cracking has been precluded by using internal ties to carry the manifold pressure-separating load, and the nozzles then have been designed with minimum radial restraint between the inner and outer shrouds.

The manifold normally is designed with radial freedom between it and the supporting member to accommodate thermal growth with a minimum of distortion. Symmetrical patterns of radial pins or thin, flexible axial cylinders or both have been used with satisfactory results.

Because thermal stresses are an important consideration in manifold design, materials with relatively low strength but with good ductility and good low-cycle fatigue strength normally are selected instead of high-strength materials with attendant lower ductility. A non-heat-treatable alloy is often utilized for ease of weld repair.

Structural analysis. – Essentially all of the analysis of the structural members is based on thin-shell theory and makes use of computerized finite-element techniques (ref. 47).

Structural limitations. – No special structural limitation criteria are used for the manifold and casing design. It should be noted that the thermal stresses play an important part in configuration selection; this consideration is dealt with early in the design phase.

Design drawings for the turbine manifold preferably include information describing proof-pressure testing requirements. Manifolds are proof-pressure tested to 120 percent of the room-temperature equivalent of the mechanical-design pressure; this value for proof pressure is obtained as follows:

$$p_p' = \left(\frac{\text{Property at room temperature}}{\text{Property at max. oper. temp.}}\right) p_{m\,d} \times 1.2 \qquad (38)$$

where

p_p' = proof pressure

$p_{m\,d}$ = mechanical-design pressure

2.4.5.3 PROBLEM AREAS

2.4.5.3.1 Welding Practices

Turbine structures with high ratios of power to weight are constructed of comparatively thin metal sections. The successful fabrication of these sections is highly dependent on the utilization of good welding practices, particularly for turbine manifold and casing assemblies; as noted, past turbine programs have required large amounts of welding development effort. Figure 47 illustrates a typical good manifold and casing configuration

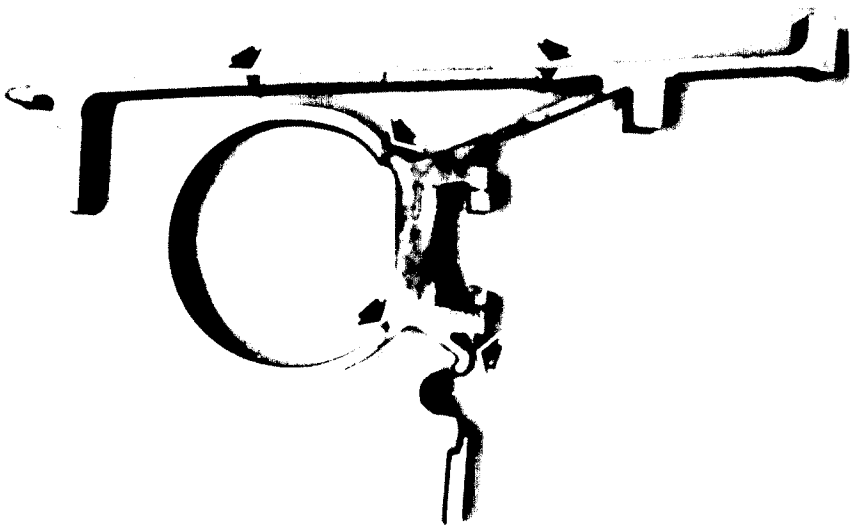

Figure 47. – Weld details in the manifold and casing of the alternate Mark 10 turbine for the F-1 engine.

with well-designed weld details; this design is used in the alternate Mark 10 turbine appearing in figure 7.

Specifications applicable to turbine manifold and casing welding procedures (ref. 48) have been established from experience in rocket turbine development. The utilization of this type of specification helps minimize time-consuming and costly weld-related problems.

2.4.5.3.2 Casing Cavities and Pockets

Moisture accumulation and casing cracks. – Care is exercised to avoid casing designs that contain circumferential pockets or sections that can collect moisture during engine operations. There have been instances during engine test when the condensate from cryogenic pumps and unavoidable spray of cooling fluids from the test facility accumulated in turbine circumferential passages and diaphragm U-sections. Between hot-fire tests, the pump's cryogenic environment froze the liquid and thereby cracked the structure. Casing designs that can accumulate moisture or provide leak passages to internal sections of the turbine are avoided in all new turbines. Designs with cylindrical-type turbine casings as shown in figures 43 and 45 are seldom subject to this kind of problem.

Accumulation of foreign matter in circumferential cavities. – Internal casing erosion that occurred during some prototype turbine development tests was attributed to the continual movement of entrapped foreign matter in circumferential casing cavities. Motion of the foreign material was sustained by impingement of leakage flow of turbine working fluid. New turbines therefore are designed without circumferential ridges that can inadvertently collect carbon particles and foreign matter.

2.4.5.3.3 Casing Flange Leakage

The best technique for preventing leakage at flange retainer bolts is to position the flange static seals between the pressure source and the bolt circle. Before any seal is designated for service in a turbine, it is subjected to performance verification tests that simulate service conditions of the intended application.

2.5 INTEGRATION AND ASSEMBLY

2.5.1 Rotordynamics

2.5.1.1 CRITICAL SPEED

Critical and nonsynchronous whirl speeds have been responsible for the development of high stresses and deflections. The deflections due to bending, shear deformation, and gyroscope

effects of the rotating masses must be accurately predicted in the rotordynamic analysis, which is based on an analytical model of the turbopump rotating assembly (ref. 45). As a general rule, if the ratio of housing weight to rotor weight is less than 3, the housing also is modeled and included in the rotordynamic analysis.

For the preliminary analysis, each bearing is assumed to be a linear-elastic translational spring. The final analysis employs an experimentally determined, usually nonlinear, load/deflection curve for the bearings, and includes bearing clearances. The physical damping forces and associated damping coefficients that act to restrict the whirl amplitude cannot be determined theoretically and therefore must be established from test data.

Drawings for prototype turbine components normally include provisions for installing displacement detectors (proximity pickups) for determining turbine rotordynamic characteristics during test operations. The critical speeds of nonsynchronous whirl are approached in incremental phases during turbine testing to avoid turbine damage. If the analytical model is verified by experimental techniques, an operating speed "redline limit" is then established.

2.5.1.2 ROTORDYNAMIC RESPONSE

In order to calculate response, some dissipative elements must be included in the model. Viscous damping is considered to be acting on the masses, and structural damping is used to represent internal material friction in the shaft and friction at connections.

The response of the shaft/disk system being designed is in turn analytically determined. The response due to point-mass imbalances of the rotor and the response due to tolerances and bearing clearances are analyzed. The response of the system at a critical speed is limited only by the damping forces acting on the rotor. Since these forces are not predictable, the rotor system is designed so that no portion of the steady-state operating range is within ±20 percent of any critical speed. The response then is determined primarily by the rotor imbalance, which can be predicted and controlled. If necessary, high-speed balancing can be performed to permit operation at a critical speed.

Additional details on shaft dynamic behavior, its analysis, and its treatment in design are presented in reference 45.

2.5.2 Bearings and Seals

The turbine design procedure must include critical evaluation of turbine bearing and seal design and installation. References 49 and 50 present the current technology in these important areas.

Two characteristics of shaft-supporting bearings are of vital importance to the turbine designer because they affect rotordynamics: bearing radial spring rate, and radial clearance. In addition, in some designs, provisions to cool the bearing must be made by the turbine designer.

Seals between rotors and stages are particularly important in turbine design because they influence the gas-path pressure distribution and because seal clearances are factors in the vibration characteristics of the rotating assembly.

2.5.2.1 BEARING RADIAL SPRING RATE

Stiffness elements supporting the rotor shaft are added to the free-body analytical model to simulate the bearing radial spring rate and to determine its effect on the critical speeds. Curves of critical speed versus bearing radial spring rate are then plotted as illustrated in figure 48.

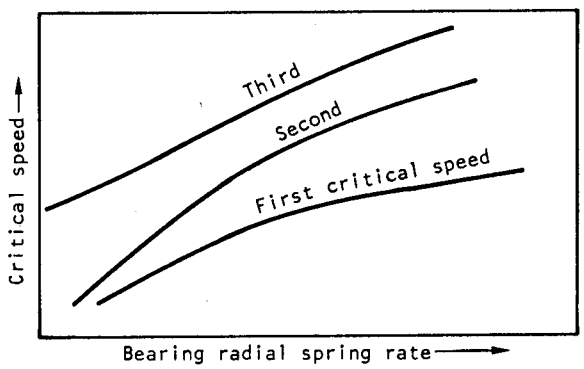

Figure 48. – Variation of critical speed with bearing radial spring rate.

The beneficial effect of changing the bearing radial spring rate is illustrated by the modification that was accomplished during the Mark 9 turbine development program. The first two critical speeds of this system were determined primarily by the bearing spring rate, as illustrated in figure 49. In the original design, the second bearing critical speed falls within the desired operating range. In the final design, as shown by the reduced values for spring rate, there were no critical speeds in the operating range of the turbine.

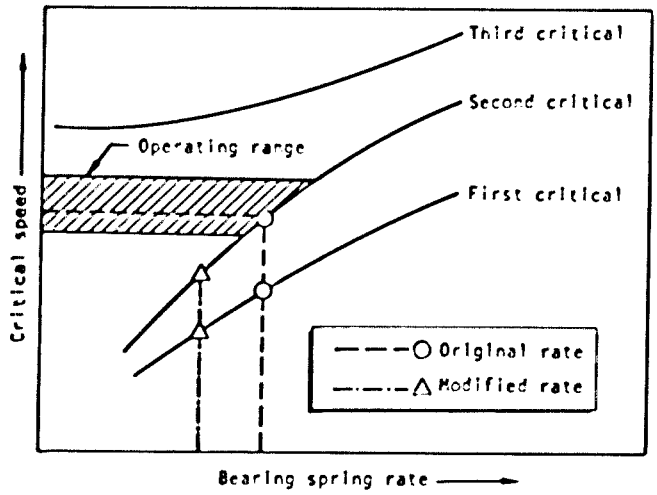

Figure 49. – Beneficial effect on critical speed resulting from a change in bearing spring rate (Mark 9 turbine).

2.5.2.2 BEARING RADIAL CLEARANCE

Turbine-bearing radial clearance is based on the results of analytical models that establish the effect of clearance on critical speed. The design values subsequently are verified by experimental tests with instrumented prototype assemblies.

2.5.2.3 COOLED BEARINGS

One- and two-row turbine configurations normally are overhung outboard of the aft turbopump bearing as shown in figures 1 through 8. Some new high-energy-fuel turbines have been designed with three rotors, and require the use of bearings that are positioned outboard of the turbine disks to provide the proper shaft support; outboard bearing installations have the disadvantage of needing additional provisions for bearing cooling and lubrication. Nuclear rocket turbines have been successfully developed with five and six rotors, the turbine shaft being independently supported by fore and aft bearings. Figure 50 illustrates the bearing and shaft spline details in the rotor assembly of the Mark 25 five-stage hydrogen turbine. Note that the blading is integrally machined with the disks.

Leakage of cryogenic bearing coolant onto the hot rotor assembly during operation has caused turbine disks to deform. This condition subsequently led to rubbing between rotor blades and adjacent nozzle trailing edges. This kind of design deficiency is corrected by the improvement of sealing provisions and the addition of alternate drain paths for any accidental leakage that could take place.

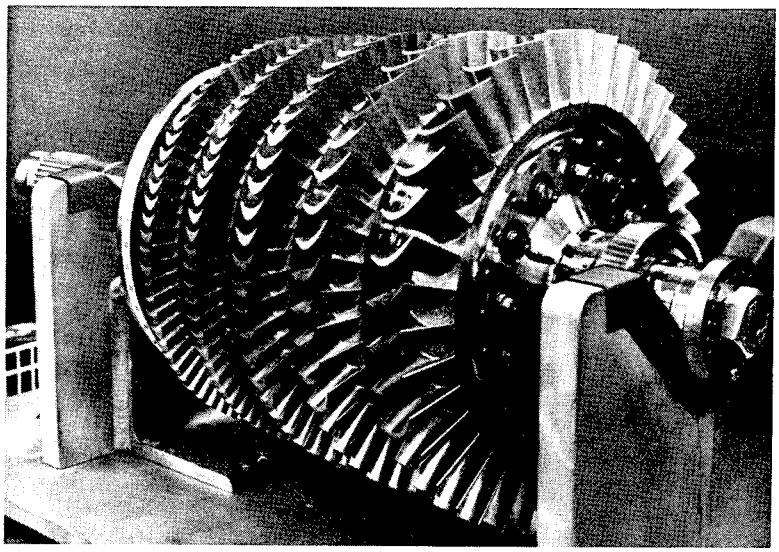

Figure 50. – Mark 25 five-stage rotor assembly utilizing outboard bearings.

2.5.2.4 SEALS BETWEEN ROTORS

Sealing between impulse-turbine rows normally is accomplished with a dynamic seal positioned between the turbine stator and disk face outer surface, as shown in figure 7. Provisions for sealing between reaction staging are more critical than those required in an impulse stage, because of the closer relationships between stage performance and the proper maintenance of gas-path pressure distribution. A labyrinth seal package, as illustrated in the designs in figures 2 and 10, is best suited for use in a reaction stage.

2.5.3 Exhaust Ducts

Turbine exhaust-duct designs have been responsible for adverse pressure gradients developing across the last-row rotor. This condition has been known to contribute to rotor vibrations and to a reduction in required turbine mass flowrates at design operating conditions. Typical corrective actions include the elimination of exhaust-duct turning and the installation of exhaust-flow straightener vanes downstream of the last rotor. The straightener vanes eliminated the tengential whirl component from the turbine exhaust; the choked condition was corrected, and normal turbine flows were restored.

2.5.4 Problem Areas

2.5.4.1 COMPONENT INTEGRATION

During the development of a new turbine configuration, the designer tries to minimize the number of components in the turbine assembly. The objective is to evolve a design that is not difficult to fabricate and maintain, will require minimum development costs, and contributes minimum component weight. Therefore, all new-design components are studied to determine which details can be integrated and fabricated as single assemblies. In some instances, the designer may be able to call for a cast or forged component that previously was comprised of two or more machined parts.

2.5.4.2 TURBINE THERMAL ISOLATION

Thermal insulation often is installed in turbopump assemblies with high-temperature turbines in order to prevent turbine radiation and soakback from adversely affecting the properties of non-high-temperature (component) materials installed adjacent to the turbine. The design of heat shields and thermal insulation is coordinated with engine systems engineers during the design phase and preferably neither is installed on the turbopump as an afterthought. The responsibility for design and installation of thermal insulation is always retained in the turbomachinery group. This practice helps protect the completed hardware from a marginal or faulty installation that may reduce turbine performance and reliability.

2.5.4.3 THERMAL GROWTH AND DEFLECTION

Turbine development experience clearly indicates that new turbine designs are prone to problems associated with component thermal growth and deflection that exceed predicted design allowances. These problems have occurred principally at the turbine/pump interface, manifold-to-casing juncture, stator retention points, turbine blade shrouds, turbine disk retainers, turbine bearing and seal retainers, and static-seal grooves. Manifold-to-casing diaphragms have developed circumferential thermal cracks that originated at the nozzle weld, and seal failure at the flange has been caused by thermal distortion of the diaphragm.

These problems have been avoided by designing structural flexibility into high-temperature, high-load-bearing turbine components such that structural growth and deflections could be sustained during operations.

2.5.4.4 COMPONENT ORIENTATION

There have been instances when prototype and development stators and rotors were improperly installed in the turbine assembly because the component design did not prevent

incorrect installation. All current turbine designs include means for preventing improper assembly; the techniques include installation pins, circumferential grooves, spline screws, flange notches, alignment grooves, tapers, interference fits, variations in bolt circle and coupling diameter and matching splines. In addition, strict assembly procedures are observed during turbine buildup; the procedures include the recording of all critical dimensions, clearances, and retaining torques.

2.6 TURBINE MATERIALS

Component material selection is based on requirements of the component installation in the turbine, operational and service life, proposed fabrication technique, and procurement and fabrication costs. The most readily available and lowest cost alloy that will meet the requirements of the design is preferred over an advanced state-of-the-art material with properties that exceed those required for the application; these materials usually have marginal availability and high procurement and fabrication costs. A listing of materials that have been used for various components in ten production and developmental rocket turbine designs is presented in table II in section 2.0. A summary of problems experienced with turbine materials during manufacturing and operation, together with corrective actions, appears in table VI.

2.7 PROVISIONS FOR INSTRUMENTATION

Design provisions for turbine instrumentation normally are made during the design phase; this practice prevents subsequent problems associated with providing instrumentation bosses in turbine casings designed with insufficient material for this purpose. Production-turbine designs normally include instrumentation provisions for measuring turbine inlet temperature and pressure and shaft speed. Turbine exhaust temperature and pressure are sensed and recorded during all turbine (turbopump) production acceptance tests; however, only large booster and space vehicle turbines have retained this added instrumentation during flight operations.

Proximity sensing devices for measuring disk axial displacement coupled with movies of turbine rotor displacement during turbine operation are used for experimentally defining rotor vibration characteristics. Supporting data for this type of investigation have been obtained by using ceramic stress-coat, temperature-sensitive paints, strain gages, and thermocouples.

Turbine instrumentation is well documented in the literature, particularly in NASA reports on turbodrive design (refs. 51 through 56).

Table VI. – Turbine Material Problems and Corrective Actions

Alloy	Fabrication problem	Corrective action	Operational problem	Corrective action
Rene 41	Manifold – Cracking during heat treatment. Cracks were weld associated and occurred in the inlet, torus, and shroud sections	(1) Changed weld filler wire from Rene 41 to Hastelloy W (2) Changed from manual to automatic welding (3) Hammer peened repair welds to relieve weld stresses (4) Screened out crack-sensitive material (5) Changed to an argon or vacuum heat-treat atmosphere	Manifold – Cracks in the inlet, torus, and shroud sections	Improved weld joint geometry (automatic welds, removed drop-through), improved parent metal ductility by more thorough acceptance testing
Inconel X-750	Manifold – Cracking of a weld during heat treatment	Improved joint fitup, changed filler wire from Inconel X-750 to Inconel 718	Rotor blades – Fatigue cracks at blade root (integrally machined disk and blade)	Shot peened blade root area after finish machining
Inconel 718	Rotor disk forging – Failure during spin test due to poor ductility	Changed solution-heat-treat temperature from 1750° to 1950° F	Rotor disks – Fatigue cracks	Increased disk thickness
16-25-6	Rotor disk forging – Penetrant indications on finish machined surface showed large inclusions	Changed from single-melt to double-melt material (consumable electrode process [slag cover] in final melt)	Rotor disks – Fatigue cracks	Included radius on fir-tree edge and shot peened
Hastelloy C	Stator casting – Straightening cracks	Revised press straightening procedure	Manifold bracket – Tensile cracks	Improved ductility by annealing after forming
310	Manifold – Cracking during stress-relief heat treatment on final assembly	Reduced heating and cooling rate to 25° F/min in stress-relieving	Manifold – Cracks at weld joint	Reduced weld residual stresses by stress-relief heat treatment of manifold to 1650° F
Alloy 713C	Cast blades – Grinding heat checks	Lowered feeds and speeds, increased frequency of wheel dressing, changed to a water-base coolant	Rotor blades – Thermal fatigue cracking	Changed to a finer and more equiaxial grain structure
Stellite 21	Stator casting – Microshrinkage	Improved foundary quality control	Cast rotor blades – Fatigue cracking	Revised design to include cast shroud
321	Manifold – Cracking during welding (parent metal)	Amount of welding reduced 50% by redesign to fabricate from large rolling forgings, material changed from air melt to vacuum melt		

3. DESIGN CRITERIA and Recommended Practices

3.1 PRELIMINARY DESIGN ANALYSIS

Final turbine design state conditions and geometry shall be based on tradeoff studies of design control parameters.

Perform design optimization studies with the parameters that influence the selection of turbine type, arrangement, size, number of stages, and performance.

Establish the effect of pressure ratio, inlet temperature, number of stages, pitchline velocity, and velocity ratio on turbine performance.

Determine how variations in mass flowrate, inlet temperature, pressure ratio, and speed influence developed turbine horsepower.

Investigate blade height requirements for changes in mass flow, inlet pressure, and number of stages.

Study the influence of pitchline velocity on pitch diameter, velocity ratio, and turbine efficiency.

Establish preliminary blading stresses, using annulus-area/speed-squared relationships ($A_a N^2$); evaluate variations in pitchline velocity and blade height.

If the primary concern is maximum performance, special care should be directed to the limiting parameters of staging, pitch diameter, speed, and blading stress.

Examples of parametric data plots that should be generated during a preliminary design and used for selecting the final turbine design state conditions are illustrated in figures 51 and 52.

3.1.1 Pressure Ratio, Mass Flowrate, and Engine Performance

The design mass flowrate (or pressure ratio), at rated horsepower and speed, shall be the optimum value for best engine and vehicle performance.

Turbines for gas-generator-cycle engines should be designed with minimum attainable mass flow, whereas staged-combustion (topping) turbine designs should aim for the lowest

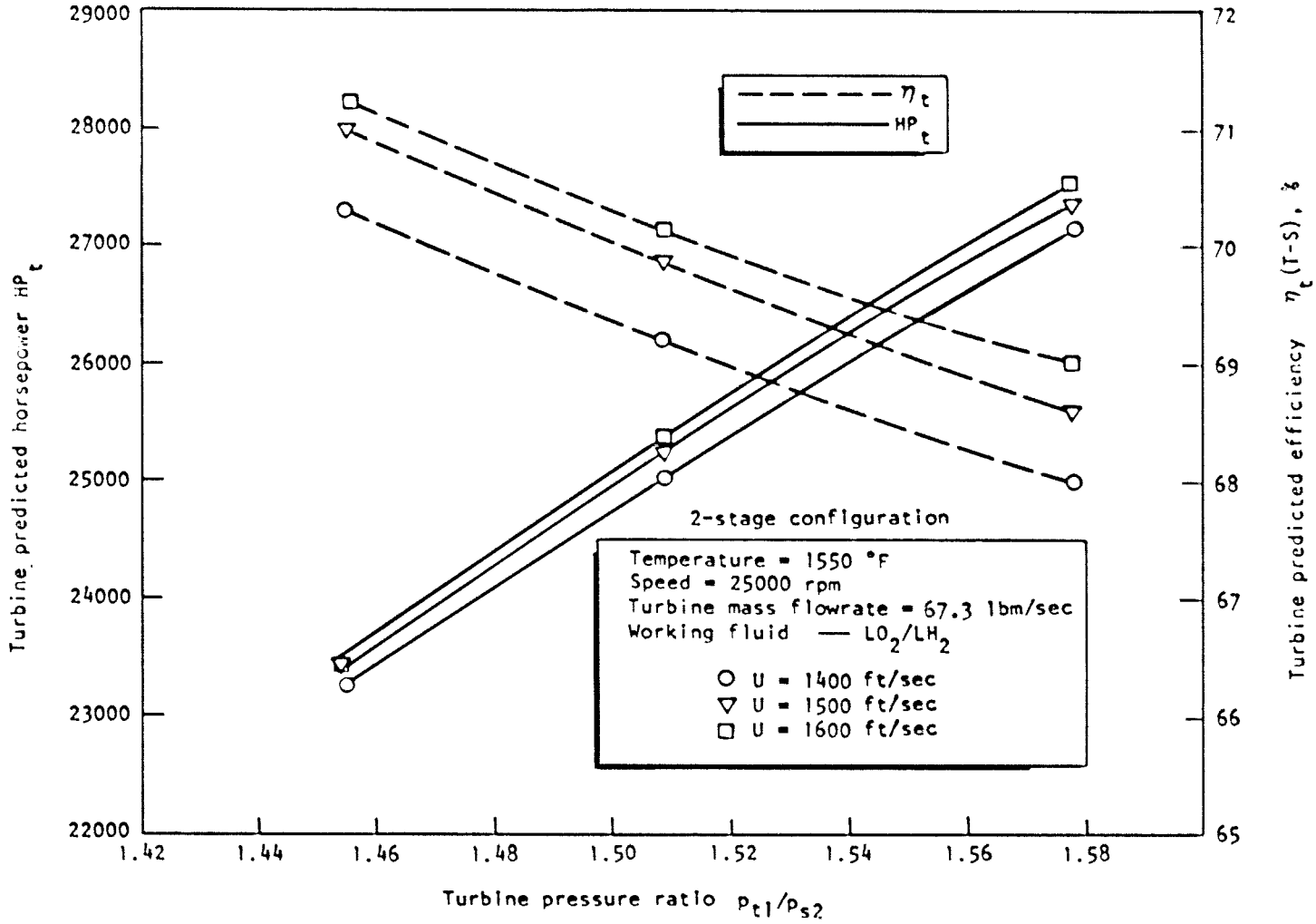

Figure 51. — Parametric data plot of horsepower and efficiency vs pressure ratio.

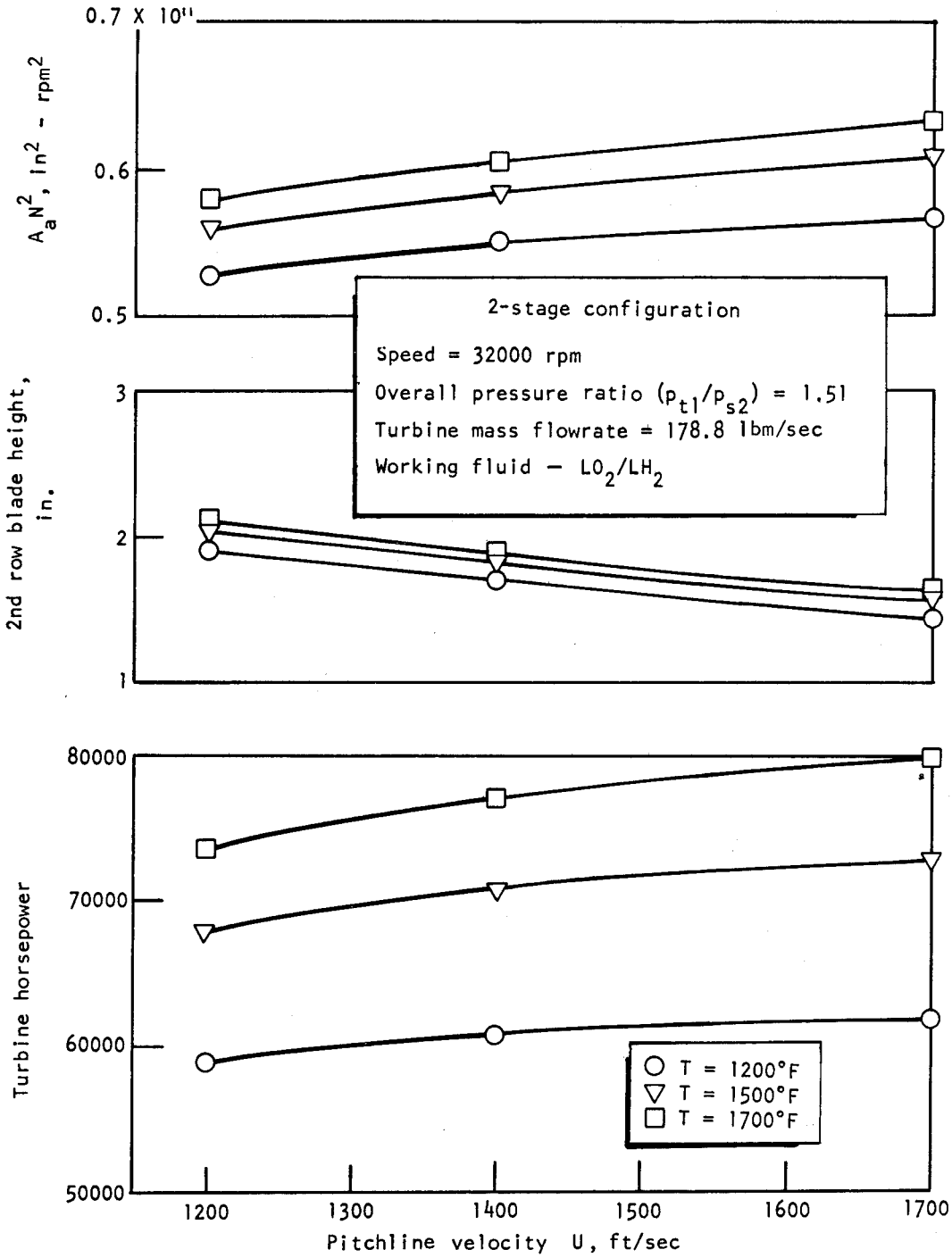

Figure 52. – Parametric data plot of horsepower, blade height, and $A_a N^2$ vs pitchline velocity.

turbine pressure ratio.

In gas-generator-cycle turbines, the high pressure ratios and accompanying large amounts of working-fluid available energy normally require the designer to select high pitchline velocities so that the turbine will operate in the desired ranges of velocity ratio and efficiency. If high pitchline velocities are precluded by stress or size limitations, the designer should evaluate series-installed turbines with dual-shaft turbopumps. The total available pressure ratio is allocated between the high- and low-pressure turbines in the series installation. The theoretical spouting velocity of each turbine is thereby reduced, and velocity ratio and turbine efficiency are improved.

For the low-pressure turbines required in staged-combustion-cycle engines, use reaction designs with 35- to 50-percent reaction.

To avoid errors in the gas-path pressure schedule, designate specific stations that locate turbine inlet and exhaust pressure points in the turbine design.

3.1.2 Working-Fluid Properties

Working-fluid gas properties shall agree with the properties used for the overall engine energy balance.

The range of turbine design pressures and temperatures is established by engine system requirements. Responsibility for verifying that the turbine working-fluid gas properties satisfy the design pressure and temperature requirements must be established prior to the initiation of the turbine final design analysis.

Some turbine working fluids do not behave as ideal gases at pressures above 2000 psi. With this type of working fluid, the gas-path available energy should be established as a process quantity when expanding between nozzle and blading pressures. Variations in temperature data, together with compressibility effects, must also be accounted for when sizing gas-path flow areas for nonideal gases.

3.1.3 Isentropic Velocity Ratio

The design isentropic velocity ratio shall be in the range of values that provides maximum turbine efficiency.

Use the design pressure ratio and data on working-fluid available energy to establish whether single- or multi-row impulse or reaction staging will provide the design velocity ratio for maximum performance.

In dual-shaft turbopump designs, evaluate the effect on velocity ratio and turbine efficiency of series- and parallel-installed turbines. Determine whether the increased efficiency normally experienced with a series-turbine installation justifies any accompanying size and weight increases in the downstream low-pressure turbine.

The use of data on velocity ratio vs turbine efficiency as illustrated in figure 53 first requires establishing whether the data are applicable to the subject design in terms of pressure ratio, sealing-arrangement clearances, nozzle and blade designs, arc of admission, and nozzle height.

3.1.4 Staging

The type of staging and number of blade rows for a turbine design shall be based on tradeoffs among turbine efficiency, mass flowrate, tau factor, turbine/pump mechanical-design requirements and weights, and engine mission requirements.

Initially, establish the energy available to the turbine and the range of velocity ratios in which candidate turbine configurations can operate.

Determine whether impulse or reaction staging is required. Reaction staging should be specified for design isentropic velocity ratios above 0.45, whereas two-row velocity-compounded impulse staging is recommended for a design velocity ratio between 0.20 and 0.30. A single-row impulse stage delivers best performance at velocity ratios between 0.30 and 0.40. For design velocity ratios below 0.15, estimated incremental gains of 10 and 23 points in overall turbine efficiency can be realized by adding one and two rows, respectively, to a single-row design.

Theoretical spouting velocities of high-energy working fluids often force operation at velocity ratios that come short of delivering maximum efficiency. This condition occurs because the pitchline velocities required for higher turbine efficiencies exceed allowable stresses in the turbine rotor. The practice in this case requires developing turbine design power with the highest allowable pitchline velocity and least number of turbine stages needed to accomplish the job.

Additional details on turbine staging design for high-energy working fluids are presented in reference 57.

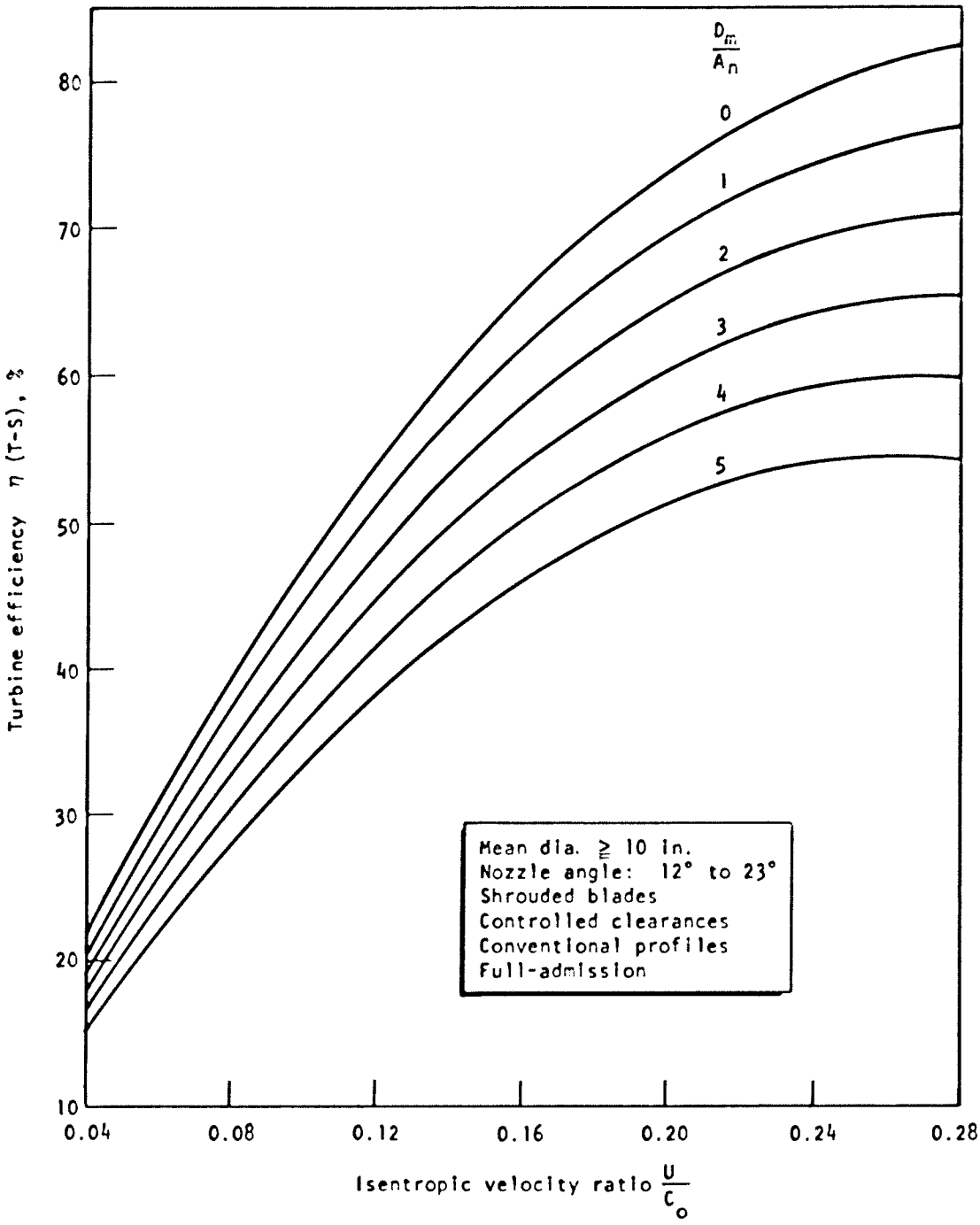

Figure 53. – Efficiency of a two-row VC turbine as a function of U/C_o and D_m/A_n.

3.2 TURBINE AEROTHERMODYNAMIC POINT DESIGN

3.2.1 Gas-Path Energy Balance, Velocity and Pressure Distribution, and Power

The turbine design analysis shall account for pressure, temperature, and energy distribution at all stations in the turbine gas path.

Firmly establish whether the turbine design point is based on nominal or maximum power conditions; mission requirements and engine system studies will establish the design-point conditions.

For evolving the turbine-stage energy balance, gas-path velocity and pressure distribution, and horsepower data at all stations from the stage inlet to exhaust, it is recommended that values for the parameters be tabulated as shown in table VII. The corresponding nozzle and blade design geometric parameters should be tabulated as shown in table VIII. The individual columns designate the nozzle throat (N_t) and nozzle outlet (N_o), the first rotor (1-R), stator(S), and second rotor (2-R) of the two-row velocity-compounded stage being analyzed.

From equation (1), calculate isentropic enthalpy drop for all pressure ratios in nozzles, vanes, and blades. This practice establishes the incremental enthalpy change Δh_s directly and therefore minimizes small variations that can occur if the difference between enthalpies at two pressure levels is calculated.

Establish the enthalpy equivalent of kinetic energy entering the stator or rotor.

Adjust turbine gas-path expansion and kinetic energy, using the respective two-dimensional loss coefficients for expansion energy, kinetic energy, Mach number, and incidence angle as determined from plots like those in figures 16 through 18.

Calculate the total available effective energy Δh_e, using the adjusted expansion and kinetic energy values (eq. 5(b)).

Perform iterative gas-path calculations as the turbine design is developed and pertinent design parameters are changed. Adjust pressures, enthalpy, and velocities.

When establishing flow areas, calculate working-fluid specific volume(s) from static temperatures at the stator and blade exits.

Establish the velocity ratio using the pitch-diameter blade velocity and total effective energy. Check whether the velocity ratio will yield the best attainable efficiency within turbine size and stress limitations.

Table VII. – Illustrative Tabulation of Parameters for Calculating Energy Distribution and Power

Turbine Gas Path Calculation Sheet Date _____

Design One stage, two row, velocity compounded
Flow 6.22 lbm/sec Speed 26 100 rpm
Working fluid data LO_2/LH_2, T_{11} = 1200° F = 1660° R
R = 397, γ = 1.370

Element	N_i	N_o	1–R	S	2–R
Inlet temperature	1660	–	–	–	–
Inlet pressure	580.80	314	123	123	107.8
Outlet pressure	314	123	123	107.8	100.18
Pressure ratio	1.85	2.545	1.00	1.142	1.075
Enthalpy ratio	NA	NA	NA	NA	NA
Inlet relative pressure	122	68.8	NA	42.9	42.45
Outlet relative pressure	66	27.0	NA	37.55	39.10
Inlet enthalpy	2306	1856	1307	1537	1531
Outlet enthalpy	1827	1259	1307	1452	1478
Isentropic enthalpy drop	479	597	0	85	53
Expansion energy coefficient	0.941	0.920	0.832	0.847	0.880
Kinetic energy coefficient-basic	NA	NA	0.664	0.694	0.760
Kinetic energy coefficient-corrected	NA	NA	0.646	0.688	0.725
Effective expansion energy	450	549	0	72	46.6
Effective kinetic energy	NA	450	418	145	58.8
Total effective energy	450	999	418	217	105.4
Outlet velocity	4750	7075	4570	3298	2296
Actual outlet enthalpy	1856	1307	1537	1531	1507
Actual outlet temperature	1422	1126	1250	1247	
Specific volume	12.48	25.25	28.05	31.90	33.91
Outlet area	2.348	3.195	5.50	8.65	13.23
Blade velocity		1424	1424	1424	1424
2 cos α		1.942	1.902	1.888	1.825
Velocity ratio (VR)		0.202	0.312	0.432	0.621
2 cos α -VR		1.740	1.590	1.456	1.204
Diagram factor		0.352	0.446	0.629	0.748
Blading work		351	207	136	79
Exit energy		648	211	81	26
Exit velocity		5700	3250	2016	
Sonic velocity		4440	4665	4670	
Mach number		1.283	0.697	0.431	
Mach no. coefficient		0.986	1.000	1.000	
Sin α		0.233	0.309	0.325	
Cos α		0.971	0.951	0.944	
Cos α -VR		0.769	0.639	0.512	
Tan β		0.303	0.484	0.625	
Exit angle relative to element		16.4	26.4	32.4	
Blade inlet angle		25	32.6	48.5	
Incidence angle		+8.1	+5.7	+16.1	
Incidence coefficient		0.986	0.992	0.954	
Outlet total enthalpy		1955	1748	1612	1533

NA = not applicable

Table VIII. – Illustrative Tabulation of Data on Gas-Path Geometry

Turbine Gas Path Data Sheet — Date _____

Number/Type stages: One stage, two row, velocity compounded
Design horsepower: 5900 HP — Design speed: 26 100 rpm

Element	N	1–R	S	2–R	Remarks
Mean diameter	12.500	12.500	12.500	12.500	
Blade height[a]	0.420	0.530	0.640/0.770	0.880	
Base diameter	12.080	11.970	11.730	11.620	
No. blades	43	97	115	93	
Type blade	Exp. N	Circ. arc.	Circ. arc	Para. arc	
Chord angle	–	78	78	70	
Blade profile	–	–	–	–	
Blade width	0.700	0.596	0.596	0.585	
Blade inlet angle	–	25	32.6	48.5	
Pitch	0.914	0.405	0.342	0.423	
Pitch/Width ratio	1.305	0.680	0.574	0.724	
Opening coefficient	–	0.274	0.292	0.383	
Edge coefficient	0.897	0.882	0.871	0.916	
Sin α	0.233	0.309	0.325	0.405	
α	13.5	18	19	23.9	
Cos α	0.971	0.951	0.944	0.913	
2 cos α	1.942	1.902	1.888	1.825	
Blade design factor	0.989	0.986	0.984	0.993	
Incidence curve	–	1–C–17	1–C–17	1–C–17	
Deflection angle	–	137	128.4	107.6	
Exp. energy coef.[b]	0.941/0.920	0.832	0.847	0.880	
Kinetic energy coef.	–	0.664	0.694	0.760	
Annular area	16.49	20.81	30.21	34.58	
Net flow area[b]	2.348/3.050	5.710	8.690	12.23	
Opening[b]	0.130/0.156	0.111	0.100	0.162	
Annulus coefficient	0.885	1.000	0.986	1.000	

[a]Dual values are entrance/exit.
[b]Dual values are throat/discharge.

Check the velocity distribution as flow passes through the gas path, and determine the influence of blading entrance and exit angles on vector form. Draw a turbine velocity diagram representative of the design-point velocity data. A diagram representative of the design data in table VII appears in figure 54.

To minimize turbine exit losses, minimize turbine exit velocity and design for an exit vector that is closest to an axial direction.

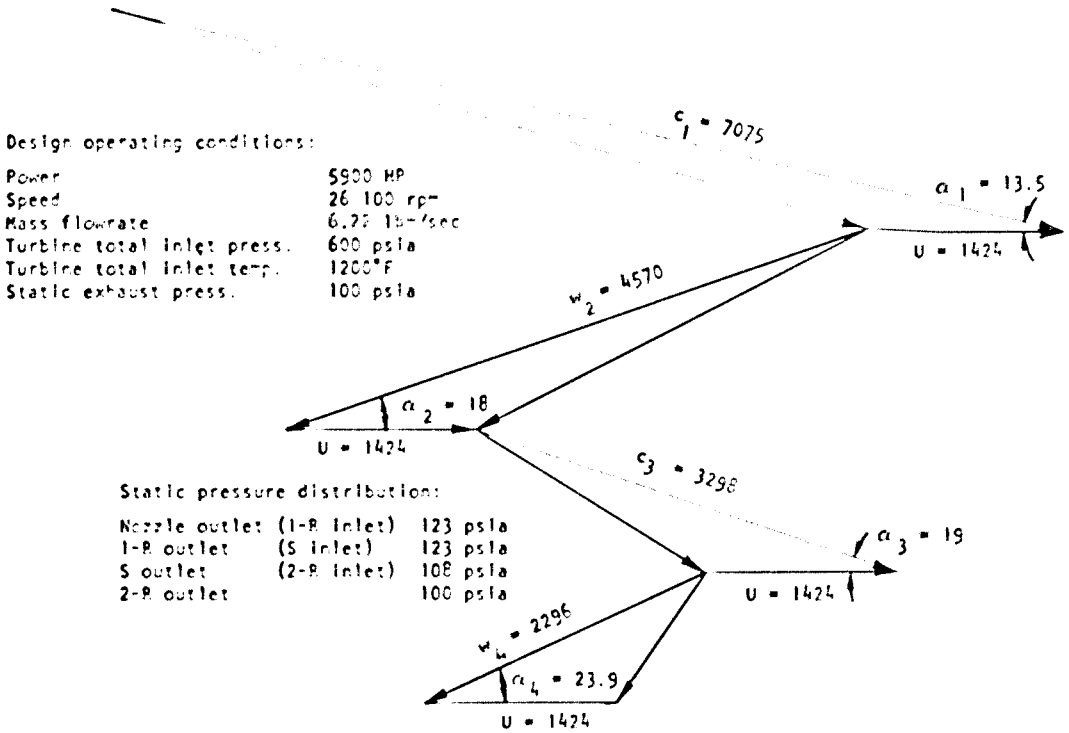

Figure 54. – Velocity diagram for two-row VC turbine.

Obtain η_{td} from equation (11). A diagram efficiency factor c_d, as plotted in figure 55 for a specific value of tip clearance, should be applied to η_{td} to establish the predicted value for turbine total-to-static efficiency η(T-S). Data for c_d appearing in figure 55 was developed from test results on production and experimental rocket engine turbines and from published information on turbines.

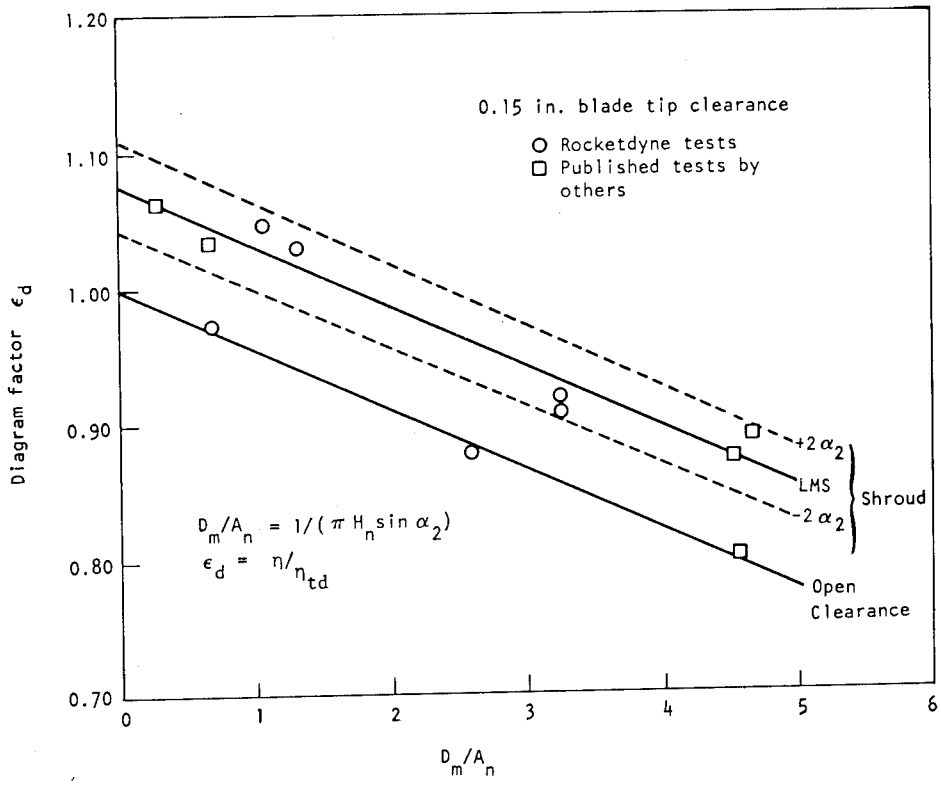

Figure 55. – Diagram efficiency factor vs D_m/A_n.

3.2.1.1 EFFECT OF DESIGN CHANGES

Any change made to the final turbine design state conditions, to the nozzle and blading geometry, or to the mechanical design shall be accounted for in the gas-path design analysis and final blading geometry.

Iterative adjustments should be made to the detailed gas-path analysis for all changes that affect gas-path areas, turbine performance, or final geometry.

Consistency must be maintained among the design values for working-fluid temperature and properties; pressures; distribution of energy and developed power; blading inlet and exit angles; and gas-path areas.

Care should be exercised to maintain work distribution among turbine rows without overloading either the fore or aft rotors when relevant changes are made to the design.

3.2.1.2 ENERGY BALANCE

The turbine design procedure shall include a turbine energy balance.

On completion of the gas-path analysis, prepare a turbine energy balance summary that tabulates the enthalpy losses from turbine inlet to exit. This summary should include losses in expansion and kinetic energy, turbine exit losses, an accounting for performance adjustments, and a summation of turbine work; any additional factors that influence the energy distribution in the gas path should be accounted for. In addition, account for all temperatures, pressures, enthalpies, and work on an enthalpy-entropy diagram as shown in figure 15.

3.2.1.3 PRESENTATION OF DATA

Turbine performance data shall be expressed in a form suitable for supporting associated engine studies.

Use torque/speed parameter maps as shown in figure 56; these maps are more useful than plots of velocity ratio versus efficiency because pertinent turbine performance data can be obtained directly from the curves. (The torque/speed parameter data plotted in figure 56 represent performance of the production F-1 turbine.)

3.2.1.4 VALIDITY OF ANALYSIS

The design analysis shall confirm that the logic and output data of the turbine computer program are consistent with the specific needs of the gas-path analysis.

Output data from computer programs utilized for turbine calculations, parametric studies, and lengthy gas-path analyses should be hand checked to substantiate computer logic, proper use of design coefficients, and performance data. In addition, make periodic checks to ensure that the program is functioning properly for the design being analyzed.

3.2.2 Partial-Admission Turbine

3.2.2.1 ARC OF ADMISSION AND BLADE HEIGHT

The final design of the partial-admission turbine shall allow for effects on performance of variations in turbine arc of admission and blade height.

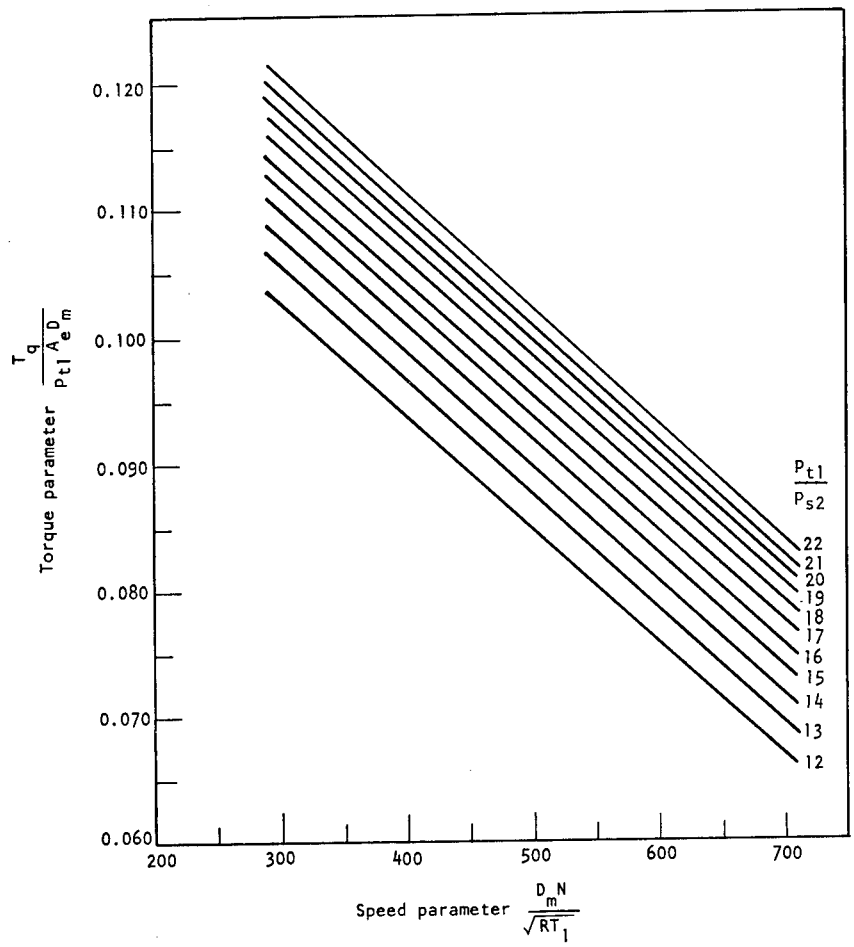

Figure 56. – Typical map of torque parameter vs speed parameter.

Evaluate performance tradeoffs as blade heights are increased and turbine arcs of admission are varied.

Determine whether changes in pitch diameter for the partial-admission design will contribute to attaining the operating-point velocity ratio and efficiency.

Establish whether an overall turbopump operational gain is attainable when pump design speed is varied; the effect from loss in pump performance may be less than the net gain in the partial-admission-turbine efficiency.

Note that as the arc of admission decreases from 100 percent to small percentages of admission, the peak turbine efficiency is attained at proportionately reduced values of design velocity ratio. This shift in peak efficiency is illustrated in the curves of velocity ratio vs stage efficiency in figure 20, and also is noted in Stenning's work (ref. 16).

Analytical techniques for predicting interstage energy quantities and losses between two successive (non-reentry type) partial-admission stages have not been adequately developed; these design variables should be established by turbine development testing. If the first stage arc of admission is small, exit kinetic energy sustains a minimum 50-percent loss before entering the partial-admission second-stage nozzle; when this loss is coupled with partial-admission losses, the effect on overall two-stage performance is excessive. Therefore, a small arc of admission should be avoided in applications requiring high turbine efficiencies.

Two-stage turbines designed with partial-admission first stages and full-admission second stages should be designed with as large an axial spacing between the first-stage rotor exit and second-stage nozzle entry as the turbine assembly allows, so that interstage losses are held to a minimum.

3.2.2.2 DISTRIBUTION OF NOZZLE ARC

The distribution of the nozzle arc shall result in best attainable performance and minimum susceptibility to blade vibration.

The partial-admission nozzle arc should be continuous and should not be distributed around the circumference. Tests have substantiated the advantage of a continuous nozzle discharge arc. The efficiency plot in figure 57 illustrates how efficiency in a 50-percent-admission turbine declines when the nozzle discharge arc is changed from one continuous 180° arc to two, three, six, and eighty-five evenly spaced sections.

The recommendation for a continuous nozzle arc may sometimes have to be violated (and efficiency penalized) in designs that cannot sustain the uneven loads applied to the rotor by a continuous partial-admission nozzle.

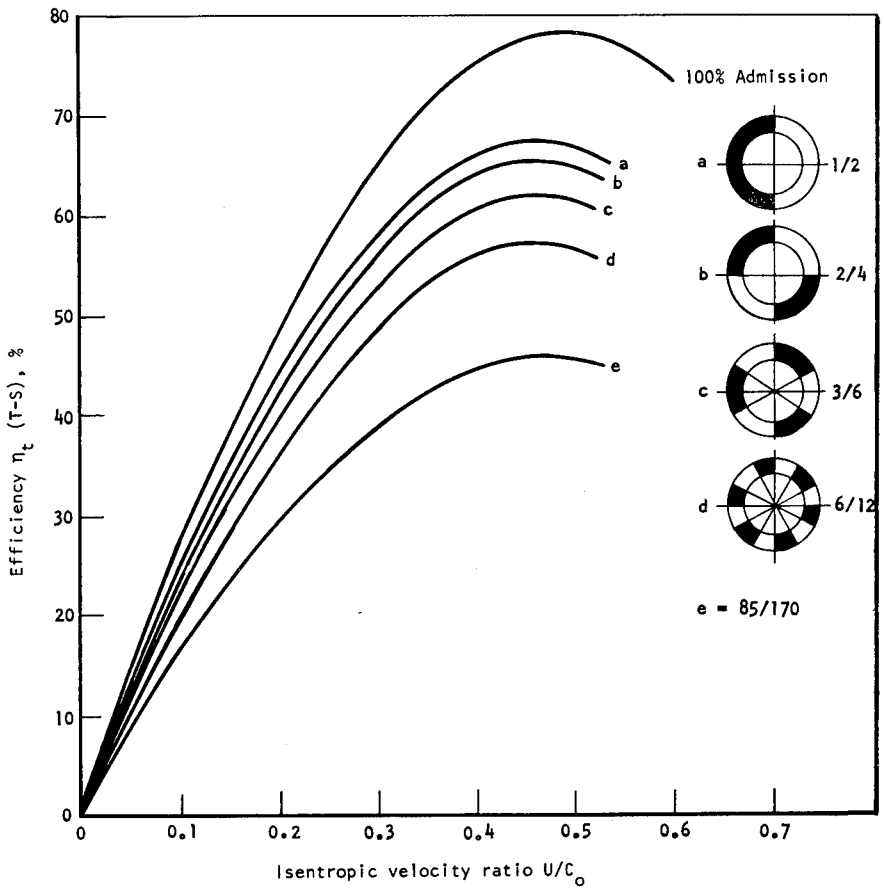

Figure 57. — Effect of nozzle arc arrangement on efficiency of a partial-admission turbine.

3.2.3 Stage Reaction

3.2.3.1 PRESSURE GRADIENTS

Impulse blading for two-row, velocity-compounded staging shall have a degree of reaction that precludes pressure gradients from developing at the blade roots.

Ten-percent reaction is recommended in a two-row, velocity-compounded stage design as a precaution against adverse blade-root pressure gradients; two-thirds of this reaction should be assigned to the second-row stator, and one-third to the second-row rotor. No reaction is prescribed in the first-row rotor. Slight adjustments in reaction percentages may be made during subsequent gas-path design iterations to obtain agreement among the path state conditions, energy distribution, and geometry.

3.2.3.2 EFFICIENCY VS BLADE SIZE

The degree of stage reaction shall help establish blading vector relationships that develop the highest efficiency with the smallest size blading.

Reaction staging should be designed with 35- to 50-percent reaction for operation in the range of best efficiency. An increase in the degree of reaction should be considered for new designs that exhibit overstressed blade conditions resulting from blade height requirements. A decrease in required flow area and blade height is realized as the percentage of reaction (and the velocity of the working-fluid passing through the rotor) increases. The reaction adjustment may slightly compromise turbine performance in order to obtain a blade height that does not exceed stress limitations. The following should also be evaluated to determine the corrective action to the blade-height/stress problem that least affects performance:

(1) Establish the gain in flow area that results from increasing blade exit angles.
(2) Evaluate the effect of adjustments in turbine speed and pitch diameter on flow area and performance.
(3) Determine whether throat opening and unguided turning can be increased.

The gas-path analyses should be adjusted to reflect any design perturbation of pressure ratio, stage reaction, and energy distribution.

3.2.4 Intake Manifold Sizing

The inlet manifold shall produce a minimum pressure loss and shall contain sufficient area to ensure the required flow of turbine working fluid at all operating conditions.

Pressure-drop allocation between the turbine inlet and nozzle inlet should be minimal consistent with requirements of the design. In gas-generator-cycle designs, limit the manifold pressure drop to a maximum of 2 percent of the available turbine inlet pressure; in staged-combustion designs, use axial-entry inlet manifolding to minimize losses. Avoid the use of sharp bends at the manifold entrance and include turning vanes adjacent to the manifold inlet, as shown in figure 44, if the inlet is perpendicular to the flow in the manifold.

Designate a flow velocity of Mach 0.25 to 0.30 when calculating required manifold areas, and increase manifold flow capacity 10 to 20 percent above the design flowrate as a precautionary measure against unforeseen manifold pressure losses. Constant-diameter torus designs should be designated whenever possible; they are easier to fabricate and less costly than constant-velocity configurations. Manifolds may be designed with noncircular cross

sections to comply with turbopump length and envelope requirements if pressure and flow characteristics are not penalized.

3.3 NOZZLE, VANE, AND BLADE GEOMETRY

The nozzle, vane, and blade geometry shall develop the required gas-path vector relationships and shall pass the working-fluid mass flowrate at design operating conditions.

Profile layout drawings should be adequate to maintain consistency among nozzle, vane, and blade designs. Appropriately scaled drawings 10- to 20-times actual size should be used to establish accurate design layouts of blade shape(s), gas path, and flow areas. The blade layout should be initiated for design conditions at the pitch diameter. Blading pitch and chord should be selected initially as a function of the blade loading coefficient; subsequent adjustments will be required as other blade design constraints become evident. The entrance and exit angles and flow areas established during the gas-path analysis are now utilized to initiate the development of pressure and suction surfaces as described in section 3.3.2. Completed blading profiles should contain smooth transitions from the entrance to exit planes and exhibit a convergence of the flow channel from the blade inlet to the minimum flow section (where the blade opening O is designated). Profile sections with large amounts of local turning should be avoided because they will produce unnecessary and therefore unacceptable local acceleration of the working fluid.

If the blading is being designed for radial equilibrium, use the geometry at the mean diameter as a reference for establishing entrance and exit angles and profile adjustments from the blade root to the tip.

A side-view layout of the whole turbine gas path should be drawn 10- to 20-times scale to define the height and width sizing relationships between adjacent nozzles and blades. This large-scale drawing also serves to develop and help illustrate details of blade spacing, blade-to-disk retention, and sealing provisions.

Convergent and divergent sections upstream and downstream of the nozzle throat should be designed into the nozzle side walls whenever possible, and the inner and outer radii should be maintained constant for the length of the nozzle. Throat sections that are capable of being physically measured should be designated.

References 58 and 59 expand the subject matter presented in this section.

3.3.1 Leading and Trailing Edges

3.3.1.1 INLET ANGLE

The blade inlet angle shall have zero angle of incidence relative to the working-fluid inlet vector angle.

The blade inlet angle should be set at the same value as the working-fluid inlet vector angle to obtain a line-to-line angle relationship between the incoming gases and the blade leading edge. This practice also applies to nozzle vane designs and to blades designed for radial-equilibrium conditions. As the inlet vector angle increases from root to tip, the blade inlet angle should be increased accordingly in the blade layout.

3.3.1.2 TRAILING-EDGE RADII

Trailing-edge radii shall minimize exit losses without sacrificing required structural strength.

To avoid excessive exit-wake losses, the nozzle and blading trailing edges should be designed with edge-coefficient values that are not less than 0.90. Establish a preliminary value for blade stress as the blade profile and height are initially developed and adjust the trailing-edge design to the minimum allowable thickness. When calculating blade stress, make sure that all critical flow areas and blading cross sections include allowances for fillet areas. Fillet areas normally vary between 0.75 and 1.25 percent of the flow area at the throat section.

The blade opening is measured at the point of tangency where the blade pressure surface meets the trailing edge radius. Whenever the trailing-edge configuration and the pitch are adjusted, care should be exercised that the proper follow-up calculations are made to verify that flow-area requirements are maintained.

3.3.2 Pressure and Suction Surfaces

3.3.2.1 VELOCITY CHANGES

Pressure and suction surfaces shall not generate or contribute to unacceptable gas-path accelerations.

Localized accelerations and losses resulting from pressure and suction surface discontinuities and excessive turning rates should be avoided by observing the construction relationships

described herein during the development of these profile surfaces. To initiate the blade design, use entrance and exit vector angles established during the gas-path final analysis. For circular arc blading, designed with parallel sides and containing no provisions for radial equilibrium, the blade inlet angle β_1 should be equal to the entrance angle formed by inlet vector w_1. The entrance angle is drawn as illustrated by the mean inlet angle β_1 in figure 23. The exit vector angle α_2 fixes the blade trailing-edge geometric angle β_2; it forms the straight-back portion of the suction surface. Calculate preliminary values of pitch, required opening, and blade chord. Between the time the design is initiated and the time the final designs are found satisfactory for fabrication, these values should be adjusted to obtain proper geometric relationships among all the design parameters.

Initiate the blade layout as follows: (1) set chord angle between 45° and 70°, (2) draw in the mean entrance angle β_1, and (3) draw the exit angle β_2 that becomes the straight-backed exit portion of the suction surface. Construct the trailing-edge radius. Layout the leading edge as an ellipse, if this is permitted by the geometry, and include the leading-edge angles β_{1p} and β_{1s}. If an ellipse can't be used for the blade being designed, use a circular section. Construct the pressure and suction surfaces with circular arcs as illustrated in figure 23.

Before the pressure and suction surfaces can be utilized in acceptable profiles, the profile layout may require adjustments in circular arc radii, chord angle, divergence angles, and pitch. Numerous trial layouts usually are drawn before a configuration that satisfies all the design requirements is developed. Resort to the use of drawing overlays to expedite the initial drawing phase. Draw the suction surface of the adjacent blade to establish the flow-path geometry; this surface must provide a continuous rate of convergence from entrance to exit. Check the required opening (O) and pitch (p) dimensions and calculate the total flow area for the nozzle or rotor; include the allowances for fillets as noted above. Establish preliminary blade stress data on the basis of this initial layout. If the blade is not overstressed, continue design checks as outlined in sections 2.3.3 through 2.3.7.

The development of parabolic pressure and suction blade surfaces is accomplished with the same basic approach as described above for circular arc blades. As before, the blade inlet angle β_1 is drawn equal to the angle formed by the inlet vector w_1. The blade exit angle β_2 is established by adjusting the exit-vector angle for efflux-angle deviation as described in section 3.3.3. After constructing the blade chord angle and inlet and exit angles, the leading- and trailing-edge divergence angles are established as illustrated in figure 22. Initiate the design with a total divergence of 25° to 30° at the leading edge, and 6° to 10° at the trailing edge. Lay out the leading edge with a preliminary selected ellipse, and lay out the trailing edge with a radius yielding a minimum trailing-edge thickness. Construct tangent parabolas at the pressure and suction surfaces as illustrated in figure 24.

If radial-equilibrium conditions are to be incorporated into the blading design, root and tip profiles are developed with entrance and exit angles prescribed by the radial-equilibrium analysis performed at this juncture in the design.

Highly loaded blade designs may limit the construction of tangent parabolas at the suction and pressure surfaces. For a design that requires excessive adjustments in the suction surface, a combination tangent-parabola and circular-arc construction is recommended. The profile sections adjacent to the leading and trailing edges are developed as tangent parabolas, and the midsection of the profile is evolved with an adjoining circular arc.

3.3.2.2 FLOW-AREA CONSISTENCY

Any change in blading design necessary for structural reasons shall not result in a change in blading flow area

The recommended practice for modifying blade designs in which stresses exceed the maximum allowable blade stresses is to simultaneously reduce blade height and increase throat opening by adjusting the suction surface profile to pass the required mass flow. This is accomplished as follows:

(1) Adjust blade height to the maximum value allowed by blade stresses.
(2) Increase the amount of unguided turning (sec. 3.3.4) downstream of the blade throat and adjust throat opening.
(3) Exercise care to distribute the increase in blade-path throat opening at the root and tip.
(4) Draw the blade throat section after the root and tip profiles are developed so that the physical blade flow area agrees with that required by the gas-path analysis.
(5) Always include fillet area provisions in all calculations of blade-path area.

For those designs that cannot accommodate the required flow area after a blade height reduction is attempted as described in (1) through (5) above, the following practices are recommended:

(6) Decrease the exit turning to effect an increase in throat area.
(7) Vary the pressure ratio (or reaction) across the gas-path element to increase the exit vector velocity and in turn reduce required flow area.

In cases (6) and (7), the gas-path analysis will have to reflect the effect these changes have on turbine performance and on overall gas-path geometry (ref. 14).

3.3.3 Deviation of Exit Vector Angle

Exit turning in subsonic vane and blade designs shall be sufficient to correct for exit-flow deviation

An exit-flow deviation correction should be made in terms of additional turning applied to the physical blade design; this correction is applied to the exit angle established by the gas-path exit vector. The recommended correction is made on the basis of exit-vector velocity and angle noted in figure 25.

3.3.4 Unguided Turning

Unguided turning in subsonic blading gas paths shall provide an improved transition from entrance to exit and preclude excessive turning rates.

Unguided turning should be incorporated into the blade suction profile, downstream of the throat, to distribute the total blade turning across a longer portion of the blade surface and prevent local accelerations caused by uneven turning rates. Turning in the flow channel should be allowed to continue beyond the throat section an additional 8° to 12° at the blade root, and up to 15° at the tip. If a design requires a total turning of 130° and 10° of unguided turning is incorporated, then 120° of turning should be used from the blade entrance to the throat. The additional 10° of unguided turning continues until it is tangent with the required blade discharge angle β_2. This point of tangency does not necessarily extend all the way to the trailing edge. The blade illustrated in figure 24 is designed with unguided turning.

3.3.5 Pitch

Blading pitch shall provide maximum control of flow path with minimum friction loss.

The pitch parameter, which is used to establish the number of vanes and blades designated in each stage, should be initially established in parametric form as a function of gas-path inlet and exit angles and the Zweifel loading coefficient (eq. (17)). The recommended Zweifel coefficients for nozzle design range from 0.7 to 0.95, and for blading from 0.90 to 1.15. Blade designs have been successfully developed with values down to 0.75; this type of deviation involves a degree of risk in attaining predicted performance.

Initially establish a blade pitch based on nominal values of the Zweifel coefficient. After obtaining agreement between the initial pitch value and the physical requirements of blade chord, height, throat opening, and area relationships, the blade layout is initiated. Pitch may again have to be modified because of blade-number/vibration constraints or because of profile and area limitations that develop during profile design process.

For straight-backed impulse blading, pitch should be established as a function of the gas exit vector angle as designated by the O'p plot presented in figure 27. Subsequently establish a pitch/chord ratio and initiate a preliminary blade layout drawing. The blade inlet and exit angle(s), pitch, opening, and flow-area geometric relationships should be drawn before the profiles are developed.

3.3.6 Radial-Equilibrium (Free-Vortex) Blading

Blading that is greater than one inch in height shall comply with radial-equilibrium conditions.

For compliance with radial-equilibrium conditions, all blading designs that are greater than one inch in height[1] should be analyzed from root to tip to determine the required variations in inlet and exit vector angle. The analysis can include as many radial sections as required to define the vanes and blading being designed. Three sections are generally sufficient to define the change in geometry from the root to the tip. The x and y coordinates that define the blading pressure and suction surfaces should be displaced at the defining sections, from root to tip, to accommodate the twist developed along the length of the blade. Thus all x and y coordinates from root to tip are in line from the blade entrance to exit. In the process of establishing the product of blade radius R and tangential velocity c_{u1} for equilibrium conditions, the static-pressure variations from root to tip are also established. The analysis, as described in reference 34, will develop the required inlet and exit vectors at all radii that are analyzed. Vector diagrams should be drawn and studied to establish consistency among vector angle and velocity relationships from blade root to tip.

No corrections for Reynolds number effects should be made in designs that utilize high-energy working fluids in the turbine inlet temperature range from 1200° to 1700° F and operate above the critical pressure ratio. Performance adjustments are required if design Reynolds numbers fall below values of 10^6.

For reasons of expediency, the use of a computer program is recommended when performing radial-equilibrium analyses. The program logic is not complex and should be written to dovetail with the output data from the turbine gas-path analysis.

3.3.7 Blade-Path Velocity Distribution

Analytical predictions of blade-path velocity distributions shall verify that no unacceptable accelerations exist on pressure or suction profiles.

[1]When blade height is less than 1 in. and greater than 0.6 in., and hub-to-tip ratio is approximately 0.9, use a radial-equilibrium blade for maximum performance. However, the justification for this blading must be great enough to override the greatly increased cost of manufacturing involved in producing this kind of blade.

On completion of a new blade profile design, velocity distributions on the pressure and suction surfaces should be established analytically. A properly designed blade will show no signs of excessive accelerations. The recommended method for calculating these velocity distributions is described in reference 29. The analysis is accomplished with a computer program whose output data are plotted to describe the velocity variations as flow progresses through the blade path. The blade design is adjusted if a local acceleration is noted along its profile. This effect is most often caused by excessive blade curvature and generally requires a redistribution of turning along the blade surface. Whenever a blade profile requires modification to correct for excessive local gas-path accelerations:

- Check whether additional unguided turning can be utilized downstream of the throat.
- Redistribute high rates of local turning along the profile surface.
- Evaluate the effect of reduced total blade turning on stage performance.
- Reestablish the velocity distribution after modifying the blade profile.

It is appropriate to note at this point that the designer must be constantly alert to the effect on predicted turbine performance resulting from adjustments to blade profiles and gas-path conditions during the blading design process. The designer should determine the influence of all blade and gas-path revisions upon energy distribution and power-producing capability of the turbine. If physical changes are required by a single blade row, a check of its effect upon the overall pressure distribution from turbine inlet to exhaust is recommended. If necessary, a new turbine gas-path design analysis should be performed to obtain agreement between physical design and gas-path design parameters.

3.3.8 Blade Shrouding and Clearance

Turbine blading shall sustain minimum blade tip clearance loss.

High-performance turbines should be designed with shrouded turbine rotor blades containing tip labyrinths that seal against stationary honeycomb seal strips mounted on the casing. Rotors are installed with zero clearance between the blade labyrinths and honeycomb seals; during initial turbine operations, the labyrinths wear sealing grooves in the honeycomb materials. Felt-metal may also be utilized for sealing with blade tip labyrinths.

Turbines that cannot incorporate a honeycomb-type seal with zero clearance should be designed with the smallest tip clearance allowed by the rotor installation. The recommended tip clearance is one percent of the rotor blade height. When establishing tip clearance:

- Check the effect of bearing axial and radial displacement on tip clearance.
- Establish the influence of shaft radial displacement during high speeds.
- Account for pressure differentials and temperature effects on seal displacement.

An interlocking rubbing shroud as shown in figure 58 is recommended for providing damping and resistance to blade torsional motion. Bumping-type shrouds should be used to reduce natural frequency (by added tip mass) and thus avoid resonance, or to limit the magnitude of blade vibratory motion to the clearance between shrouds.

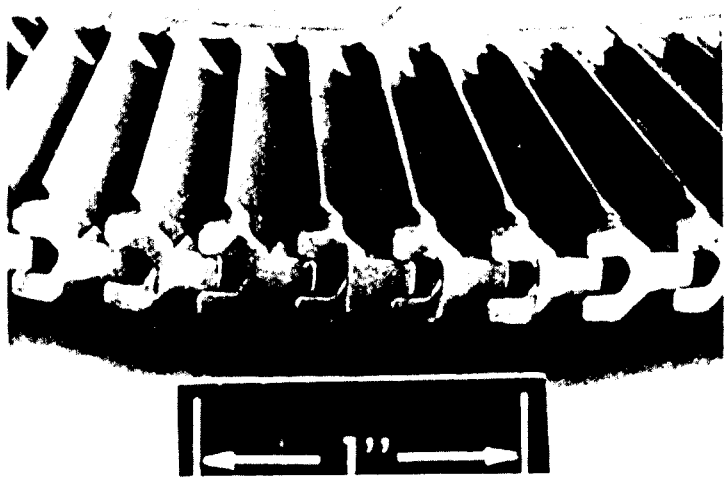

Figure 58. – Interlocking rubbing shroud.

Unshrouded blading designs should have provisions for recessing the blade tip clearance volume into the turbine casing as a circumferential groove adjacent to the blade tip. The blade tip should extend a minimum of 0.005 in. into the clearance groove.

3.4 MECHANICAL DESIGN AND STRUCTURAL ANALYSIS

Turbine structural integrity shall be ensured by safety factors adequate for the application.

The design of turbine components should be based on mechanical design parameters that are in excess of predicted maximums. This practice compensates for uncertainty in predicting the exact conditions represented by the maximum operating loads. The mechanical design speed should be 10 percent greater than the predicted maximum speed, and pressures and torques 20 percent greater than the expected maximum values. For thermal loading considerations, use temperatures equal to the predicted maximum values.

Turbine components should be designed with adequate safety factors on primary stresses maintained to both yield and ultimate strengths. For manifolding, casings, shafts, structural supports, and fasteners, incorporate a safety factor of 1.5 on ultimate (FS_u) and a safety factor of 1.1 on yield (FS_y). These factors should be based on the use of minimum guaranteed material properties and mechanical design stresses.

Turbine components should also be designed with adequate safety factors on the total imposed cyclic strain, including both primary and secondary stresses. Secondary stresses are limited by low-cycle fatigue considerations, because a small change in imposed strain will result in a large change in life. The design safety factor should be applied to the strain rather than to life. Maintain safety factor of 1.4 on the strain that will produce failure in the required number of duty cycles. This factor is applied to the total strain cycle, including effects of primary and secondary loads, for the mechanical-design conditions; minimum material fatigue properties are used. For long-life applications, a more conservative approach for low-cycle fatigue is to apply the safety factor to the number of cycles. A fatigue safety factor of this kind should be based on cycles to failure and should be no less than 4; i.e., the number of cycles to failure should be four times the number of duty cycles.

3.4.1 Blading

3.4.1.1 MECHANICAL DESIGN

3.4.1.1.1 Structural Adequacy

Turbine blading shall withstand all predicted mechanical and thermal stresses.

Both steady-stress and fatigue considerations should be included in the determination of blade structural adequacy. The recommended safe operating stress range is indicated in the modified Goodman diagram appearing in figure 33. This safe operating region is based on mechanical-design stresses at the worst-tolerance conditions. The indicated limitations must be imposed on all critical locations in the blade; these generally include the root-fillet tangency point and the neck of the mechanical attachment. Additional locations such as the area adjacent to the tangency point of the hole fillet should also be examined.

To establish an optimum design with a minimum number of iterations, it is recommended that a plot of $A_a N^2$ versus temperature, like that shown in figure 30, be used in establishing the preliminary design.

3.4.1.1.2 Blade Attachment

The method of blade attachment shall provide required strength and reliability with minimum weight, ease of fabrication, and low cost.

The designer should evaluate which of the following techniques of attaching blades to disks best meets design and application requirements:

(1) Cast blades with fir-tree attachments to the disk
(2) Blades integrally machined with the disk
(3) Cast blades mechanically retained with split disks.

Method (1) normally best meets the needs of production designs. Initial tooling costs can be distributed for the number of assemblies fabricated during the production run. This method generally is recommended except for specialized applications treated below.

Experimental or prototype designs, which have hardware requirements for only one or two assemblies for performance evaluation purposes, should be integrally machined with the disk. Configurations that contain tip shrouds, however, are difficult and costly to machine in this manner.

Prototype and model turbine rotors that undergo performance evaluation tests with cold gases instead of high-temperature working fluids can be assembled with cast blades that contain cast retaining sections below the blade root section in place of comparatively expensive machined fir-trees. This design normally is used with split-disk sections that part axially and retain the blades below the blade root.

Extreme care should be exercised with designs that utilize blading welded to the disk. Welds are prone to develop cracks. In addition, weld geometry, tooling, and welding techniques have to be developed. Welding can be expensive and troublesome when compared to alternate attachment methods discussed above.

3.4.1.1.3 Blade-Root Geometry

The geometry of blade-root fillet and blade-central-hole bottom shall not result in overlapping stresses.

The turbine-blade central-hole/fillet-radius tangency points should not coincide with those of other blade fillet radii. The tangency point for the lightening-hole/fillet radius should be positioned outboard of the blade-to-platform fillet (fig. 31) to eliminate interaction between the two stress concentrations. In addition, the blade-to-platform fillet radius should be greater than the leading- and trailing-edge thicknesses to minimize the stress concentrations at these critical points.

3.4.1.1.4 Stacking

Stacking of rotor blades shall compensate for the power bending moment and minimize undesirable bending moments.

The blades should be stacked with the centers of gravity of the shroud and blade positioned to induce a centrifugal bending moment that will compensate for the power bending moment at the critical locations in the blade and attachment and minimize other centrifugal bending moments. The stacking should be accomplished by shifting the shroud and blade and by tilting the blade to minimize the stresses at each of the critical locations.

3.4.1.1.4.1 Tolerances

The blading dimensional tolerances shall maintain the beneficial effects of stacking and tilt.

To maintain the benefits of blade tilt and stacking, tolerances consistent with the severity of the stress field should be established. Blade thickness variations of 0.003 and 0.004 in. are recommended in highly stressed blades. The influence of tolerance variations upon blade natural frequency should be established.

3.4.1.1.5 Axial Spacing

Axial spacing between nozzles and blades shall have a minimal effect upon vibrational excitation of the blades.

The axial spacing between the trailing and leading edges of adjacent vane and blade rows influences the magnitude of vibratory force on the downstream blade; the disturbance is reduced with increased axial distance. A nominal spacing equal to 25 percent of the chord length of the upstream stator is recommended for minimum vibrational excitation.

3.4.1.1.6 Tip Clearance

In turbines without honeycomb seals adjacent to blade tip labyrinths, tip clearances shall be adequate to prevent rubbing.

Tip clearances should be designated large enough to avoid rubbing during operation at design conditions, during thermal transient conditions, and during passage through rotor critical speeds. Premature fatigue failures normally will result from vibratory stresses induced by the rotor blade tip rubbing the stationary housing during operation. Selection of the minimum running clearance should also include the effects of thermal and centrifugal growths, tolerance stackups, shaft runouts, and rotordynamic deformations.

3.4.1.1.7 Blade Resonance

Blades shall be free of vibration resonances within the turbine operating speed range.

The basis for this condition is developed in section 2.4.1.2. Once the natural frequencies are calculated, however, it is essential that a 15-percent margin be maintained between the operating speeds and resonant speed (fig. 34). The first and second harmonics of the first tangential bending mode and the first harmonic of the second tangential bending mode are of primary concern. Additional modes may be of interest in marginal cases.

The analytical prediction of blade natural frequencies is based on simplified assumptions; therefore, laboratory vibration testing of rotor blades is recommended to verify the predicted results for each blade design. The natural frequencies of stator blades normally are far enough from the operating speed range that vibration testing is not required.

3.4.1.2 STRUCTURAL ANALYSIS

The structural analysis shall verify that the combined stress at all locations on the blade is less than the prescribed allowable stress.

Calculate direct centrifugal stress σ_c, centrifugal bending stress σ_{cb}, and gas gending stress σ_p from equations (22), (23), and (24), respectively; then obtain mean stress σ_m from equation (25).

In using equations (22) and (23), make sure that K_t' is established as a function of fillet radius and blade thickness from a curve like that shown in figure 32. Note also that section moduli must be calculated about the maximum and minimum blade axes.

In using equation (24), note that the moments about the principal axes should reflect maximum and minimum power conditions at which the turbine operates.

Determine vibratory stress from equation (26) or (27), paying particular attention to the conditions under which these equations are to be used. Verify that the blade will operate in a safe operating range (figures 33 and 34). Verify analytical results by component vibration testing.

Calculate thermal stress (for long-life applications) by the technique given in reference 39.

3.4.2 Nozzle

3.4.2.1 CONFIGURATION

The nozzle configuration shall provide for thermal growth and transmission of structural loads without disrupting the orientation of gas-path flow angles.

Designs that transmit turbine casing loads through the nozzle should concentrate the loading through the heavy leading-edge section of the nozzle vane. Maintain thickness relationships that provide uniform thermal expansion and avoid large thermal strains. However, in high-horsepower turbines operating above 1200° F and 500 psi, the recommended practice is to separate the manifold/nozzle assembly from the turbine casing, as shown by the design in figure 7. The manifold and nozzle thus are not subjected to casing loads.

3.4.2.2 PASSING FREQUENCY

Nozzle passing frequency shall not coincide with any rotor blade natural frequency and thereby excite resonance.

The following nozzle vane and rotor blade corrective practices should be evaluated for use in a given application whenever the relation of forcing frequency to natural frequency requires adjustment:

(1) Add or modify turbine blade shrouds.
(2) Vary blade dimensions and weight.
(3) Change number of nozzle vanes.
(4) Increase or decrease turbine (turbopump) design speed.
(5) Include blade damping devices.

3.4.2.3 FLOW-AREA CONSISTENCY

The nozzle flow area shall remain constant enough to ensure consistency in flow characteristics in production-run turbines.

It is recommended that the required physical nozzle flow area be noted on design drawings as a functional dimension. All component flowchecks that establish nozzle effective area should be accomplished with the test nozzle assembly installed in series with a calibrated orifice.

Cast nozzles are recommended for new turbine designs in preference to machined or welded configurations; a cast nozzle will provide the best dimensional accuracy consistent with ease of fabrication and low cost.

3.4.3 Stator

The stator shall sustain the power torque, provide thermal flexibility, and withstand predicted loads.

Size the support struts, retaining flanges, and vanes so that adequate rigidity and firm alignment are maintained under all test and operational loads.

Radial growth should be provided for in the design by allowing the stator vane to expand as follows:

(1) Incorporate a gap at the junction to the stator inner shroud, as shown in figure 59; provide for a seal at this gap to maintain gas-path pressure distribution.
(2) Provide thin yielding cylinders and diaphragms.
(3) Provide radial freedom at the retention point.

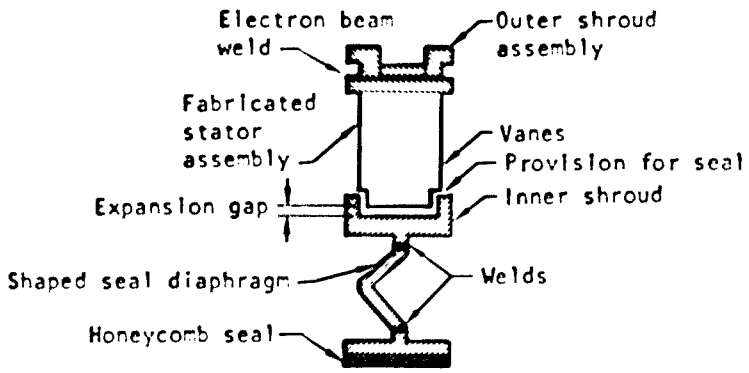

Figure 59. – Stator design with radial expansion gap.

Position the stator with retaining techniques as shown in figures 6, 36, and 37.

Honeycomb seals (figures 5 and 59) should be installed on casing sections that do not deflect and thereby distort the sealing surface. Provide sufficient cross-sectional area in the retaining flange for the seal strip so that a structurally sound honeycomb seal can be welded or brazed without difficulty.

Stators operating above 1100° F should be designed with multivaned segments or with individual stator vanes, whereas low-horsepower, low-temperature units should be cast, single-ring configurations.

To prevent overloading the stator in highly loaded stage designs, avoid transmitting external loads through stator vane assemblies, particularly in the manifold nozzle vanes. A monocoque or other supporting structure is recommended for carrying the loads around the stator vanes, thereby allowing the stator assembly freedom of thermal motion. Figure 7 illustrates this type of configuration.

3.4.4 Rotor Assembly

The dynamic loading on the rotor assembly shall be as low as possible.

The dynamic loading should be minimized by following the design practices given below and by proper balancing. Specific rotor balance limits should be noted on the rotor assembly drawing.

The required balance accuracy must be established from the limitations on radial bearing load, shaft bending, and shaft deflection. A low-speed (1000 to 2000 rpm) multiplane balance has proved adequate for most applications.

It is recommended that the basic rotor component be balanced and subsequently rebalanced as each component is added. In the assembly, each additional correction should be made on the added component. When the low-speed balance is inadequate or a very accurate balance is required, balancing at the design speed is recommended.

3.4.4.1 DISK

3.4.4.1.1 Configuration

Disk geometry shall not induce inplane bending.

The turbine disk should be designed with an axially symmetrical profile to obtain a configuration that will experience a minimum bending-stress contribution from disk geometry. To further minimize stress, it is recommended that the transition radius located between the rim and neck of the disk be generously sized to minimize stress concentrations.

3.4.4.1.2 Structure

3.4.4.1.2.1 Speed Capability

The rotor disk shall have adequate margins on burst and yield speeds.

It is recommended that the disk be designed to have (1) a burst speed equal to or greater than 120 percent of the maximum design speed and (2) a yield speed equal to or greater than 105 percent of the maximum design speed.

3.4.4.1.2.2 Yield Strength

The stresses within the disk shall not result in unacceptable yielding of the disk.

It is recommended that a safety factor be maintained on the maximum radial stress and rim tangential compressive stress for the mechanical-design conditions so that yielding does not occur. A factor of 1.1 is recommended.

3.4.4.1.2.3 Critical Speed Margin

The disk shall have an adequate margin between the operating speed and the lowest critical speed.

Limit operation to speeds at or below 85 percent of the lowest critical speed of the second and higher diametral modes to ensure a structurally adequate design. A disk found to operate at or near critical speeds should be modified to correct potential critical-speed problems. The following practices are recommended:

(1) Vary thickness of the disk.
(2) Adjust turbopump speed.
(3) Structurally couple a two-row disk configuration with a large-diameter curvic coupling.
(4) Redesign a single-row curvic into a double-row curvic coupling.

3.4.4.1.3 Structural Testing

3.4.4.1.3.1 Spin Test

Disk spin tests shall satisfy quality-control requirements and shall preyield localized high-stress areas

It is recommended that the configuration of the disk during spin test be as near as possible to the final configuration with exception of the blade area, where a solid mass may be left to simulate blade weight. All noncritical surfaces should be machined to their finished dimensions and critical surfaces to within 0.020 or 0.030 in. of finished dimensions. All through-holes should be in the disk during the spin test. It is recommended that the spin test speed(s) should subject all areas of the disk to strains in excess of the equivalent room-temperature mechanical-design strains. The spin speed should not exceed 90 percent of the spin-configuration burst speed or 95 percent of the yield speed.

3.4.4.1.3.2 Vibration Tests

Disk vibration tests shall ensure that the operating speed range is free of critical speeds

Since disk vibration is a possible source of failure and the analysis of disks is based on simplifying assumptions, laboratory vibration tests of turbine rotor disks should be

conducted. These tests should be carefully designed to verify the calculated natural frequencies and to establish that no forcing frequencies exist in the proposed speed range.

3.4.4.2 SHAFT

The turbine shaft shall have an adequate safety factor on the combined stress state imposed by the mechanical-design parameters.

The safety factor on the turbine shafting as determined from the modified Soderburg relationship of equation (37) considers both the steady and alternating stress. Unless reliable data establishing other values is available, the alternating component of torsional load should be assumed to be equal to 5 percent of the steady torsional load. A safety factor of 1.5 based on mechanical-design parameters is recommended.

3.4.4.3 FASTENERS

The axial preload on fasteners in rotor assemblies shall preclude fastener unloading during operation.

To maintain an adequate axial preload on fasteners during operations, a safety factor of 1.5 should be maintained between the applied load causing separation and the total applied load at operating conditions. The load causing separation is a function of the initial preload, differential thermal growth, Poisson-type shortening, curvic-coupling growth, and the component spring rates. Applied loads result from pressure-separating, bending, and curvic-separating effects. The fastener loading will change with temperature, speed, and power; therefore, various run times should be considered during the design analysis.

3.4.4.3.1 Locking Devices

All locking devices for threaded retainers shall withstand maximum loads without yielding or failing.

The dynamic-load-carrying capacity of locking devices for threaded retainers should be established analytically and substantiated experimentally. Designate tab-lock designs that permit safety locking without requiring any movement of nuts or bolts after the required fastener torque has been applied. The condition of locking devices should be inspected and noted during controlled disassembly of the turbine.

3.4.4.4 TORQUE TRANSMISSION

The torque transmission device shall provide adequate torque transmission capability as well as the capability for balance and retention of components

Torque transmission, balance, and component retention should be accomplished with couplings that maintain piloting even when they are deformed by thermal and centrifugal loads. Designs incorporating either curvic couplings or interference fits between rotating components have proven satisfactory. The recommended ratio for curvic pitch diameter to turbine pitch diameter is 0.4 to 0.5. A detailed presentation of recommended practices is given in reference 45.

Limit the design length of male threads in the coupling device so that the threads are not exposed to turbine fluids; this practice precludes subsequent accumulation of foreign matter on the threads that will result in thread binding.

3.4.5 Casing, Manifold, and Diaphragm

3.4.5.1 CONFIGURATION

The configuration and construction of casings, manifolds, and diaphragms shall be

(1) Specifically suited to the operational temperature, pressure, and developed power of the turbine
(2) Light in weight
(3) Simple in form
(4) Easy to fabricate

Low power, low temperature. – For this kind of turbine, the diaphragm should serve as the principal structural member through which turbine casing and torus loads are transmitted to the turbopump housing. With this configuration, the casing stresses pass through the nozzle, as illustrated in the turbine appearing in figure 3. Upon completion of the design layout, check all details for compliance to minimum component size and weight, ease of fabrication, component cost, and ease of assembly.

Low inlet pressure. – Use integrated manifold and casing designs similar to those in figures 6 and 43, wherein the structural loads are transmitted across the manifold outer surface. For this design, castings are not practical because of the weight/strength penalty imposed. Fabricate the thin casing and manifold sections from sheet metal or from forgings machined into thin sections. Locate attachment flanges on the manifold outer surface and on the diaphragm inner bolt circle.

Moderate inlet pressure. – For pressures up to 500 psi, use the welded torus and casing as shown in figures 4 and 44. The mounting flanges should be designed as part of a continuous structural ring (or rings) welded to the torus; avoid the "dog-ear" manifold flange.

High inlet pressure. – For inlet pressures above 500 psi, the structural support for the torus should be separated from the turbine casing so that operational loads sustained by the casing (coupled with loads contributed by high turbine manifold pressures) do not alter the orientation of the manifold and nozzle relative to the rotor assembly. The design details for this type of manifold installation appear in figures 7 and 45.

Configuration for test. – For casings and manifolds intended to be used in performance evaluation tests, weight and sizing requirements should be considered secondary to those dealing with ease of fabrication, assembly, and instrumentation; a typical model test turbine manifold and casing appears in figure 46. Aluminum should be used in the fabrication of this hardware whenever the test turbine is scheduled to be evaluated with cold working fluids. The design should be built with a minimum of machining operations, at a minimum cost, and with the capability of accepting design modifications with a minimum amount of rework.

3.4.5.2 STRUCTURE

The turbine inlet manifold, diaphragm, and casing shall withstand the design pressure loads, externally applied loads, and differential thermal loads.

Section thicknesses should be made uniform and as small as is consistent with strength requirements for the primary load. This practice will generally reduce the thermal stresses and minimize the cyclic plastic strain. In addition, it is recommended that the manifold be designed to transmit the external loads imposed by ducts, mounts, and associated hardware around the torus and vanes rather than through them.

In high-pressure manifolds, the flow downstream of the inlet port should separate circumferentially and flow in two directions around the manifold. This dual-entry-and-flow configuration is recommended for the purpose of equalizing manifold pressure and load distribution. An example of this geometry for a high pressure manifold appears in figure 44.

In high-temperature and high-power applications, the diaphragm design should provide the turbine with sealing provisions and the structural support to withstand distortion during operations. The diaphragm should be short coupled from the torus to the diaphragm inner attachment point. A recommended diaphragm design for a highly loaded turbine appears in figure 7. Note the short radial length of the diaphragm in this design compared to the one used in the lower power J-2 oxidizer turbine in figure 6.

The width and thickness of the diaphragm inside-diameter flange should be sized to sustain all operational loads (structural and thermal) and to maintain a proper seal at that juncture.

Provide for thermal growth with a symmetrical pattern of radial pins or the equivalent.

Use materials with good ductility and good low-cycle fatigue strength.

Verify the structural adequacy analytically and conduct proof-pressure tests as described previously.

3.4.5.3 PROBLEM AREAS

3.4.5.3.1 Welding Practices

Welding practices shall conform to established successful specifications and procedures.

Manifolds and turbine casing construction should be butt welded with 100-percent penetration; welds should be accessible for X-ray inspection. For reliability and reproducibility, the weld process (ref. 48) should control (1) the type of weld; (2) weld preparation; (3) bead width and height; (4) wire size and feed rate; (5) weld dropthrough requirement; and (6) fit tolerances. Avoid using fillet welds in turbine manifold and shroud configurations. Whenever thin-sheet-metal diaphragms are welded to comparatively thick torus cross sections, the design should contain a transition section from the thick torus to the thin-diaphragm weld joint to prevent thermal stress concentrations and cracking. Figure 60(a) illustrates representative kinds of welds recommended for turbine fabrication, and figure 60(b) the types that should be avoided because of potential cracking.

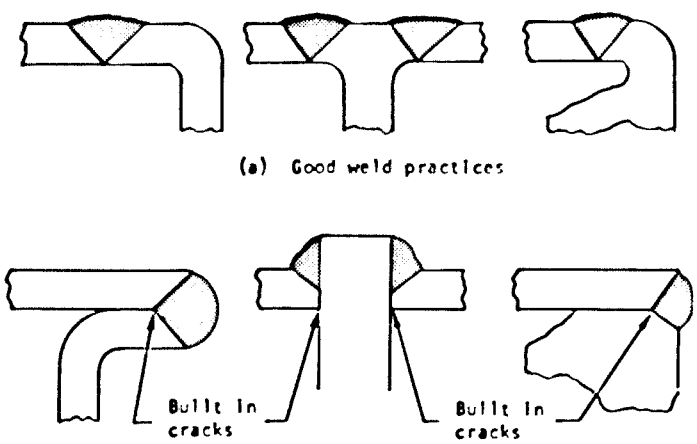

Figure 60. – Good and bad weld practices.

3.4.5.3.2 Casing Cavities and Pockets

The turbine casing design shall preclude

(1) The accumulation of liquids and subsequent condensation on the casing outer surface, and

(2) The collection and entrapment of foreign matter on the casing internal surface.

The casing configuration should approach a smooth-wall cylindrical section as shown in figures 43 and 45. Avoid ridges, pockets, or U-sections that can accumulate moisture or leaking test-stand fluid. Avoid any possible leakage path that leads to the internal sections of the turbine.

The internal geometry should be free of pockets or cavities formed by the juncture of two casing sections. Modify any casing design that can form this kind of intersection when it is connected to the engine system ducting.

3.4.5.3.3 Casing Flange Leakage

The casing flange design shall preclude leakage through the flange bolt holes.

Turbine flanges should be designed with the static-seal groove positioned between the flange bolt circle and the pressure source being sealed. Designate only high-temperature-resistant static seals that have been tested to verify their capability to withstand turbine operating conditions at flanges, seal cavities, and instrumentation ports. Seals designated for reduced temperature environments should comply with selection criteria for this type of service. In high-pressure turbines, the flange is more likely to leak because the high loads deflect the flange sealing surfaces. The solution is to make the flange heavy enough to withstand the loads, then lighten it by scalloping.

3.5 INTEGRATION AND ASSEMBLY

3.5.1 Rotordynamics

3.5.1.1 CRITICAL SPEED

Rotordynamic analytical models of the complete rotating assembly shall be adequate to predict dynamic responses at critical and nonsynchronous whirl speeds.

The complete turbopump rotating assembly, of which the turbine is a component, should be analyzed. Construct an analytical model, for use with a digital computer, of the critical speeds and radial motions for the full range of operating conditions. Establish response versus time for an applicable range of acceleration rates. Verify that acceptable component deflections and stresses exist under unusual dynamic loads and at operation near a critical speed or a nonsynchronous whirl speed. Consult reference 45 for additional details on this kind of analysis of rotordynamics.

3.5.1.2 ROTORDYNAMIC RESPONSE

The combination of rotor geometry, rotor mass distribution, and operating speeds shall not result in unacceptable shaft stress amplification and shaft deflection.

To minimize deflection and stress amplification, adjustments are made to shaft stiffness, bearing stiffness, and rotor mass distribution. When possible, the maximum operating speed should not exceed 80 percent of the lowest synchronous speed. If this is not possible, the dynamic characteristics of a given turbine rotor should be experimentally evaluated in a turbine test facility over the full range of operating speeds to verify analytically predicted critical-speed responses.

3.5.2 Bearings and Seals

3.5.2.1 BEARING RADIAL SPRING RATE

The bearing radial spring rate shall suitably locate the critical speeds with respect to operating speeds.

Satisfactory operation between critical speeds should be achieved by shifting the critical speed curves by proper choice, location, and design of the bearings. As a means of avoiding excessive rotor radial displacement, the bearings should be designed and located such that the resulting critical speeds are separated from the operating speeds by the margins noted in section 3.5.1. The bearing radial spring rate has a pronounced effect upon critical speed and the amplitude of rotor motion. Therefore, calculations should be performed for the maximum permissible assembly imbalances over the entire operating range and, if necessary, bearing clearances should be increased to accommodate free-free rotor motion at the bearings.

3.5.2.2 BEARING RADIAL CLEARANCES

The bearing clearances shall preclude excessive orbital motion of the rotor about the centerline and excessive bearing reaction forces.

A certain amount of bearing radial clearance is necessary to minimize the bearing reaction forces due to rotor imbalance. The presence of clearance also facilitates operation at or near a critical speed by reducing the tendency of rotor imbalance alone to excite rotor motion. For the same reason, clearance can facilitate rapid transition through a critical speed. On the other hand, radial clearance should be kept small to minimize whirl of the system. Thus, the selection of bearing clearance is a compromise between two opposing conditions: the clearance should be small enough to minimize whirl, but large enough to permit rotor motion due to the maximum permissible assembly imbalances.

Bearing installations for the rotor assembly should be designed with provisions to preload angular contact-type bearings for the purpose of minimizing shaft non-synchronous whirl amplitudes; this practice helps reduce disk flexure during operation and the probability of cracks originating at the rotor hub.

3.5.2.3 COOLED BEARINGS

Designs for cooling and lubricating bearings installed outboard of the turbine rotor shall provide adjustable flowrates and pressures for the coolant.

The adjustment of cooling and lubrication flowrates and pressures for the bearing can be accomplished with variable orifices or with interchangeable coolant supply lines.

3.5.2.3.1 Coolant Leakage

The turbine design shall preclude accidental leakage of bearing coolant from impinging on the hot turbine disk.

Design the seal housing adjacent to the turbine diaphragm inner diameter with leakage flow paths that preclude impingement of any bearing coolant that might leak into the turbine housing. Establish a differential pressure distribution in the seal housing to help direct leakage flows away from the turbine.

3.5.2.4 SEALS BETWEEN ROTORS

Clearances in impulse-turbine dynamic seals located between the turbine stator and disk face shall not contribute to disk vibration and seal damage.

The seal clearance that will preclude any contributory effect on disk vibration should be established on a tentative basis during design. The final value should be based on the results of development tests (ref. 50). The influence of shaft axial displacement and deflection upon seal clearance should also be considered when establishing the seal configuration. The

best design is one that can be installed as a subassembly. Avoid configurations that disturb the stator installation whenever the seal is installed or disassembled.

3.5.3 Exhaust Ducts

Exhaust ducts shall not result in adverse pressure gradients across the last-row rotor.

Exhaust-duct configurations designed with flow parallel to the turbine axis are recommended because they contribute a minimum pressure gradient across the last-row disk. Installations limited to the use of nonaxial exit-duct designs should incorporate a centerbody or exhaust-flow straightener vanes to control pressure distribution adjacent to the last-row blades.

3.5.4 Problem Areas

3.5.4.1 COMPONENT INTEGRATION

The number of welds, flanged components, and sealing points in turbine hardware shall be minimized to simplify the design, reduce fabrication costs, and lower component weight.

Strive to integrate the turbine design with single machined detail parts, castings, and forgings. The manifold and shroud assembly in figure 61 illustrates how a design consisting of a number of separate parts can be integrated to form an improved design. In the original design (fig. 61(a)), the shroud-and-manifold assembly was fabricated by welding (1) the discharge flange section, (2) the center section, (3) the stator retainer section, and (4) the nozzle attachment section into a single subassembly. In the improved integrated design (fig. 61(b)), a single unit forged shroud (A) is machined and welded to the manifold section (B).

Turbine tooling and fixture design should be initiated as soon as the manifold/casing design is established, because of procurement lead time required for the manifold assembly.

3.5.4.2 TURBINE THERMAL ISOLATION

When necessary, the turbine design shall protect adjacent components in the engine system from turbine thermal radiation and soakback.

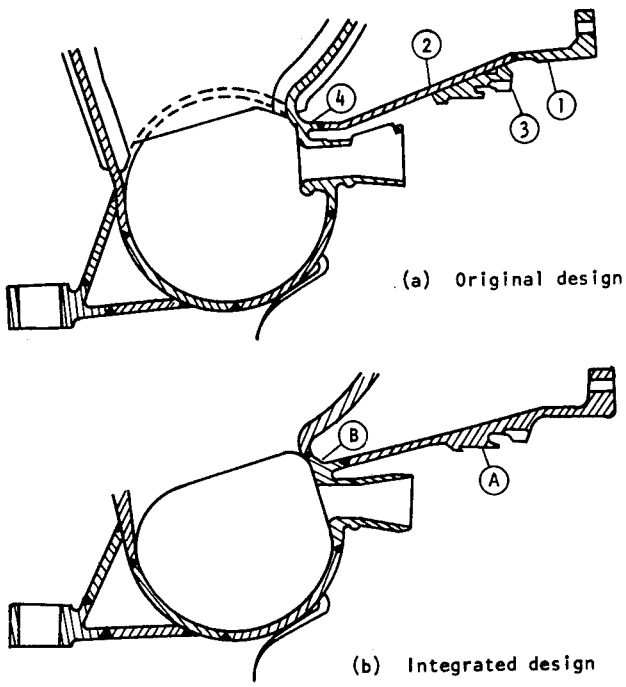

Figure 61. – Integration of shroud and manifold components.

An insulating heat shield is recommended for use on external turbine surfaces to prevent thermal radiation to adjacent engine components. The shielding design should in no way interfere with turbine operation, complicate engine installation, or contribute to turbine casing stresses. A typical turbine heat shield is shown in the F-1 turbine assembly in figure 4. All turbine insulation designs and installations should be accomplished by the turbomachinery group, or the insulation should be designed and installed in accordance with established criteria, subject to the approval of the turbomachinery group.

3.5.4.3 THERMAL GROWTH AND DEFLECTION

Turbine design shall minimize the effects of differential expansion and distortion of adjacent components.

Care should be exercised during the turbine mechanical design to concentrate on factors that help maintain rotating-element alignment and orientation during operations, so that the

gas path is not disturbed. Analyze all components for effects of differential expansions due to temperature effects and structural loading concentrations. The following procedures should be carried out:

- Check the method used to mount the turbine to the pump, and include allowances for turbine radial growth.
- Provide for proper transfer of loads between the turbine manifold and casing.
- Design stator vanes to sustain thermal radial growth without constraint.
- Allow for adequate diaphragm expansion and sealing during all operating conditions.
- Check nozzle vane and rotor blade shrouding for circumferential growth allowance.
- Provide the turbine bearing and seal retainers with adequate support to sustain all operating loads; allow for both structural and thermal loads.

3.5.4.4 COMPONENT ORIENTATION

The geometry of rotors, blades, stators, vanes, and shafting shall prevent the improper assembly and orientation of components.

Alignment grooves, tapers, interference fits, and variations of bolt-circle and curvic-coupling diameters should be incorporated into the turbine design to prevent the improper assembly of symmetrical rotor and stator components. Indexing and assembly-orientation markings may be made on components after controlled assembly and balance operations (where required) are completed. During prototype assembly, an assembly check should be made to establish the orientation and rotation direction(s) specified in all nozzle, vane, rotor, blade, and stator drawings. The rotor design drawing should include information describing the orientation of components, weight distribution for balance purposes, and retaining torque values.

3.5.4.5 TURBINE/TURBOPUMP INTERFACE

3.5.4.5.1 Manifold-to-Pump Coupling

The design of the manifold-to-pump coupling shall prevent excessive load concentrations at the attachment points.

When the turbine manifold is coupled to the pump, the attachment flanges should be interconnected by scalloped or circumferential structures as shown in figures 44 and 45. This type of interconnected flange design provides a better distribution of turbine loads than that provided by "dog-ear" flanges that are independently attached to the manifold.

Designs with turbine inlet temperatures up to 1000° F should utilize radial-type turbine-to-pump retainers to accommodate any differential component growth experienced during operations. Examples of this type of retainer appear in figures 4 and 6. Turbines designed for higher temperatures and pressures should utilize the manifold/casing type of retention technique shown in figures 7 and 8, so that thermal differential expansions between these components are kept to a minimum.

3.5.4.5.2 Turbine/Engine Accessories

The turbine structure shall not be required to sustain loads from engine accessories or ducting.

In particular, designs with the gas generator mounted directly on the turbine manifold should be avoided. Excessive static and dynamic loads are imposed on the turbine manifold if the gas generator is mounted directly upon it. The turbine designer should check the overall engine layout during the design and development phases to ensure that the objectives of this design criterion are observed for any other engine accessory.

3.6 TURBINE MATERIALS

Turbine materials shall possess physical and thermal properties adequate to meet all conditions during test and operation.

Material selection should be based on careful evaluation of the following properties:

(1) Capability to withstand thermal and structural loads at design and emergency power levels for required service life
(2) Compatibility with turbine working fluid under all conditions of service
(3) Fabricability as required for the necessary dimensional tolerances
(4) Cost and availability.

Recommended materials and their uses are presented in table II. Note that the turbine designation in table II relates to the information in table I and thus identifies the design conditions under which the materials were successfully used.

Several precautions should be observed in the use of certain materials:

- For stainless-steel welded structures, use 347 or 321. Avoid the use of 310 because welding problems can develop.
- Avoid welding Hastelloy C detail parts to Rene 41 manifold assemblies that will subsequently under go the heat-treat cycle for Rene 41; the Hastelloy C becomes brittle and unsuitable for load carrying.

- The process specification for fabricating manifolds from Rene 41 should include provisions for preventing strain'age cracking of Rene 41 welds, as follows:
  (1) Specify Hastelloy W weld rods
  (2) Solution anneal in an inert atmosphere (e.g., argon) with controlled heating and cooling rates.

3.7 PROVISIONS FOR INSTRUMENTATION

The turbine design shall specify the nature, location, and installation of all gas-path instrumentation.

Design details for instrumentation of prototype turbine configurations should be established when component drawings are evolved; this practice avoids problems associated with space limitation, accessibility, instrumentation-boss location, and adverse effects upon casing stresses if instrumentation provisions are made after hardware is fabricated.

To preclude leakage, manifold and casing instrumentation flanges should be designed to maintain "total flatness" at the sealing surface. High-temperature instrumentation flanges >2.0 in. in diameter should be designed with provisions for 0.001 in. flatness. This practice, coupled with proper sealing provisions, precludes leakage.

Instrumentation for the following minimum measurements is recommended for a prototype two-row velocity-compounded turbine:

- Turbine total inlet temperature
- Turbine static inlet pressure
- Static pressure between the nozzle and first-row blading
- Static pressure between the first-row blading and stator
- Static pressure between stator and second-row blading

Inter-row pressure data are obtained with piezometer ring installations. Prototype turbine dynamometer tests utilize dynamometer shaft-speed output data, and turbine exhaust pressure either is measured in the turbine exhaust duct or atmospheric pressure is used as a reference with an atmospheric exhaust setup. The detailed descriptions and data contained in references 51 through 56 are recommended as instrumentation guides for new turbine design.

APPENDIX A
GLOSSARY

Symbol	Definition
Aerothermodynamics	
A	area
A_a	annulus area
A_e	turbine effective area
A_n	nozzle nominal outlet area
b	blade or vane axial width
C_e	end loss (edge) coefficient
C_i	incidence coefficient
C_m	Mach number coefficient
C_o	theoretical spouting velocity
C_p	specific heat at constant pressure
c_o	absolute fluid velocity, stator inlet
c_1	absolute fluid velocity, stator outlet
c_2	absolute fluid velocity, rotor outlet
c_{u1}	fluid tangential velocity
D_m	nozzle or blade row outlet mean diameter
E_{d1}	diagram factor, stator
E_{d2}	diagram factor, rotor
F	active fraction of nozzle admission
f	nozzle arc length

Symbol	Definition
g	acceleration due to gravity
H	blade or vane height
HP	horsepower
h	enthalpy
Δh_c	total effective energy available for work
Δh_{c1}	kinetic energy, stator outlet
Δh_{c2}	kinetic energy, rotor outlet
Δh_{cs}	effective expansion energy
Δh_{cv}	effective kinetic energy
Δh_f	stator and rotor blade losses
Δh_r	enthalpy drop in rotor
h_{s0}	static enthalpy, stator inlet
h'_{s1}	static enthalpy, rotor inlet (=stator outlet)
h_{s2}	isentropic static enthalpy (exhaust)
h'_{s2}	static enthalpy, rotor outlet (=exhaust)
Δh_s	stage isentropic enthalpy drop
h_{t0}	total enthalpy, stator inlet
h'_{t1}	total enthalpy, rotor inlet
h'_{t2}	total enthalpy, exhaust
Δh_v	kinetic energy entering a stator or rotor
Δh_{v0}	kinetic energy, stator inlet
Δh_{v1}	kinetic energy, rotor inlet

Symbol	Definition
Δh_{v2}	kinetic energy, exhaust
Δh_w	stage actual enthalpy drop (blading work)
Δh_{wd}	diagram work for a single-row stage
J	energy conversion factor
K	opening coefficient, O/p
K	ratio of fluid velocity leaving wheel to velocity entering wheel for full admission
LMS	least mean square
M	Mach number
N	rotational speed (nominal); nozzle
N_t	nozzle throat
N_o	nozzle outlet
O	nozzle or blade throat opening
PC	pressure compounded
p	nozzle or blade circumferential pitch
p_{so}	static pressure, stator inlet
p_{s1}	static pressure, rotor inlet (+stator outlet)
p_{s2}	static pressure, rotor outlet (+exhaust)
p_{to}	total pressure, stator inlet
p_{t1}	total pressure, rotor inlet
p_{t2}	total pressure, exhaust
R	specific gas constant; rotor; radius
1-R	first rotor

Symbol	Definition
2-R	second rotor
R_1	blade radius, pressure surface
R_{su}	blade radius, suction surface
R_s	stage reaction, percent
r_1	leading-edge radius
r_2	trailing-edge radius
S	entropy
S	stator
T	working-fluid temperature
T_{t1}	turbine inlet temperature
(T-S)	total-to-static
(T-T)	total-to-total
t_1	leading-edge thickness
t_2	trailing-edge thickness
U	pitchline velocity
VC	velocity compounded
$\dot{w}_p$	mass flowrate of thrust-chamber propellant
$\dot{w}_t$	mass flowrate of turbine working fluid
w_1	relative fluid velocity, rotor inlet; also denotes inlet vector
w_2	relative fluid velocity, rotor outlet; also denotes outlet vector
Z	number of blades or vanes
O p	opening coefficient

Symbol	Definition
p/b	pitch/width ratio
U/C_o	isentropic velocity ratio
α	gas vector angle
α_1	exit vector angle, vane
α_2	exit vector angle, blade
β	blade physical angle
β_1	blade inlet angle
$\Delta\beta_1$	blade leading-edge divergence
β_{1p}	blade inlet angle, pressure surface
β_{1s}	blade inlet angle, suction surface
β_2	blade discharge angle
$\Delta\beta_2$	blade trailing-edge divergence
β_{2p}	blade discharge angle, pressure surface
β_{2s}	blade discharge angle, suction surface
γ	$\frac{\text{specific heat at constant pressure}}{\text{specific heat at constant volume}}$
Δ	increment or difference
ϵ_d	diagram efficiency factor
η_{FA}	turbine efficiency with full admission
η_{LW}	efficiency reduction from windage, partial-admission turbine
η_{PA}	efficiency, partial-admission turbine
η_{TSM}	turbine efficiency correction

Symbol	Definition
η_c	turbine efficiency with clearance
η_{c_0}	turbine efficiency with zero clearance
η_t	turbine efficiency
$\eta_{t,d}$	turbine diagram efficiency
θ	blade deflection angle
θ_d	design value, blade deflection angle
ρ	density
τ	tau factor, $\tau = \dot{w}_t / \dot{w}_p$
ϕ	chord angle
φ^2	expansion-energy loss coefficient
ψ	blade (or vane) loading coefficient (Zweifel number)
ψ^2	kinetic-energy loss coefficient

Structures and Stress

A	cross-sectional area
A_a	annulus area
A'	net area = (gross area − bolt hole area)
A_d	disk gross cross-sectional area
ΔA_i	area increment
A_s	amplification factor in a damped system
D_p	pitch diameter
d_i	inner diameter of hub shear section
d_o	outer diameter of hub shear section

Symbol	Definition
e	elongation
F_b	disk burst factor
F_c	centrifugal weight of blade, $F_c = MR\omega^2$
F_d	disk design factor
F_m	mode receptiveness factor
F_{te}	endurance limit for the required number of cycles
F_{tu}	ultimate tensile strength
F_{ty}	tensile yield strength
FS	factor of safety
FS_u	factor of safety, ultimate
FS_y	factor of safety, yield
f_{n1}, f_{n2}	forcing frequencies, first and second mode, resp.
g	acceleration due to gravity
K_t	stress-concentration factor, 1
K_t'	stress-concentration factor, 2
K_{tf}	fatigue notch factor for tensile stress
K_{tsf}	fatigue notch factor for shear stress
L_b	limit design factor for bending
L_s	limit design factor for shear
M	mass
M_{cmin}	bending moment about the minimum-moment-of-inertia axis
M_{cmax}	bending moment about the maximum-moment-of-inertia axis

Symbol	Definition
$M_{g\,min}$	gas bending moment about minimum principal inertia axis
$M_{g\,max}$	gas bending moment about maximum principal inertia axis
N	rotational speed (nominal)
N_b	burst speed
N_{CR1}	critical speed associated with the 1st bending mode
N^*_{CR1}	critical speed associated with 2nd harmonic of the exciting frequency and the 1st bending frequency
N_{CR2}	critical speed associated with the 2nd bending mode
N_{CR3}	3rd diametral critical speed
N_{CR4}	4th diametral critical speed
N_d	mechanical-design speed
N_y	yield speed
P_{md}	mechanical-design pressure
P'_p	proof pressure
R	radius
R	ratio of alternating stress to gas bending stress
R_1	ratio of maximum to nominal turbine speed
R_2	fraction of gas bending stress that is alternating
R_w	ratio of actual blade weight to that of a solid untapered blade
T_q	torque
T_{t1}	turbine inlet temperature
Z_{min}	section modulus about minimum axis
Z_{max}	section modulus about maximum axis

Symbol	Definition
ρ	density
σ_{AT}	disk average tangential stress
$\sigma_{ATburst}$	disk average tangential stress at burst
σ_{ATcorr}	corrected disk average tangential stress
σ_a	alternating normal stress
σ_{alt}	alternating stress
σ_c	direct centrifugal stress
σ_{cb}	centrifugal bending stress
σ_m	mean stress at any point in the blade
σ_{max}	maximum tangential stress
σ_o	steady normal stress
σ_p	gas bending stress
σ'_p	gas bending stress induced by gas force on the blade profile only
σ_{td}	local tangential stress at discontinuity
σ_{ti}	local tangential stress
σ_{tmax}	maximum tangential stress
σ'_{tmax}	peak tangential stress
τ_a	alternating shear stress
τ_o	steady shear stress
ω	rotational speed in rad/sec

Material[1]	Identification
alloy 713C	austenitic nickel-chromium-aluminum casting alloy
FLOX	mixture of liquid fluorine and liquid oxygen
GH_2	gaseous hydrogen
GN_2	gaseous nitrogen
Hastelloy B	trade name of Union Carbide Corp. for austenitic nickel-molybdenum-iron alloy
Hastelloy C	trade name of Union Carbide Corp. for austenitic nickel-molybdenum-chromium-iron alloy
Hastelloy W	trade name of Union Carbide Corp. for austenitic nickel-molybdenum-iron-chromium alloy
hydrazine	N_2H_4, propellant grade per MIL-P-26536B
IN 100	trade name of International Nickel Co. for nickel-cobalt-chromium-aluminum alloy
Inconel 718	trade name of International Nickel Co. for nickel-chromium-iron alloy
Inconel X-750	trade name of International Nickel Co. for austenitic nickel-chromium-iron alloy
IRFNA	inhibited red fuming nitric acid, propellant grade per MIL-P-7254
LF_2	liquid fluorine
LH_2	liquid hydrogen, propellant grade per MIL-P-27201A
LOX or LO_2	liquid oxygen, propellant grade per MIL-P-25508D
N_2O_4	nitrogen tetroxide, propellant grade per MIL-P-26539
Rene 41	trade name of General Electric Co. for an austenitic nickel-chromium-cobalt-molybdenum alloy
RP-1	kerosene-base high-energy hydrocarbon fuel per MIL-P-25576

[1]Additional information on metallic materials herein can be found in the 1972 SAE Handbook, SAE, Two Pennsylvania Plaza, New York, NY; in MIL-HDBK-5B, Metallic Materials and Elements for Aerospace Vehicle Structures, Dept. of Defense, Washington, DC, Sept. 1971; and in Metals Handbook (8th ed.), Vol. 1: Properties and Selection of Metals, Am. Society for Metals (Metals Park, OH), 1961.

Material	Identification
Stellite 21	trade name of Union Carbide Corp. for a cobalt-base alloy
Titanium 6-2-4-2	designation of Titanium Metals Corp. for a titanium alloy containing 6Al-2Sn-4Zr-2Mo
Udimet 630	trade name of Special Metals, Inc. (New Hartford, NY) for a nickel-iron-chromium-columbium alloy
Udimet 700	trade name of Special Metals, Inc. for a nickel-cobalt-chromium-molybdenum alloy
UDMH	unsymmetrical dimethylhydrazine, propellant grade per MIL-P-25604D
16-25-6	trade name of Timken Roller Bearing Co. for an austenitic iron-base 16Cr-25Ni-6Mo alloy
19-9DL	trade name of Universal Cyclops for an austenitic iron-base 19Cr-9Ni alloy
50/50	50:50 mixture of hydrazine and UDMH
310 321 347	AISI designations for austenitic stainless steels

Vehicles and Engines	Identification
Agena LR81-BA-11	engine for Agena upper stage; 15 000 lbf thrust; uses IRFNA/UDMH; manufactured by Bell Aerospace Company, Division of Textron
Atlas	launch vehicle using MA-5 engine system containing 2 booster, 2 vernier, and 1 sustainer engines; boosters provide 330 000 to 370 000 lbf thrust; sustainer, 60 000 lbf thrust; uses LOX/RP-1; engine system manufactured by Rocketdyne Division, Rockwell International Corp.
E-1	development backup engine for F-1
F-1	engine for S-IC; 1 500 000 lbf thrust; uses LOX/RP-1; manufactured by Rocketdyne
H-1	engine for S-IB; 200 000 lbf thrust; uses LOX/RP-1; manufactured by Rocketdyne

Vehicles and Engines	Identification
H-2	advanced version of H-1 engine with new turbomachinery
J-2	engine for S-II; 200 000 lbf thrust; uses LOX/LH_2; manufactured by Rocketdyne
J-2S	uprated J-2 engine; 250 000 lbf thrust
J-2X	advanced J-2 engine with redesigned turbomachinery
Jupiter	launch vehicle using S3D engine that developed 150 000 lbf thrust; used LOX/RP-1; engine manufactured by Rocketdyne
M-1	1 500 000-lbf-thrust engine designed and developed by Aerojet Liquid Rocket Co.; used LOX/LH_2
NERVA	Nuclear Engine for Rocket Vehicle Application developed by Aerojet Liquid Rocket Co.; 750 000 lbf thrust; uses H_2 as working fluid
Redstone	launch vehicle using Rocketdyne A-7 engine system providing 78 000 lbf thrust; engine used LOX/alcohol
RL10	engine for Centaur upper stage; 15 000 lbf thrust; uses LOX/LH_2; manufactured by Pratt & Whitney Aircraft Division of United Aircraft Corp.
Saturn V	launch vehicle for Apollo manned mission to the moon
S-IB	booster using a cluster of eight H-1 engines
S-IC	first stage (booster) of the Apollo Saturn V vehicle; uses five F-1 engines
S-II	second stage of the Apollo saturn V vehicle; uses a cluster of five J-2 engines
S-IVB	third stage of the Apollo Saturn V vehicle; uses a single J-2 engine
Thor	launch vehicle using MB-3 engine system; 170 000 lbf thrust; uses LOX/RP-1; engine system manufactured by Rocketdyne
X-8	experimental throttleable rocket engine; 90 000 lbf thrust; uses LOX/LH_2; developed by Rocketdyne

Vehicles and Engines	Identification
X-15	experimental rocket-powered aircraft manufactured by North American Rockwell; used XLR-99 engine
XLR-99	variable-thrust engine (15 000 to 55 000 lbf) manufactured by Thiokol Chemical Corp.; used LOX/NH_3

APPENDIX B

Conversion of U.S. Customary Units to SI Units

Physical quantity	U.S. customary unit	SI unit	Conversion factor[a]
Bending moment	in.-lbf	N-m	0.1130
Energy	Btu	J	1054
Enthalpy (specific)	Btu/lbm	J/kg	2324
Force	lbf	N	4.448
Length	ft	m	0.3048
	in.	cm	2.54
Mass	lbm	kg	0.4536
Power	hp	W	745.7
Pressure	psi ($lbf/in.^2$)	N/m^2	6895
Rotational speed	rpm	rad/sec	0.1047
Section modulus	$in.^3$	m^3	1.639×10^{-5}
Specific gas constant	$\frac{\text{ft-lbf}}{\text{lbm-}^\circ\text{R}}$	$\frac{\text{J}}{\text{kg-K}}$	5.380
Specific heat	$\frac{\text{Btu}}{\text{lbm-}^\circ\text{R}}$	$\frac{\text{J}}{\text{kg-K}}$	4184
Stress	psi ($lbf/in.^2$)	N/m^2	6895
Temperature	°F	K	$K = \frac{5}{9}(^\circ F + 459.67)$
	°R	K	$K = \frac{5}{9}(^\circ R)$
Tensile strength	psi ($lbf/in.^2$)	N/m^2	6895
Thrust	lbf	N	4.448

[a]Multiply value given in U.S. customary unit by conversion factor to obtain equivalent value in SI unit. For a complete listing of conversion factors, see Mechtly, E. A.: The International System of Units. Physical Constants and Conversion Factors. Second revision, NASA SP-7012, 1973.

REFERENCES

1. Anon.: Turbopump Systems for Liquid Rocket Engines. NASA Space Vehicle Design Criteria Monograph (to be published).

2. Glassman, A. J., ed.: Turbine Design and Application. Volume One. NASA SP-290, 1972.

3. Glassman, A. J.: Computer Program for Preliminary Design Analysis of Axial-Flow Turbines. NASA TN D-6702, 1972.

4. Wong, R. Y.; and Nusbaum, W. J.: Experimental Investigation of a 3.0 Inch Mean Diameter Full Admission Three-Stage Turbine Suitable for Small Auxiliary Power Units. NASA TN D-2639, 1965.

5. Nusbaum, W. J.; and Holeski, D. E.: Cold-Air Investigation of Prototype SNAP-8 Turbine. NASA TN D-1529, 1962.

6. Johnston, I. H.; and Dransfield, D. C.: The Test Performance of Highly Loaded Turbine Stages for High Pressure Ratio. Aeronautical Research Council, Reports and Memoranda, R & M 3242, 1962.

7. Kofskey, M. G.: Performance Evaluation of Two-Stage Turbine Designed for a Ratio of Blade Speed to Jet Speed of 0.146. NASA TM X-146, 1960.

8. Stewart, W. L.: Analytical Investigation of Multistage Turbine Efficiency Characteristics in Terms of Work and Speed Requirements. NACA RM E57K22b, 1958.

9. Ainley, D. G.; and Mathieson, G. C. R.: An Examination of the Flow and Pressure Losses in Blade Rows of Axial Flow Turbines. Rept. No. R 86, National Gas Turbine Establishment, Mar. 1951.

10. Ainley, D. G.; and Mathieson, G. C. R.: A Method of Performance Estimation for Axial Flow Turbines. Aeronautical Research Council, R & M 2974, 1951.

11. Emmert, H. D.: Current Design Practices for Gas Turbine Power Elements. Trans. ASME, vol. 72, 1950, p. 189.

12. Carter, A. F.; Platt, M.; and Lenherr, F. K.: Analysis of Geometry and Design-Point Performance of Axial Flow Turbines. Part 1 – Development of the Analysis Method and the Loss Coefficient Correlation. NASA CR-1181, Northern Research and Engineering Corp. (Cambridge, MA), Sept. 1968.

13. Platt, M.; and Carter, A. F.: Analysis of Geometry and Design-Point Performance of Axial Flow Turbines. Part 2 – Computer Program. NASA CR-1187, Northern Research and Engineering Corp. (Cambridge, MA), Oct. 1968.

14. Carter, A. F.; and Lenherr, F. K.: Analysis of Geometry and Design-Point Performance of Axial-Flow Turbines Using Specified Meridional Velocity Gradients. NASA CR-1456, Northern Research and Engineering Corp. (Cambridge, MA), Dec. 1969.

15. Flage, E. E.: Analytical Procedure and Computer Program for Determining the Off-Design Performance of Axial Flow Turbines. NASA CR-710, Flight Propulsion Div., General Electric Co. (Cincinnati, OH), Feb. 1967.

16. Stenning, A. H.: Design of Turbines for High-Energy-Fuel Low-Power-Output Applications. Mass. Inst. of Tech. Publ. Off. (Cambridge, MA) 1953.

17. Moffitt, T. P.; and Klag, F. W.: Experimental Investigation of the Partial Admission Performance Characteristics of a Single Stage Mach 2 Supersonic Turbine. NASA TM X-80, 1959.

18. Klassen, H. A.: Cold-Air Investigation of Effects of Partial Admission on Performance of 3.75 Inch Mean Diameter Single Stage Axial Flow Turbine. NASA TN D-4700, 1968.

19. Hawthorne, W. R.: Aerodynamics of Turbines and Compressors. Volume X of High Speed Aerodynamics and Jet Propulsion. Princeton University Press, 1964.

20. Boxer, E.; Sterrett, J. R.; and Wiodarski, J.: Application of Supersonic Vortex-Flow Theory to the Design of Supersonic Impulse Compressor or Turbine Blade Sections. NACA RM L52B06, 1952.

21. Colclough, C. D.: Design of Turbine Blades Suitable for Supersonic Relative Inlet Velocities and the Investigation of Their Performance in Cascades: Part I, Theory and Design. J. Mech. Eng. Sci., vol. 8, no. 1, Mar. 1966, p. 110.

22. Goldman, L. J.: Analytical Investigation of Supersonic Turbomachinery Blading. Part II – Analysis of Impulse Turbine-Blade Sections. NASA TN D-4422, 1968.

23. Goldman, L. J.; and Scullin, V. J.: Analytical Investigation of Supersonic Turbomachinery Blading. Part I – Computer Program for Blading Design. NASA TN D-4421, 1968.

24. Goldman, L. J.: Supersonic Turbine Design and Performance. Paper 72-GT-63, ASME Gas Turbine and Fluids Eng. Conf. and Prod. Show (San Francisco, CA), Mar. 1972.

25. Hamrick, J. T.; Ginsburg, A.; and Osborn, W. M.: Method of Analysis for Compressible Flow Through Mixed Flow Centrifugal Impellers of Arbitrary Design. NACA TR 1082, 1952.

26. Zweifel, O.: The Spacing of Turbo-Machine Blading Especially With Large Angular Deflection. The Brown Boveri Review, Brown Boveri & Co., Ltd. (Baden, Switz.), Dec. 1945.

27. Ainley, D. G.; and Mathieson, G. C. R.: An Examination of the Flow and Pressure Losses in Blade Rows of Axial-Flow Turbines. Aeronautical Research Council, R & M 2891, 1955.

28. Huppert, M. C.; and MacGregor, C. A.: Comparison Between Predicted and Observed Performance of Gas-Turbine Stator Blade Designed for Free-Vortex Flow. NACA TN 1810, 1949.

29. Katsanis, T.: FORTRAN Program for Calculating Transonic Velocities on a Blade-to-Blade Stream Surface of a Turbomachine. NASA TN D-5427, 1969.

30. Katsanis, T.: FORTRAN Program for Quasi-Three-Dimensional Calculation of Surface Velocities and Choking Flow for Turbomachine Blade Rows. NASA TN D-6177, 1971.

31. McNally, W. D.: FORTRAN Program for Calculation of Compressible Laminar and Turbulent Boundary Layers in Arbitrary Pressure Gradient. NASA TN D-5681, 1970.

32. Sasman, P. K.; and Crisci, R. J.: Compressible Turbulent Boundary Layer With Pressure Gradient and Heat Transfer. AIAA J., vol. 4, no. 1, Jan. 1966, pp. 19-25.

33. Stewart, W. L.: Analysis of Two-Dimensional Compressible Flow Loss Characteristics Downstream of Turbomachine Blade Rows in Terms of Boundary Layer Characteristics. NACA TN 3515, 1955.

34. Horlock, J. H.: Axial Flow Turbines. Butterworth & Co., Ltd. (London), 1966.

35. Kofskey, M. G.; and Nusbaum, W. J.: Performance Evaluation of a Two-Stage Axial-Flow Turbine for Two Values of Tip Clearance. NASA TN D-4388, 1968.

36. Hong, Y. S.: Axial Turbine Loss Analysis and Efficiency Prediction Method. Rept. D4-3220, The Boeing Company, 1966.

37. Anon.: Metallic Materials and Elements for Aerospace Vehicle Structures. MIL-HDBK-5B, Department of Defense, Sept. 1971.

38. Traupel, W.: Thermische Turbomaschinen. Vol. 2. Springer-Verlag (Berlin), 1960.

39. Manson, S. S.: Thermal Stress and Low Cycle Fatigue. McGraw-Hill Book Co., 1966.

40. Prescott, J.: Applied Elasticity. Dover Publications, 1961.

41. Millenson, M. B.; and Manson, S. S.: Determination of Stresses in Gas-Turbine Disks Subjected to Plastic Flow and Creep. NACA Rep. No. 906, 1948.

42. Pestel, E. C.; and Leckie, F. A.: Matrix Methods in Elastomechanics. McGraw-Hill Book Co., 1963.

43. Ehrich, F. F.: A Matrix Solution for the Vibration Modes of Nonuniform Discs. Trans. ASME, vol. 78, 1956, p. 109.

44. Mykelstad, J.: Vibration Analysis. McGraw-Hill Book Co., 1956, pp. 90-91.

45. Anon.: Liquid Rocket Engine Turbopump Shafts and Couplings. NASA Space Vehicle Design Criteria Monograph, NASA SP-8101, Sept. 1972.

46. Peterson, R. E.: Stress Concentration Design Factors. John Wiley & Sons, Inc., 1953, pp. 14-17 and p. 64.

47. Przemieniecki, J. S.: Theory of Matrix Structural Analysis. McGraw-Hill Book Co., 1968.

*48. Anon.: Process Specification RAO 607-034. Rocketdyne Div., North American Rockwell Corp., unpublished, July 1970.

49. Anon.: Liquid Rocket Engine Turbopump Bearings. NASA Space Vehicle Design Criteria Monograph, NASA SP-8048, Mar. 1971.

50. Anon.: Liquid Rocket Engine Turbopump Rotating Shaft Seals. NASA Space Vehicle Design Criteria Monograph (to be published).

51. Petrash, D. A.; Schum, H. J.; and Davison, E. H.: Component Performance Investigation of J-71 Experimental Turbine. NACA RM E57E29, Jan. 1958.

52. Plohr, H. W.; Holeski, D. E.; and Forrette, R. E.: Design and Experimental Investigation of a Single Stage Turbine With Downstream Stator. NACA RM E56K10, Jan. 1957.

53. Whitney, W. J.; Szanca, E. M.; Moffitt, T. P.; and Monroe, D. E.: Cold-Air Investigation of a Turbine for High-Temperature-Engine Application. I - Turbine Design and Overall Stator Performance. NASA TN D-3751, 1967.

54. Schulze, W. M.; Ashby, G. C.; and Erwin, J. R.: Several Combination Probes for Surveying Static and Total Pressure, and Flow Direction. NACA TN 2830, 1952.

55. Whitney, W. J.; Schum, H. J.; and Behning, F. P.: Cold-Air Investigation of a Turbine for High-Temperature-Engine Application. IV - Two-Stage Turbine Performance. NASA TN D-6960, 1972.

56. Kofskey, M. G.; and Nusbaum, W. J.: Design and Cold-Air Investigation of a Turbine for a Small Low-Cost Turbofan Engine. NASA TN D-6967, 1972.

57. Whitney, W. J.: Cold-Air Investigation of a Three-Stage Turbine With a Blade-to-Jet-Speed Ratio of 0.135 Designed for a 20 000-Pound-Thrust Hydrogen-Oxygen Rocket Turbopump Application. NASA TM X-414, 1960.

58. Beckwith, I. E.; and Moore, J. A.: An Accurate and Rapid Method for the Design of Supersonic Nozzles. NACA TN 3322, 1955.

59. Crown, J. C.: Supersonic Nozzle Design. NACA TN 1651, 1948.

*Dossier for design criteria monograph "Liquid Rocket Engine Turbines." Unpublished, 1971. Collected source material available for inspection at NASA Lewis Research Center, Cleveland, Ohio.

NASA SPACE VEHICLE DESIGN CRITERIA MONOGRAPHS ISSUED TO DATE

ENVIRONMENT

SP-8005	Solar Electromagnetic Radiation, Revised May 1971
SP-8010	Models of Mars Atmosphere (1967), May 1968
SP-8011	Models of Venus Atmosphere (1972), Revised September 1972
SP-8013	Meteoroid Environment Model–1969 (Near Earth to Lunar Surface), March 1969
SP-8017	Magnetic Fields–Earth and Extraterrestrial, March 1969
SP-8020	Mars Surface Models (1968), May 1969
SP-8021	Models of Earth's Atmosphere (90 to 2500 km), Revised March 1973
SP-8023	Lunar Surface Models, May 1969
SP-8037	Assessment and Control of Spacecraft Magnetic Fields, September 1970
SP-8038	Meteoroid Environment Model–1970 (Interplanetary and Planetary), October 1970
SP-8049	The Earth's Ionosphere, March 1971
SP-8067	Earth Albedo and Emitted Radiation, July 1971
SP-8069	The Planet Jupiter (1970), December 1971
SP-8084	Surface Atmospheric Extremes (Launch and Transportation Areas), May 1972
SP-8085	The Planet Mercury (1971), March 1972
SP-8091	The Planet Saturn (1970), June 1972
SP-8092	Assessment and Control of Spacecraft Electromagnetic Interference, June 1972
SP-8103	The Planets Uranus, Neptune, and Pluto (1971), November 1972
SP-8105	Spacecraft Thermal Control, May 1973

STRUCTURES

SP-8001	Buffeting During Atmospheric Ascent, Revised November 1970
SP-8002	Flight-Loads Measurements During Launch and Exit, December 1964
SP-8003	Flutter, Buzz, and Divergence, July 1964
SP-8004	Panel Flutter, Revised June 1972
SP-8006	Local Steady Aerodynamic Loads During Launch and Exit, May 1965
SP-8007	Buckling of Thin-Walled Circular Cylinders, Revised August 1968
SP-8008	Prelaunch Ground Wind Loads, November 1965
SP-8009	Propellant Slosh Loads, August 1968
SP-8012	Natural Vibration Modal Analysis, September 1968
SP-8014	Entry Thermal Protection, August 1968
SP-8019	Buckling of Thin-Walled Truncated Cones, September 1968
SP-8022	Staging Loads, February 1969
SP-8029	Aerodynamic and Rocket-Exhaust Heating During Launch and Ascent May 1969
SP-8030	Transient Loads From Thrust Excitation, February 1969
SP-8031	Slosh Suppression, May 1969
SP-8032	Buckling of Thin-Walled Doubly Curved Shells, August 1969
SP-8035	Wind Loads During Ascent, June 1970
SP-8040	Fracture Control of Metallic Pressure Vessels, May 1970
SP-8042	Meteoroid Damage Assessment, May 1970
SP-8043	Design-Development Testing, May 1970
SP-8044	Qualification Testing, May 1970
SP-8045	Acceptance Testing, April 1970

SP-8046	Landing Impact Attenuation for Non-Surface-Planing Landers, April 1970
SP-8050	Structural Vibration Prediction, June 1970
SP-8053	Nuclear and Space Radiation Effects on Materials, June 1970
SP-8054	Space Radiation Protection, June 1970
SP-8055	Prevention of Coupled Structure-Propulsion Instability (Pogo), October 1970
SP-8056	Flight Separation Mechanisms, October 1970
SP-8057	Structural Design Criteria Applicable to a Space Shuttle, Revised March 1972
SP-8060	Compartment Venting, November 1970
SP-8061	Interaction with Umbilicals and Launch Stand, August 1970
SP-8062	Entry Gasdynamic Heating, January 1971
SP-8063	Lubrication, Friction, and Wear, June 1971
SP-8066	Deployable Aerodynamic Deceleration Systems, June 1971
SP-8068	Buckling Strength of Structural Plates, June 1971
SP-8072	Acoustic Loads Generated by the Propulsion System, June 1971
SP-8077	Transportation and Handling Loads, September 1971
SP-8079	Structural Interaction with Control Systems, November 1971
SP-8082	Stress-Corrosion Cracking in Metals, August 1971
SP-8083	Discontinuity Stresses in Metallic Pressure Vessels, November 1971
SP-8095	Preliminary Criteria for the Fracture Control of Space Shuttle Structures, June 1971
SP-8099	Combining Ascent Loads, May 1972
SP-8104	Structural Interaction With Transportation and Handling Systems, January 1973

GUIDANCE AND CONTROL

SP-8015	Guidance and Navigation for Entry Vehicles, November 1968
SP-8016	Effects of Structural Flexibility on Spacecraft Control Systems, April 1969
SP-8018	Spacecraft Magnetic Torques, March 1969
SP-8024	Spacecraft Gravitational Torques, May 1969
SP-8026	Spacecraft Star Trackers, July 1970
SP-8027	Spacecraft Radiation Torques, October 1969
SP-8028	Entry Vehicle Control, November 1969
SP-8033	Spacecraft Earth Horizon Sensors, December 1969
SP-8034	Spacecraft Mass Expulsion Torques, December 1969
SP-8036	Effects of Structural Flexibility on Launch Vehicle Control Systems, February 1970
SP-8047	Spacecraft Sun Sensors, June 1970
SP-8058	Spacecraft Aerodynamic Torques, January 1971
SP-8059	Spacecraft Attitude Control During Thrusting Maneuvers, February 1971
SP-8065	Tubular Spacecraft Booms (Extendible, Reel Stored), February 1971
SP-8070	Spaceborne Digital Computer Systems, March 1971
SP-8071	Passive Gravity-Gradient Libration Dampers, February 1971
SP-8074	Spacecraft Solar Cell Arrays, May 1971
SP-8078	Spaceborne Electronic Imaging Systems, June 1971
SP-8086	Space Vehicle Displays Design Criteria, March 1972
SP-8096	Space Vehicle Gyroscope Sensor Applications, October 1972
SP-8098	Effects of Structural Flexibility on Entry Vehicle Control Systems, June 1972

SP-8102	Space Vehicle Accelerometer Applications, December 1972

CHEMICAL PROPULSION

SP-8087	Liquid Rocket Engine Fluid-Cooled Combustion Chambers, April 1972
SP-8081	Liquid Propellant Gas Generators, March 1972
SP-8109	Liquid Rocket Engine Centrifugal Flow Turbopumps, December 1973
SP-8052	Liquid Rocket Engine Turbopump Inducers, May 1971
SP-8048	Liquid Rocket Engine Turbopump Bearings, March 1971
SP-8101	Liquid Rocket Engine Turbopump Shafts and Couplings, September 1972
SP-8094	Liquid Rocket Valve Components, August 1973
SP-8097	Liquid Rocket Valve Assemblies, November 1973
SP-8090	Liquid Rocket Actuators and Operators, May 1973
SP-8080	Liquid Rocket Pressure Regulators, Relief Valves, Check Valves, Burst Disks, and Explosive Valves, March 1973
SP-8064	Solid Propellant Selection and Characterization, June 1971
SP-8075	Solid Propellant Processing Factors in Rocket Motor Design, October 1971
SP-8076	Solid Propellant Grain Design and Internal Ballistics, March 1972
SP-8073	Solid Propellant Grain Structural Integrity Analysis, June 1973
SP-8039	Solid Rocket Motor Performance Analysis and Prediction, May 1971
SP-8051	Solid Rocket Motor Igniters, March 1971
SP-8025	Solid Rocket Motor Metal Cases, April 1970
SP-8041	Captive-Fired Testing of Solid Rocket Motors, March 1971

NASA-Langley, 1974